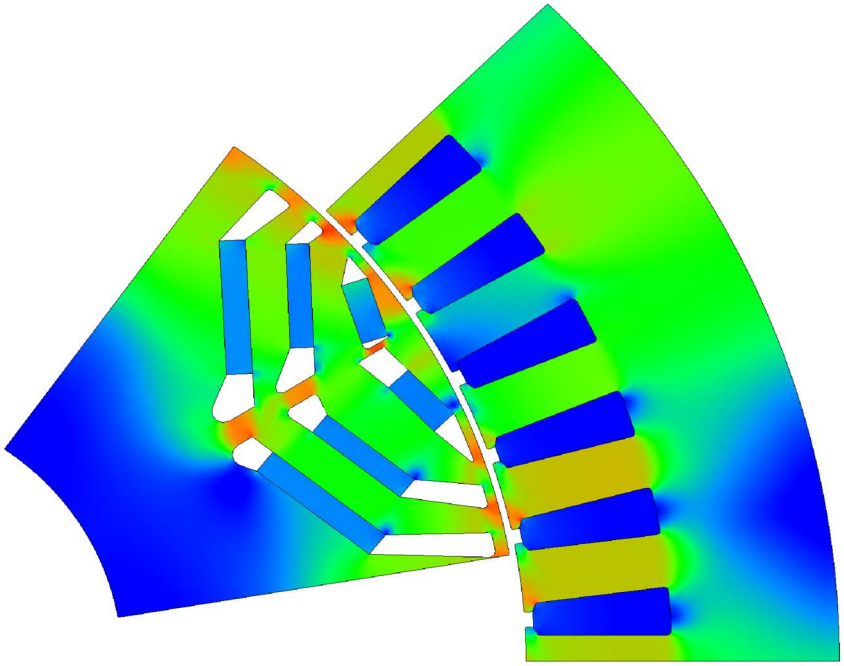

Design and Analysis of Asymmetric Electrical Machines for Automotive Applications

Master's thesis in Sustainable Electric Power Engineering and Electromobility

JACOB NILSSON

DEPARTMENT OF ELECTRICAL ENGINEERING
DIVISION OF ELECTRIC POWER ENGINEERING

CHALMERS UNIVERSITY OF TECHNOLOGY
Gothenburg, Sweden 2025
www.chalmers.se

Design and Analysis of Asymmetric Electrical Machines for Automotive Applications

JACOB NILSSON

Department of Electrical Engineering
Division of Electric Power Engineering
CHALMERS UNIVERSITY OF TECHNOLOGY
Göteborg, Sweden 2025

Design and Analysis of Asymmetric Electrical Machines for Automotive Applications

JACOB NILSSON

Department of Electrical Engineering
Division of Electric Power Engineering
Chalmers University of Technology
SE–412 96 Göteborg
Sweden
Telephone +46 (0)31–772 1000

Cover:
Contour plot of magnetic flux density in an asymmetric 3V machine.

Göteborg, Sweden 2025

Design and Analysis of Asymmetric Electrical Machines for Automotive Applications
JACOB NILSSON
Department of Electrical Engineering
Division of Electric Power Engineering
Chalmers University of Technology

Abstract

The study has designed and optimised six different rotor topologies all with three different magnet grades with a common stator geometry. To first evaluate the maximum performance given the constrained volume and magnet mass for each topology and magnet grade with asymmetric magnet size and placement. Secondly the optimisation targets were changed from maximising performance to minimising cost and losses at two operating points important for WLTP efficiency. A brief analysis of the risk of demagnetisation during normal operation and ASC was also conducted.

It was found that the asymmetric machine can deliver more torque per magnet mass and that the 3V N52 machine delivers the most torque for this size. In general, the V-rotors outperformed the U-rotors, and the V-rotors became more asymmetric from the optimisations. The asymmetric machines can not generate the same peak torque in both directions as a symmetric can and does therefore have a worse power factor in generator mode. Despite this the machines maintain a respectable WLTP efficiency at the same time as the material cost has greatly been reduced by the cost and efficiency optimisation.

Keywords: Asymmetric, IPM, JMAG, Optimisation, Permanent Magnet, PMSM, Reluctance

Acknowledgements

This work has been carried out at the Department of Electrical Engineering at Chalmers University of Technology. With financial support given by Polestar Performance AB in the form of providing facilities, software and computational hardware making this thesis possible. I want to specifically thank my supervisor Andreas Carlsson at Polestar for the opportunity and the guidance throughout the project. I also want to thank Zoltan Nadudvari from Powersys for getting me started with optimisation in JMAG Designer.

Jacob Nilsson
Göteborg, Sweden, 2025

Acronyms

ASC Active Short Circuit. 5, 22, 23, 42–47

ASM Asynchronous Machine. 3

DC Direct Current. 3

EESM Electrically Excited Synchronous Machines. 1, 3

EM Electric Machine. 20, 21

EMF Electromotive Force. 4, 5, 42

FW Field Weakening. 18

IPM Interior Permanent Magnet. 3, 5, 8, 41, 47

MMF Magnetomotive Force. 4

MTPA Maximum Torque per Ampere. 3, 14, 18, 38, 41, 42

MTPL Maximum Torque per Loss. 38

OEM Original Equipment Manufacturer. 1

OP1 Operation Point One, Low Speed Acceleration. 19–21, 37, 38, 40, 41

OP2 Operation Point Two, High Speed Steady State. 19–21, 37, 38, 40, 41

PMSM Permanent Magnet Synchronous Machine. 1, 3, 5, 8

PWM Pulse Width Modulation. 9

REE Rare Earth Element. 2, 28

RMS Root Mean Square. 9

SPM Surface-Mounted Permanent Magnet. 3

SynRM Synchronous Reluctance Machines. 1, 3

UNECE United Nations Economic Commission for Europe. 10

WLTC Worldwide Harmonized Light Vehicles Test Cycle. 10, 47

WLTP Worldwide Harmonised Light Vehicles Test Procedure. 5, 10, 21, 36–41

Contents

Chapter 1

Introduction

In today's automotive industry, electrification is of the highest focus and development of more powerful, efficient, sustainable electric drive units at a low costs is the focus of many researchers and engineers [1]–[3]. Many different technologies are currently being investigated for traction applications such as the Electrically Excited Synchronous Machines (EESM) and the Synchronous Reluctance Machines (SynRM). Since EESMs requires significant investments into both new production and validation due to the different nature of the machine. It is challenging and costly for an Original Equipment Manufacturer (OEM) to change to this technology [4]. SynRMs are on the other hand simpler but they have a relative low torque density and a low power factor compared to the Permanent Magnet Synchronous Machine (PMSM) requiring bigger converters [1]. Therefore, methods to reduce the rare-earth content in existing permanent magnet machines is investigated and if changing the magnet type to a less rare earth element type isn't an option, more efficient use of the magnet is necessary to reduce the total magnet mass.

One technology that achieves this is the use of asymmetric rotors in internally mounted permanent magnet machines [5]–[10]. As electrical machines used in the automotive industry will primarily only rotate in one direction during its lifetime, having a symmetric pole may not be the most efficient solution, since a symmetric machine machine has the peak of the reluctance torque and the magnet torque at different current angles. An asymmetric rotor can bring the peak of the reluctance torque and the peak of the magnet torque closer to each other and therefore increase the overall torque.

As of today, there are very few if any asymmetric machines on the market, however as the current economic climate is challenging and new and more cost-effective solutions must be found these machines may pose as an attractive option for many automotive OEMs.

1.1 Purpose and Objective

The purpose of this study is to investigate asymmetric machines as a technology for traction applications and compare to an existing machine in production to find benefits and drawbacks. The main goals is to find if asymmetric machines can reduce cost and magnet mass and at the same time deliver the same or better performance as the reference machine whilst being viable to produce for automotive applications. The performance, cost, and efficiency will be the main focus of the study. Different rotor topologies and asymmetries are to be designed and optimised together with the reference stator. The rotor topologies to be investigated are 1V, 2V and 3V as well as 1U, 2U and 3U, each with three different magnet strengths: N35, N42 and N52. The effects of the asymmetries in the different topologies with different magnets will be analysed to

determine where asymmetries are the most effective and why.

1.2 Limitations

The scope of the project is limited by a number of factors. To be able to directly compare asymmetric rotors topologies to symmetric rotor topologies only one stator design will be used, the same as in the already optimized symmetric reference machine. The results will also only be compared with the reference machine in the same vehicle at the same operating points. The outer diameter is the same as for the reference and the same axel diameter is used. The maximum length of the machine is also equal to the reference, but it is allowed to be shorter, so that it would fit into the same vehicle. There will not be any investigation into different core materials, no thermal considerations will be taken and no investigation into non rare earth metal magnets will be made.

1.3 Societal, Ethical and Ecological Aspects

The study aims to find ways to better utilise magnets since permanent magnets typically used for traction applications contain Rare Earth Element (REE)s such as neodymium, giving high remanence, and dysprosium added to increase the coercivity and temperature range. Mining and processing of REEs releases dust which contains other toxic metals and chemicals into the environment [11]–[13]. The released dust has an negative effect on humans, soil, vegetation and wildlife. Some REEs contain radioactive elements since they are often found in deposits which also contain radioactive materials such as uranium and thorium that contaminate the surrounding environment. This is a big problem since the majority of the worlds REEs are extracted and processed in China where there is poor working conditions and little to no information data available regarding the effects on the people working with REEs and how they affect the environment [11], [13].

Chapter 2

Theory

There are many different types of electric machines such as Direct Current (DC), Asynchronous Machine (ASM), EESM, Synchronous Reluctance Machines (SynRM) and Permanent Magnet Synchronous Machine (PMSM). The study only covers PMSMs and more specifically IPMs so the theory section is limited to the theory required to understand the Interior Permanent Magnet (IPM) although the underlying principles are the same for all types of electric machines.

2.1 Working Principles of PMSMs

The PMSMs operate on the principle of electromagnetic torque production through the interaction of a rotating magnetic field generated by current in the stator and the magnetic field from permanent magnets in the rotor. The magnetic field from the stator is rotating due to a most often three phase sinusoidal current being driven through the motor coil windings. The three phases are shifted, in the case of three phase by 120°, to be equally distributed so that the stator flux has a constant amplitude. The magnetic field rotor is attracted to and tries to align with the stator's magnetic field and therefore produces a torque. In steady state the rotor rotates at the same synchronous speed as the stator's rotating magnetic field and torque is produced by having the magnetic field in the stator lead the rotor so that the rotor constantly tries to catch up. In a Surface-Mounted Permanent Magnet (SPM) the optimal load angle is ideally 90° ahead of the rotor, but for IPMs the Maximum Torque per Ampere (MTPA) is further ahead due to the reluctance of the rotor also creating a torque that is shifted compared to the magnet torque.

To understand the inner workings of an electric machine it is important to understand the fundamental electromagnetic theory that covers how the coils in the stator and the magnets in the rotor of a PMSM create a magnetic field and how the torque is produced.

2.2 Fundamental Electromagnetic Equations

A current creates a magnetic field around it The magnetic field directly proportional to the enclosed current as per Ampère's law

$$\oint_{\partial l} H \cdot \mathrm{d}l = \iint_{S} J \cdot \mathrm{d}S = I_{\mathrm{encl}} \tag{2.1}$$

where H is the magnetic field, J is the current density and I_{encl} is the total current that is enclosed by the closed curve l and passing through the open surface surface S of which l is the perimeter [14]. Ampère's law show the relation between the magnetic field and the current creating said magnetic field. The curve l can be any arbitrary closed curve around a current

and the line integral of the magnetic field will always equal the enclosed current. This version of Ampère's law is only valid in static and quasi-static conditions, but since a electric machine is much smaller than the wavelength of the frequency's that they operate at, the simplified version holds.

If Ampère's law is considered in a magnetic circuit consisting of an iron core with an air gap and a coil wound around it with N turns as shown in Figure 2.1. Then the enclosed current is the current in the coil times the number of turns,

$$IN = \mathcal{F} \tag{2.2}$$

which equals the Magnetomotive Force (MMF) of the coil [14].

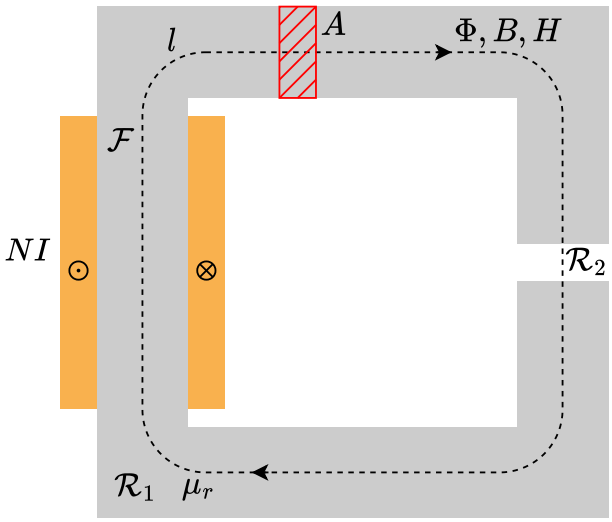

Figure 2.1: Magnetic circuit consisting of an iron core with an air gap and a coil.

The MMF is analogous to Electromotive Force (EMF) of a electric circuit, but instead of driving a current through a resistance according to Ohm's law. The MMF drives a magnetic flux, Φ, through a path with a reluctance, $\mathcal{R}$, according to Hopkinson's law,

$$\mathcal{F} = \Phi\mathcal{R} \tag{2.3}$$

The reluctance is dependent on the properties of the material and the total reluctance for the circuit is the sum of the reluctance of all paths. For simplicity the leakage flux is neglected, then the reluctance of the circuit in Figure 2.1 is the sum of the reluctance of the iron and the air gap, $\mathcal{R}_1 + \mathcal{R}_2$. The reluctance of each part is

$$\mathcal{R} = \frac{l}{\mu_0 \mu_r A} \tag{2.4}$$

where l is the equivalent length of the flux path, μ_0 is the permeability of vacuum, μ_r is the relative permeability and A is the mean area of the flux path. The magnetic flux, Φ, is only dependent on the total reluctance and will, similarly to the current in an electric circuit, be the same in the entire circuit. However, the air gap have a much greater reluctance since the permeability of iron is many magnitudes greater than that of air. Therefore, the magnetic field, H, will be much greater in the air gap than in the iron. Similar to how voltage division works in an electric circuit over resistance.

The magnetic field must always follow a closed path shown with Gauss's law for magnetism

$$\oiint_{\partial S} B \cdot \mathrm{d}S = 0 \tag{2.5}$$

meaning that the total magnetic flux through any given closed surface is zero [14]. That is, there are no monopoles in magnetism and magnetic flux cannot have a non zero divergence.

Faraday's law of induction show how a magnetic flux interacts with an electric circuit to produce an EMF,

$$\varepsilon = \oint_{\partial\Sigma} E \cdot \mathrm{d}l = -\iint_{\Sigma} \frac{\partial B}{\partial t} \cdot \mathrm{d}S = -\frac{\mathrm{d}\Phi_{\Sigma}}{\mathrm{d}t} \tag{2.6}$$

by the change of the magnetic flux within a closed loop $\partial\Sigma$ [14]. Where Σ is any surface with $\partial\Sigma$ is its perimeter, E is the electric field, B is the magnetic flux density and Φ_{Σ} is the magnetic flux through the surface Σ. The EMF is produced both by the magnetic flux density changing and by the loop $\partial\Sigma$ moving in space so the when the rotor rotates the magnetic flux in the coil changes and thereby induces a voltage in the coils in the stator.

Inductance is a measure of how much the rate of change of the current through a conductor is opposed [14]. As per Ampère's law in (2.1) the current through a conductor creates a magnetic field. That magnetic field in turn produces an EMF in the same conductor when the current is changing as per Faraday's law in (2.6) opposing the change of the current. Inductance is defined as the ratio between the induced voltage and the rate of change of the current.

$$\varepsilon = L\frac{\mathrm{d}I}{\mathrm{d}t} \tag{2.7}$$

In the case of the electric machine it is useful to consider the inductance of a multi turn coil where it is useful to define the flux linkage

$$\psi = N\Phi \tag{2.8}$$

as the magnetic flux times the number of turns of the coil. Assuming no leakage flux the inductance,

$$L = \frac{\psi}{I} = \frac{N\Phi}{I} = \frac{N\frac{\mathcal{F}}{\mathcal{R}}}{\frac{\mathcal{F}}{N}} = \frac{N^2}{\mathcal{R}} \tag{2.9}$$

is from Faraday's law the flux linkage, ψ, over the current [14], [15]. Since the flux linkage is proportional to the current the inductance can be written independent of the current by inserting (2.2), (2.3) and (2.8) resulting on the inductance only being dependent on the number of turns and the reluctance of the magnetic circuit around the coil.

2.3 Permanent Magnets

As per (2.1) a magnet field is created by a circulating current and current is the flow of electric charge [16]. There is therefore a magnetic moment created by the electrons circulating around an atom. Most often the orientation of the atomic magnetic moment is random is therefore cancelled out on a macroscopic level, but they can be aligned with an external magnetic field. Then the magnetic moment of each atom is in the same direction and all the small circulating currents cancel out in the middle but can be seen as an equivalent larger current on the surface of the material. Permanent magnets are then very good at retaining the magnetisation and have a high residual flux density, B_r, when the external magnetic field is removed.

The magnetisation of ferromagnetic materials is characterised by a hysteresis loop and permanent magnets has a very big hysteresis loop. Meaning they have a very high coercive force, H_c, which is the reverse magnetic field which is required to demagnetise the material. Both B_r and H_c are dependent on the temperature of the magnet and they will have a lower B_r at higher temperature and considerably lower H_c.

2.4 Alpha-Beta and *dq*-Transformation

Alpha-Beta Transformation, also known as Clarke Transform, transforms a balanced three phase system into an balanced orthogonal two phase system. Balanced meaning that the zero component is zero and no information is lost [17]. The *dq*-transformation then transforms the stationary two phase system into a rotating two phase system that rotates together with the rotor. Where the direct axis, the *d*-axis, is aligned with the permanent magnet flux linkage of the rotor and the quadrature axis, the *q*-axis, is orthogonal to the *d*-axis in electrical degrees as seen in Figure 2.2.

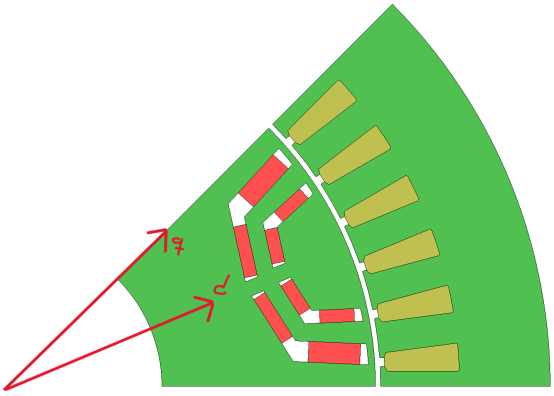

Figure 2.2: One pole of an eight pole 2U machine with *d*- and *q*-axis illustrated.

Since the machine has eight poles and therefore four pole pairs, the electrical frequency is four times the mechanical frequency. That is, the voltage, current, etc. has four periods in one full turn of the rotor.

The simplified amplitude invariant Clarke Transform expressed in matrix form is

$$\begin{bmatrix} x_\alpha \\ x_\beta \end{bmatrix} = \begin{bmatrix} \frac{2}{3} & -\frac{1}{3} & -\frac{1}{3} \\ 0 & \frac{1}{\sqrt{3}} & -\frac{1}{\sqrt{3}} \end{bmatrix} \begin{bmatrix} x_u \\ x_v \\ x_w \end{bmatrix} \tag{2.10}$$

where x is any balanced three phase quantity with phases u, v and w in that order phase shifted by 120°. Together with the simplified *dq*-transform on matrix form

$$\begin{bmatrix} x_d \\ x_q \end{bmatrix} = \begin{bmatrix} \cos\theta & \sin\theta \\ -\sin\theta & \cos\theta \end{bmatrix} \begin{bmatrix} x_\alpha \\ x_\beta \end{bmatrix} \tag{2.11}$$

where θ is the displacement angle in electrical degrees. An example of a balanced three phase signal with the first, fifth and seventh harmonic transformed with first Alpha-Beta- and then *dq*-transform described in (2.10) and (2.11) is shown in Figure (2.3).

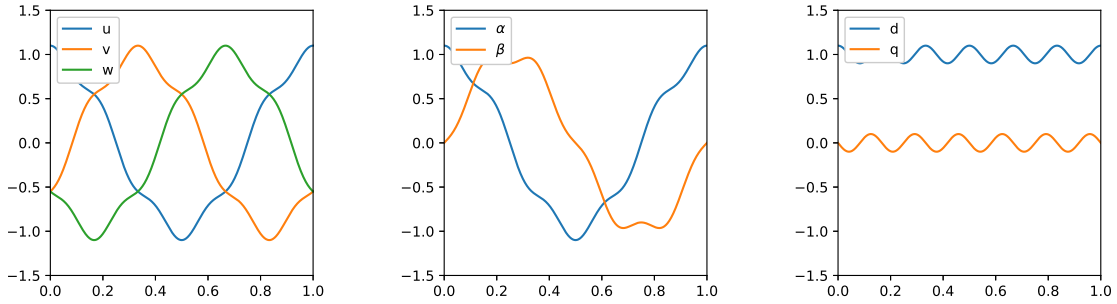

Figure 2.3: Balanced three phase signal with first, fifth and seventh harmonic transformed with Alpha-Beta- and dq-transform.

The first harmonic is transformed into a constant value with the same amplitude and the fifth and seventh harmonic appear as a sixth harmonic in the dq-frame [17].

2.5 Reluctance Torque and Magnet Torque

To calculate the torque of an electric machine the energy balance can be studied [18]. To simplify the calculations the quantities are shown in terms of space vectors in the rotating reference frame of the rotor. Any given quantity in space vector form is

$$\underline{x}_s = x_d + jx_q \tag{2.12}$$

where x_d and x_q is the quantity in the rotating dq-form described in the previous section.

The energy entering the machine at any given moment must equal the energy that exits giving in differential form

$$\mathrm{d}W_{\text{elec}} = \mathrm{d}W_{\text{loss}} + \mathrm{d}W_{\text{field}} + \mathrm{d}W_{\text{mech}} \tag{2.13}$$

where W_{elec} is the electrical energy put into the system, W_{loss} is the losses in form of heat in the windings, iron losses are neglected, W_{field} is the energy stored in the magnetic field and W_{mech} is the mechanical energy taken out from the system. The differential of the electrical energy is the power

$$\mathrm{d}W_{\text{elec}} = P\mathrm{d}t = \frac{3}{2}\Re\left\{\underline{u}_s^* \underline{i}_s\right\}\mathrm{d}t \tag{2.14}$$

where the factor 3/2 comes from the transformation from three-phase to two-phase when using amplitude invariant dq-transformation, $\underline{u}_s*$ is the complex conjugate of the stator voltage and $\underline{i}_s$ is the stator current. The stator voltage in an electric machine can be expressed as

$$\underline{u}_s = R_s\underline{i}_s + \frac{\mathrm{d}\underline{\psi}_s}{\mathrm{d}t} + j\omega\underline{\psi}_s \tag{2.15}$$

where R_s is the stator resistance, $\underline{\psi}_s$ is the stator flux linkage and ω is the electrical frequency. The voltage can be described as the sum of three parts, the voltage drop of the resistance in the stator, the voltage induced by the change of flux in time and the induced voltage from rotation. With the expression for voltage in (2.15) put in (2.14) gives

$$\mathrm{d}W_{\text{elec}} = \frac{3}{2}\Re\left\{\left(R_s\underline{i}_s + \frac{\mathrm{d}\underline{\psi}_s}{\mathrm{d}t} - j\omega\underline{\psi}_s\right)\underline{i}_s\right\}\mathrm{d}t = \frac{3}{2}R_s i_s^2\mathrm{d}t + \frac{3}{2}\Re\left\{\left(\frac{\mathrm{d}\underline{\psi}_s}{\mathrm{d}t} - j\omega\underline{\psi}_s\right)\underline{i}_s\right\}\mathrm{d}t \tag{2.16}$$

and the different parts in (2.13) can then be identified in (2.16). The losses

$$\mathrm{d}W_{\text{loss}} = \frac{3}{2}R_s i_s^2\mathrm{d}t \tag{2.17}$$

and the energy in the magnetic field is can be found when machine is at stand still. That is $\omega = 0$, since then then the mechanical energy output is zero and all the electrical energy besides the losses goes into the magnetic field giving

$$\mathrm{d}W_{\text{field}} = \frac{3}{2}\Re\left\{\frac{\mathrm{d}\underline{\psi}_s}{\mathrm{d}t}\underline{i}_s\right\} \tag{2.18}$$

leaving only one part of (2.16) left for the mechanical energy

$$\mathrm{d}W_{\text{mech}} = \frac{3}{2}\Re\left\{-j\omega\underline{\psi}_s\underline{i}_s\right\} \tag{2.19}$$

The torque can be expressed with the mechanical energy on differential from as

$$\mathrm{d}W_{\text{mech}} = T_e\frac{\omega}{p}\mathrm{d}t \tag{2.20}$$

where T_e is the electromagnetic torque and p is the number of pole pairs. Combining (2.19) and (2.20) gives an expression for the torque,

$$T_e = \frac{3p}{2}\Im\left\{\underline{\psi}_s^*\underline{i}_s\right\} = \frac{3p}{2}\left(\underline{\psi}_s \times \underline{i}_s\right) \tag{2.21}$$

as the cross product of the space vectors of the flux linkage and the current in the stator. This can be written in dq-form as

$$T_e = \frac{3p}{2}\left(\psi_d i_q - \psi_q i_d\right) \tag{2.22}$$

which can be used for motor control. For an IPM the flux linkage can be divided into the flux linkage from the permanent magnets and the flux linkage form the coils giving

$$T_e = \frac{3p}{2}\left(\left(\psi_{d,m} + \psi_{d,\text{coil}}\right) i_q - \left(\psi_{q,m} + \psi_{q,\text{coil}}\right) i_d\right) \tag{2.23}$$

where $\psi_{d,m}$ and $\psi_{q,m}$ is the permanent magnet flux linkage in the d- and q-axis respectively as well as $\psi_{d,\text{coil}}$ and $\psi_{q,\text{coil}}$ is the flux linkage from the coils in the d- and q-axis respectively. From (2.9) it is know that $\psi = LI$ so (2.23) can be written as

$$T_e = \frac{3p}{2}\left(\psi_{d,m} i_q - \psi_{q,m} i_d + L_d i_d i_q - L_q i_d i_q\right) \tag{2.24}$$

where L_d and L_q are the respective inductances of the d- and q-axis. The d-axis is per definition aligned with the permanent magnet flux in a symmetric PMSM so the permanent magnet flux linkage in the q-axis is therefore zero and the torque equation can be further simplified and be written in it's most common form

$$T_e = \frac{3p}{2}\left(\psi_m i_q + \left(L_d - L_q\right) i_d i_q\right) \tag{2.25}$$

with torque contributions from two phenomena: magnet torque, $\psi_m i_q$, from the permanent magnets and reluctance torque, $\left(L_d - L_q\right) i_d i_q$, from the saliency.

2.6 Losses

There are many different types of losses in an electrical machine. The major ones for an IPM is covered briefly in the following section.

2.6.1 Iron

Iron losses, also referred to as core losses, are a major component of power dissipation in electrical machines and consists of two parts: hysteresis and eddy current losses [19]. A widely adopted empirical approach for estimating these losses is the Steinmetz equation

$$P_{\text{Fe}} = c_{\text{se}} f^{\alpha} \hat{B}^{\beta} \tag{2.26}$$

where P_{Fe} is the iron loss per unit mass, c_{se}, α and β are material dependent coefficients, f is the frequency of the magnetic flux and $\hat{B}$ is the peak magnetic flux density [19]. This formulation assumes a perfectly sinusoidal flux and combines both hysteresis and eddy current effects into one empirical relationship. However, in practical applications, the flux density is often non-sinusoidal, especially in systems with power electronics. As a result, several extensions to the classical Steinmetz equation have been proposed.

One of the earliest improvements is the Jordan model, which separates the total core loss into hysteresis and eddy current

$$P_{\text{Fe}} = c_{\text{hy}} f \hat{B}^2 + c_{\text{ec}} f^2 \hat{B}^2 \tag{2.27}$$

with the respective coefficients for the two loss phenomenon. A more comprehensive approach is Bertotti's model

$$P_{\text{Fe}} = c_{\text{hy}} f \hat{B}^2 + c_{\text{ec}} f^2 \hat{B}^2 + c_{\text{ex}} f^{1.5} \hat{B}^{1.5} \tag{2.28}$$

which adds the excess losses as a function of the flux density and frequency.

2.6.2 Copper

The resistive losses in the windings are often called the copper losses is for a three phase electric machine

$$P_{\text{Cu}} = 3 R_s I_{\text{RMS}}^2 \tag{2.29}$$

where R_s is the phase resistance of one phase and I_{RMS} is the Root Mean Square (RMS) value of the phase current [15].

2.6.3 Magnet

Permanent magnets are typically electrically conductive, meaning they will have eddy current losses in the same way as the iron core.

2.6.4 Other

There are other losses in an electric machine such as windage, frictional, Pulse Width Modulation (PWM), skin effect etc. which is not considered in this study and will not be covered.

2.7 Optimisation Methods and Algorithms

Optimisation is the process of finding the most effective solution to a problem from a set of feasible alternatives, based on one or more criteria [20]. An optimisation problem involves determining the values of variables that minimise or maximise an objective function with a set of constraints. Optimisation plays a central role in engineering design, where the goal is to create systems that meet performance and cost requirements. Traditional gradient-based methods work well for problems where derivatives of the objective and constraint functions are available and the problem as one maximum. However, these methods may struggle with discontinuous, noisy, or multi-modal functions.

In many practical scenarios, optimisation involves more than one objective that often conflict with each other. Multi-objective optimisation problems seek to simultaneously optimise two or more conflicting objectives [20]. These problems do not yield a single optimal solution but a set of trade-off solutions known as Pareto front which represents the trade-off surface among the objectives. A solution is Pareto-optimal if no other solution exists that improves at least one objective without worsening another.

Genetic algorithms are a class of random search methods inspired by natural selection and genetics. Over multiple generations, the population evolves towards better solutions that outline the best solutions given the constrains, the Pareto front [20]. They are particularly effective for solving complex optimisation problems with non-differentiable, non-linear, or discontinuous functions such as optimising the design of an electric machine whose variables impact many different aspects of the machine at the same time.

2.8 WLTP

Worldwide Harmonised Light Vehicles Test Procedure (WLTP) is a standard test procedure set by the United Nations Economic Commission for Europe (UNECE) to create a uniform way of testing the emissions and electric range of light-duty vehicles [21]. The class of a vehicle and thereby the Worldwide Harmonized Light Vehicles Test Cycle (WLTC) used during WLTP is determined by the power to weight ratio of the vehicle. The weight in question is the kerb weight minus 75 kg, that is the weight that the vehicle has in a ready to drive condition without the driver. The three different classes and their respective power to weight ratios are shown in table 2.1.

Table 2.1: Vehicle classification for WLTC

Class	Power to weight ratio
1	$\leq$22 W/kg
2	>22 W/kg - $\leq$34 W/kg
3	>34 W/kg

There are also two sub classes for class 3. Class 3a and class 3b which is set depending on if the vehicle has a top speed below or above 120 km/h respectively. The most common vehicle class 3b with the WLTC is shown in Figure 2.4.

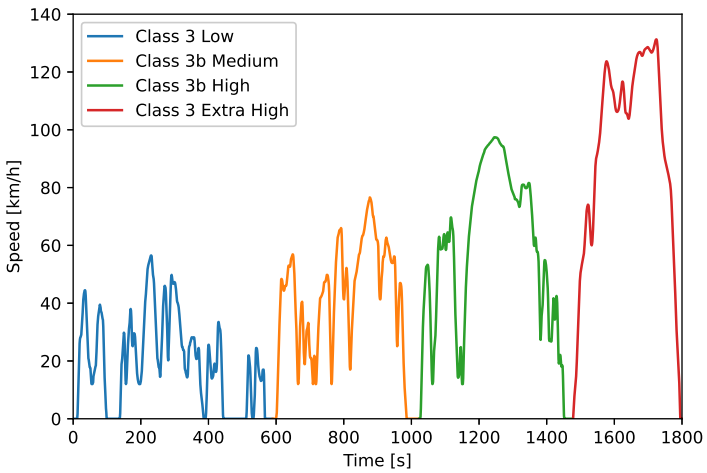

Figure 2.4: WLTC Class 3b divided into the four phases Low, Medium, High and Extra High.

The WLTC phases simulate urban, suburban, rural and highway scenarios respectively and is meant to represent a typical driving cycle. The speed over time cycle can then be simulated with a vehicle model to determine the torque to follow the speed profile.

Chapter 3

Method

The study has been conducted in the CAE software JMAG Designer to simulate the machines and run multi-objective optimisation to find the optimal solution for the respective rotor topologies.

3.1 Model Simplifications

To speed up the optimisations the motor model is simplified in a number of ways. The number of steps is reduced and the mesh element size is increased. To find the optimal simulation setup where the time is minimised without sacrificing too much precision a simple study was conducted prior to the optimisations started. The number of time steps, rotor skewing and mesh size was investigated and compared with a base line model which was used during the post processing. The settings for the optimisation and post process models are shown in table 3.1.

Table 3.1: Comparison of simplifications made in simulation model for optimisation.

	Post Process Model	Optimisation Model
Time steps	91	61
Rotor skew	6 segment step-skew	3 segment linear skew
Stator mesh size	1.2 mm	2 mm
Rotor mesh size	1.2 mm	2 mm
Magnets mesh size	1 mm	1.5 mm
Air gap mesh	90 circumferential divisions	60 circumferential divisions
	5 radial divisions	3 radial divisions

The optimisation model simplifications reduced the total solve time to 16 % of the post process model solve time. At the same time the torque, voltage, copper and iron losses all has less than 1.5 % mean deviation of the post processed model with a so small standard deviation for the relative results to be considered valid. The final cases are however run with the post processes model due the better accuracy. The optimised model is necessary since the study would be impossible to complete within the time frame since the total saved time is 65 days of simulation.

The mesh for the different models is shown in Figure 3.1a and 3.1b.

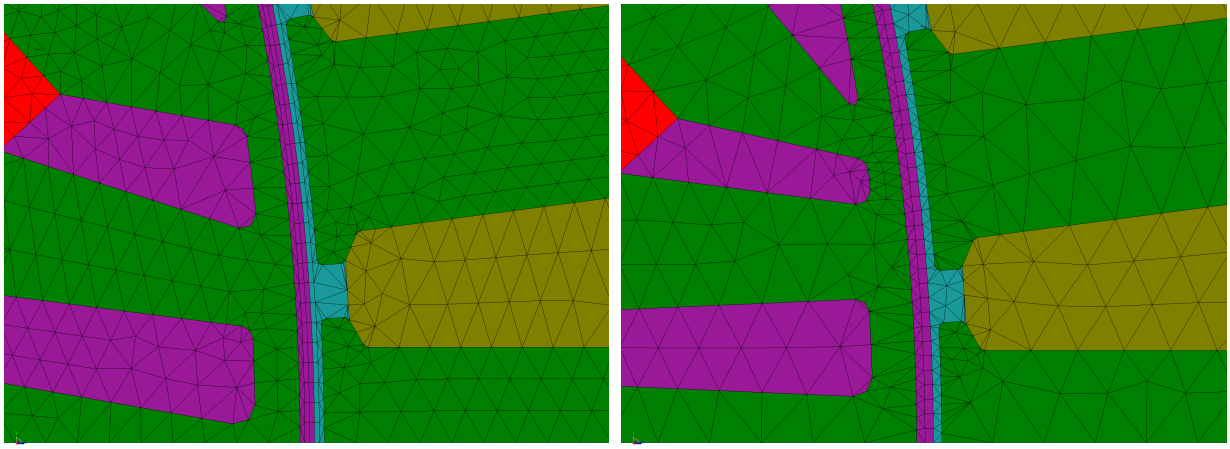

(a) Post-process model. (b) Optimisation model.

Figure 3.1: Mesh of the post-process and optimisation models.

3.2 Concept Design

The first part of the study focuses on comparing the rotor topologies and magnet grades and finding the combination with the most performance potential to be investigated further in the efficiency optimisation and detailed design.

3.2.1 Operating Points, Optimisation Limits and Targets

Each case is simulated at three operating points: low speed acceleration (OP1), high speed steady state (OP2) and peak torque at the knee point speed. OP1 characterises as typical city driving with an acceleration from a stop sign and OP2 represents highway cruising. These two operating points are selected due to being typical operating points of a machine in a traction application and high efficiency at these points is important for the drive cycle efficiency of the machine. They are not very relevant for the first part of the study where the peak torque and power is of interest. However, the losses are still considered in the optimisation so that the solutions are reasonable from a loss perspective and there is a maximum limit set for the total losses at the respective operating points. For the first two operating points there is a target torque and speed and the current is adjusted to reach the set operating point. For peak power the current is instead set to the maximum available phase current and the optimisation objective functions are set to maximise the torque and the power. The introduced asymmetries in the rotor will have an effect on the optimal current angle, so the current angle for each operating point is an optimisation variable to ensure that the optimised motor is evaluated at MTPA. The optimisation is limited by the available voltage and a set maximum magnet volume which is the same for all topologies. The maximum volume is however scaled with the remanence of each magnet grade so that the sum of all magnets in each rotor topology have a comparable magnet moment for all magnet grades. The maximum allowed magnet volume for the respective magnet grades are presented in table 3.2.

Table 3.2: Scaling of maximum allowed magnet volume for each magnet grade for the performance optimisation.

Magnet Grade	Remanence at 20 °C	Maximum Magnet Volume
N35	1.21 T	1.083 pu
N42	1.32 T	1 pu
N52	1.45 T	0.92 pu

Each optimisation is run for 450 generations with a population size of either 40, 60 or 80 depending on the number of parameters in the optimisation. The objective functions are presented in table 3.3.

Table 3.3: Objective functions for the efficiency optimisation.

Parameter	Objective	Weight
OP1 Torque	$\geq$0.18 pu	2
OP2 Torque	$\geq$0.05 pu	2
Peak Torque	Maximise	10
Peak Power	Maximise	6
Magnet Volume	According to Table 3.2	10
OP1 Total Loss	$\leq$5 %	6
OP2 Total Loss	$\leq$5 %	4

3.2.2 Rotor Model Parametrisation

Each rotor topology is drawn and fully constrained in JMAG Designer Geometry Editor using variables for the constrains that the optimisation will use.

As the initial case for the U-Rotor optimisation simple U-shaped rotors are drawn with one, two and three layers go give a starting point for the optimisation algorithm to proceed from. Figure 3.2 shows the initial case 1U rotor and the magnet size and position constrains.

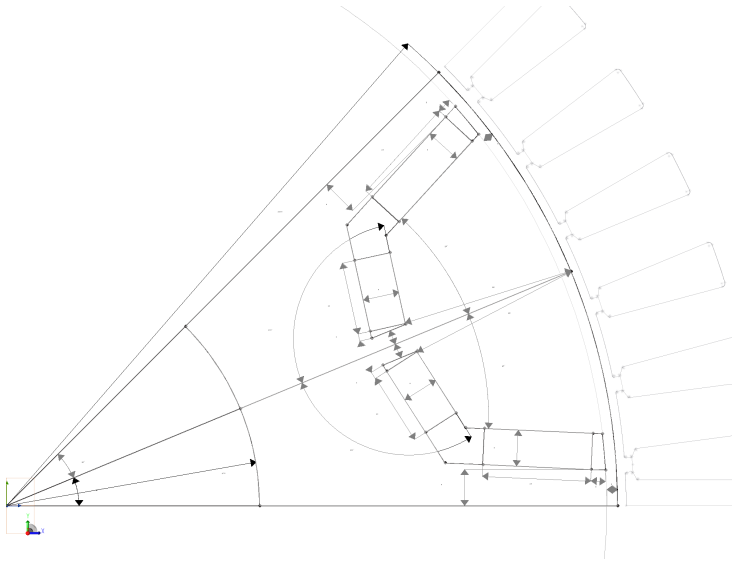

Figure 3.2: One pole of the initial 1U rotor model in JMAG Designer Geometry Editor.

The initial case is constrained symmetrically around the center line of the pole. However, each side is completely independent to enable the optimisation to find an asymmetric solution. Each magnet is rectangular and have a width and thickness as well as an angle relative to the pole center line. The position of the magnets are defined by the distance from the center line for the inner magnets or the outer rotor diameter for the outer magnets to the gap plus the gap width. All magnet positions are independent from each outer and are swept continuously in the optimisation. In table 3.4 a full list of constrains are shown for the 1U rotor.

Table 3.4: Rotor constrain variables used for optimisation of 1U rotor.

Constrain variable	Description
Bridge_li_w	Bridge lower inner width
Bridge_lo_w	Bridge lower outer width
Bridge_ui_w	Bridge upper inner width
Bridge_uo_w	Bridge upper outer width
FP_l_w	Flux path lower width
FP_u_w	Flux path upper width
Gap_li_w	Gap lower inner width
Gap_lo_w	Gap lower outer width
Gap_ui_w	Gap upper inner width
Gap_uo_w	Gap upper outer width
M_li_ang	Magnet lower inner angle
M_li_d	Magnet lower inner distance from outer diameter
M_li_t	Magnet lower inner thickness
M_li_w	Magnet lower inner width
M_lo_ang	Magnet lower outer angle
M_lo_t	Magnet lower outer thickness
M_lo_w	Magnet lower outer width
M_ui_ang	Magnet upper inner angle
M_ui_d	Magnet upper inner distance from outer diameter
M_ui_t	Magnet upper inner thickness
M_ui_w	Magnet upper inner width
M_uo_ang	Magnet upper outer angle
M_uo_t	Magnet upper outer thickness
M_uo_w	Magnet upper outer width
Rotor_o_d	Rotor outer diameter

For the 1U rotor there are 25 constrains for the magnets as well as the outer rotor diameter and together with the current amplitude and current angle for each of the three operating points, as well as the speed and active length of the machine the total number of variables for the 1U optimisation is 33. For the 2U and 3U, each layer is independent from the others and they are constrained in the same way as the first layer giving a total of 57 and 81 variables for 2U and 3U respectively.

The V-rotor topologies are parametrised a similar way to the U-rotors. The one layer V-rotor is shown in Figure 3.3.

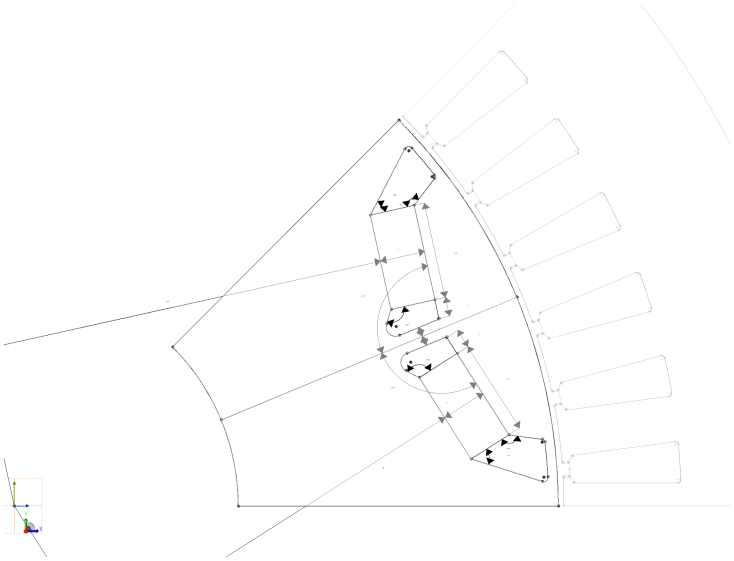

Figure 3.3: One pole of the initial 1V rotor model in JMAG Designer Geometry Editor.

The V-rotors are simpler than the U-rotors since they have half the number of magnets, but instead the angles of the flux blocking gaps are optimised. The initial case is once again symmetric around the center of the pole, but the independent constrains will allow the optimisation to converge to an asymmetric solution. All constrains for the 1V rotor is shown in table 3.5 and they follow the same naming convention as the 1U.

Table 3.5: Rotor constrain variables used for optimisation of 1V rotor.

Constrain variable	Description
Bridge_lo_w	Bridge lower outer width
Bridge_li_w	Bridge lower inner width
Bridge_uo_w	Bridge upper outer width
Bridge_ui_w	Bridge upper inner width
Gap_li_w	Gap lower inner width
Gap_li_ang	Gap lower inner angle
Gap_loo_ang	Gap lower outer outer angle
Gap_loi_ang	Gap lower outer inner angle
Gap_ui_w	Gap upper inner width
Gap_ui_ang	Gap upper inner angle
Gap_uoo_ang	Gap upper outer outer angle
Gap_uoi_ang	Gap upper outer inner angle
M_l_ang	Magnet lower angle
M_u_d	Magnet lower distance from origin
M_l_t	Magnet lower thickness
M_l_w	Magnet lower width
M_u_ang	Magnet upper angle
M_u_d	Magnet upper distance from origin
M_u_t	Magnet upper thickness
M_u_w	Magnet upper width
Rotor_o_d	Rotor outer diameter

There are in total a few less parameters for the V-rotors with a total of 29, 49 and 69 for the 1V, 2V and 3V respectively.

3.2.3 Optimisation Result Extraction and Post Processing

When each optimisation is complete a number of cases from the peak power versus peak torque Pareto front are selected. An example from the 3V N52 simulation results is shown in Figure 3.4.

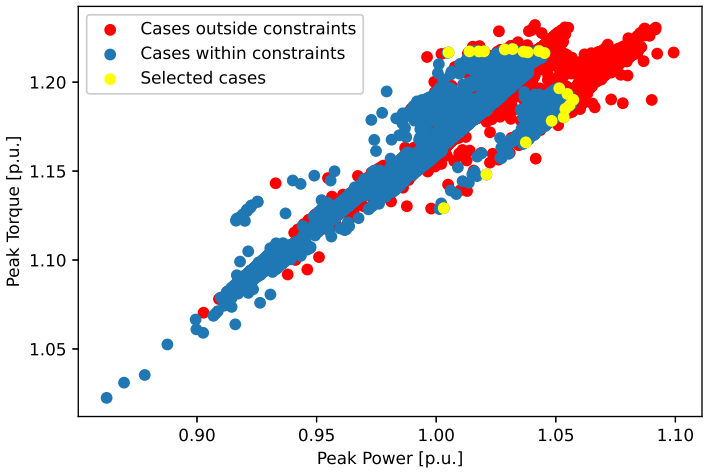

Figure 3.4: Peak torque versus peak power for all 3V N52 cases with selected cases from the Pareto front highlighted in yellow.

The 20 selected cases represents the Pareto front of the respective rotor topology with the respective magnet grade and are post processed in a more accurate post processing model described in section 3.1.

3.2.4 Motor Mapping

The best performing machine from the pareto front is mapped using the internal motor mapping function in JMAG Designer. The phase current is stepped from zero to the maximum phase current and the load angle is stepped from 0°, in reference to the q-axis, to 180°. It is necessary to map current angles up to 180° since the rotor is asymmetric it is not possible to mirror the second quadrant over the d-axis to get the third quadrant for braking operation which is possible with a symmetric machine. The speed-torque map is created using MTPA+FW which maximises the torque for a given current when the voltage is lower than the allowed voltage [22]. When the voltage is higher than the allowed voltage the flux is weakened by increasing the load angle until the voltage is low enough.

3.2.5 Reluctance Versus Magnet Torque

To find the reluctance and magnet parts of the total torque the best performing machines for the respective rotor topologies and magnets grades are simulated a in two different cases. The first being a normal case where everything is kept constant and the load angle is swept from 0° to 180°. The resulting torque is the total machine torque over load angle. Then the magnet material is replaced by air to simulate only the reluctance torque of the machine. The magnet torque is then calculated by subtracting the reluctance torque from the total.

3.3 Efficiency and Cost Optimisation

For the second part of the study the focus is shifted from performance to efficiency. Rotor topologies from the previous stage are selected and used as initial cases for the new optimisation.

3.3.1 Operating Points, Optimisation Limits and Targets

The efficiency optimisation is simulated on the same three cases as the peak performance optimisation in section 3.2.1, but now with more focus on the two low power operating points. The goal of the optimisation is to minimise the cost of the machine and the losses at Operation Point One, Low Speed Acceleration (OP1) and Operation Point Two, High Speed Steady State (OP2) while remaining a certain peak power and torque. The cost of the machine is estimated by calculating the volume of rotor, stator, magnets and windings and multiplying by their respective price per volume. The optimisation will therefore premiere a shorter, since the diameter is fixed, machine with less magnet volume since the magnets has the highest price per volume. The losses in OP1 and OP2 also consider the inverter losses which are estimated by a current dependent quadratic equation curve fitted on data provided by the inverter team.

Table 3.6: Objective functions for the efficiency optimisation.

Parameter	Objective	Weight
OP1 Torque	$\geq$0.18 pu	2
OP2 Torque	$\geq$0.05 pu	2
Peak Torque	$\geq$1 pu	5
Peak Power	$\geq$1 pu	5
Cost	Minimise	10
OP1 Torque Ripple	$\leq$10 %	1
OP2 Torque Ripple	$\leq$10 %	1
Peak Torque Ripple	$\leq$15 %	1
OP1 Total Losses	Minimise	6
OP2 Total Losses	Minimise	8

3.3.2 Optimisation Result Extraction and Post Processing

Since the optimisations minimises for three objectives the Pareto front of interest is now three dimensional. As an example for how the selected cases are extracted is the results from the 2U N35 optimisation is shown in Figure 3.5.

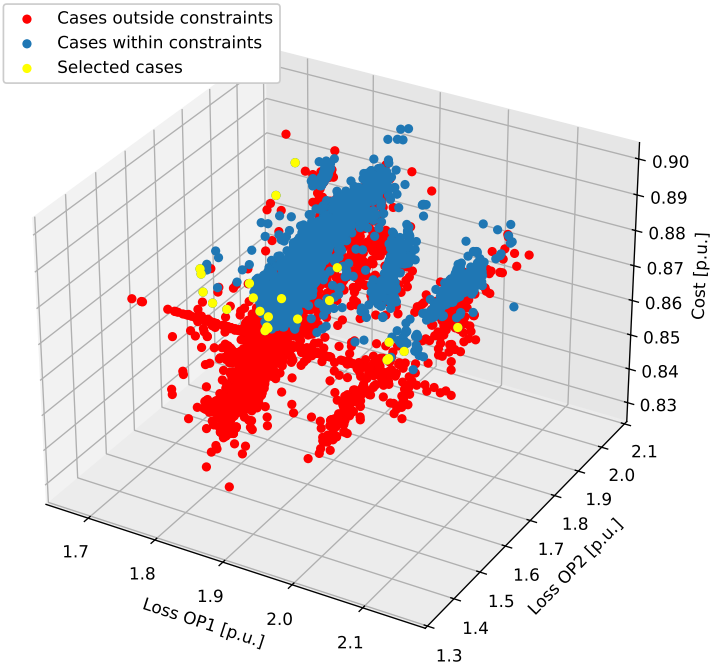

Figure 3.5: Electric Machine (EM) material cost versus total EM losses in OP2 versus total EM losses in OP1 for all cases in 2U N35 the optimisation. With cases within optimisations contains described in section 3.3.1 highlighted in blue and selected cases highlighted in yellow.

It is quite hard to find where the Pareto front is in three dimensions so the plot is projected into multiple two dimensional plots in Figure 3.6, 3.7 and 3.8.

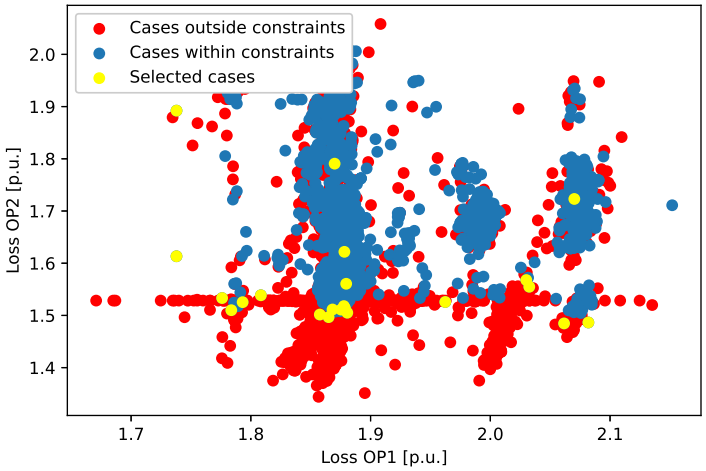

Figure 3.6: Total EM losses in OP2 versus total EM losses in OP1 for all cases in 2U N35 the optimisation. With cases within optimisations contains described in section 3.3.1 highlighted in blue and selected cases highlighted in yellow.

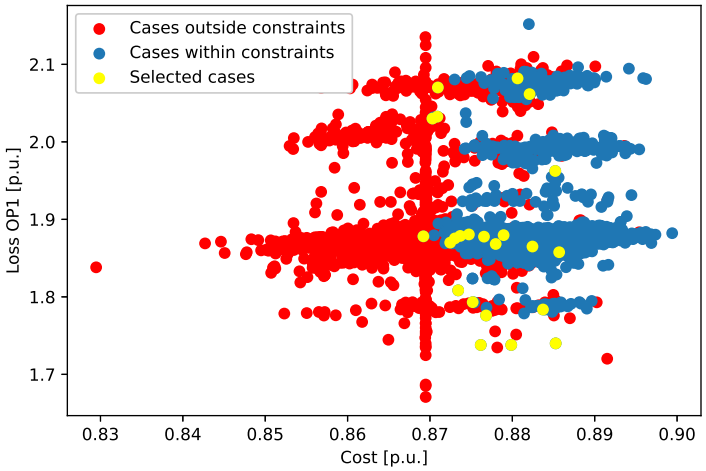

Figure 3.7: Total EM losses in OP1 versus EM material cost for all cases in 2U N35 the optimisation. With cases within optimisations contains described in section 3.3.1 highlighted in blue and selected cases highlighted in yellow.

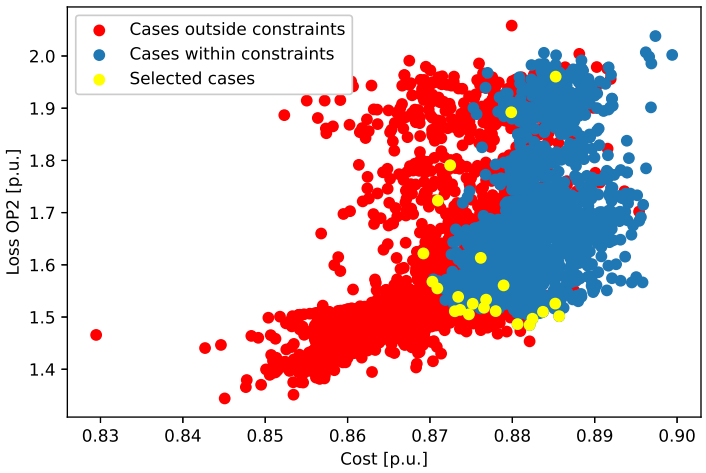

Figure 3.8: Total EM losses in OP2 versus EM material cost for all cases in 2U N35 the optimisation. With cases within optimisations contains described in section 3.3.1 highlighted in blue and selected cases highlighted in yellow.

There are in total 20 cases selected for each optimised rotor topology and magnet grade on the Pareto front. That are post processed in a more accurate post processing model described in section 3.1.

3.3.3 WLTP Efficiency

To calculate the efficiency of the machine for a WLTP drive cycle the cycle is simulated for a rear wheel drive car model were speed and torque is extracted. The drive cycle simulation is not part of this study and will not be described. The drive cycle simulation was not simulated with the actual machines, only a similar one so that the speed and needed torque to reach said speed could be extracted. With the speed and torque profile the losses for each operating point could be extracted form the loss map created according to section 3.2.4 giving the total WLTP efficiency

$$\eta_{\text{WLTP}} = \frac{E_M + E_G - E_{M,\text{Loss}}}{E_M + E_G + E_{G,\text{Loss}}} \tag{3.1}$$

where E_M is the total energy consumed by the machine in motor mode over the cycle, E_G is the total energy produced by the machine in generator mode over the cycle, $E_{M,\text{Loss}}$ and $E_{G,\text{Loss}}$ is the total energy losses for the respective modes over the cycle.

3.4 Demagnetisation Investigation

With the final design of the optimised machine the risk of demagnetisation is investigated during normal operation and Active Short Circuit (ASC).

3.4.1 Normal Operation

To determine coercivity needed for the magnets to not become demagnetised during normal operation the current and load angle is swept from zero to maximum phase current in 11 steps for all angles 0° to 180° with a step of 10°. The maximum magnetic field strength in all the six magnets of every skew segment in the 3V N35 machine is evaluated. Also the area of which the magnetic field strength in any given magnet surpasses the coercivity of the used magnets is extracted to evaluate how much, if any part, of the magnet has the risk of becoming demagnetised. The map is simulated at the maximum rated temperature of the magnets to ensure that the worst case is tested. A 3V machine with explanation of the magnet naming convention is seen in Figure 3.9.

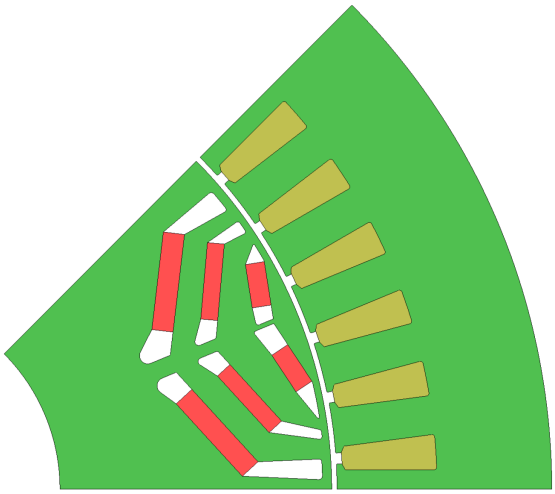

Figure 3.9: A 3V machine with magnets referred to as an upper and a lower magnet for the inner, middle and outer magnet layers. The upper magnets are leading as the machine is spinning counter clockwise and the outer magnet layer is the one closest to the stator.

3.4.2 ASC

In the case of a failure the electric machine can be put into ASC to bring the machine to a safe state. ASC can harm the machine with both high currents and high magnetic fields risking to demagnetise the permanent magnets. To simulate ASC a short circuit is created during normal operation by using switches in the JMAG-Designer Circuit editor. The setup can be seen in Figure 3.10a and3.10b.

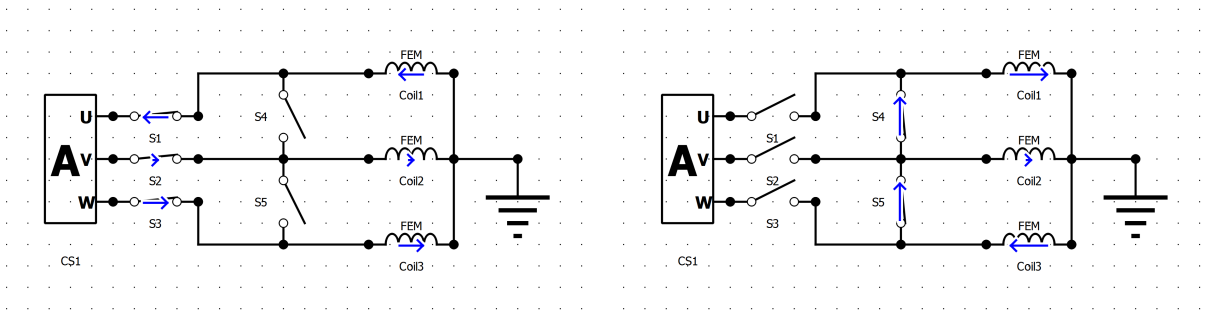

(a) JMAG-Designer circuit configuration during normal operation.

(b) JMAG-Designer circuit configuration during ASC.

Figure 3.10: JMAG-Designer circuit configuration for simulating ASC.

Switch one, two and three are closed during operation and switch four and five are open. After one electrical period switch one, two and three open and four and five closes short circuiting the machine and disconnecting the current source. The short circuit is kept for eight electrical periods before the switches are switched back to normal operation. This simulation is performed with irreversible magnets to simulate demagnetisation.

Chapter 4

Analysis

The analysis chapter presents and analyses the results of the study.

4.1 Peak Performance Concept

The following section presents and analyses the results of the first part of the study where the peak torque and power for the different rotor topologies where investigated.

4.1.1 Peak Power and Torque

The maximum torque and power lines for the asymmetric 2V N42 is shown in Figure 4.1a as well as the symmetric 2V N42 used as a reference is shown in Figure 4.1b.

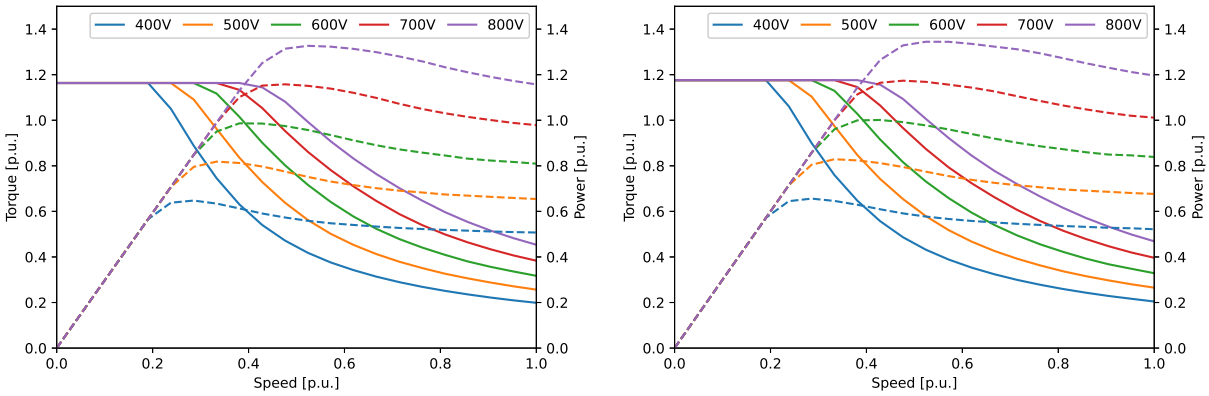

(a) Asymmetric 2V N42 machine torque and power max lines at different DC-link voltages.

(b) Symmetric 2V N42 machine torque and power max lines at different DC-link voltages.

Figure 4.1: Asymmetric 2V N42 and symmetric reference machine peak torque and peak power.

The peak power and torque of the two machines is similar, but the symmetric machine just outperforms the asymmetric one despite having 5.9 % magnets than the asymmetric machine. The symmetric reference machine is the result of an optimisation run with the same prerequisites as the asymmetric optimisations described in section 3.2 with the only difference that the rotor is constrained to be symmetric.

In Figure 4.2 the peak torque for each rotor topology is shown. The torque and power over speed plots can be found for every rotor topology in Appendix A.

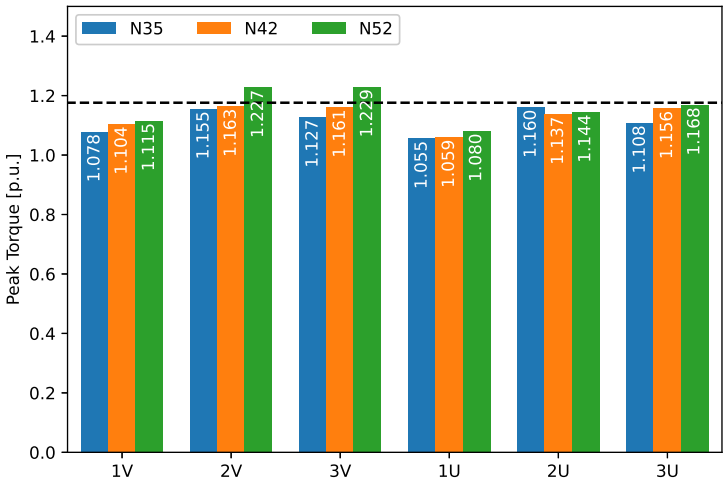

Figure 4.2: Peak torque for the asymmetric machines compared with the symmetric 2V N42 machines shown with the black dashed line.

The only machines that outperform the symmetric reference machine is the 2V and 3V N52 machines. In general the machines with higher grade magnets produces a higher torque with the exception of 2U. There is a significant performance increase from the one layer machines to the two layer machines while the three layer machines have similar performance as the two layer machine. This can be due to the size of the rotor and there not being enough space for the three layers. For example both 3V and 3U N35 perform worse than the 2V and 2U N35 machines. This can be caused by the fact that there is not enough space so the q-axis flux gets choked by the extra layer of magnets and the thicker magnets are needed to get the same magnet torque, hence the reluctance torque is lower. 2U is also an outlier when it comes to V- versus U-topology since the V outperforms the U in all other instances. This can because the U-topology likely would premiere a smaller rotor diameter and will be discussed further later.

The peak power of each machine is shown in Table 4.3.

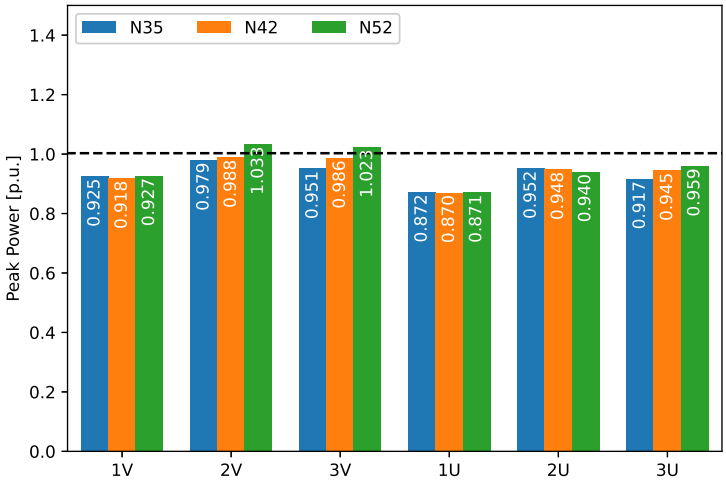

Figure 4.3: Peak power for the asymmetric machines compared with the symmetric 2V N42 machines shown with the black dashed line.

The peak power tells a similar story as the peak torque although with some differences. N52 magnets superiority has been reduced and the N35 seems to perform better relative to N52 in power compared to torque.

4.1.2 Magnet Mass Versus Peak Torque

Since all the machines have a different magnet mass due to the optimisations finding different optimal solutions for the different machines and the interest of the study is to investigate if the asymmetric machines can reduce the needed magnets. Figure 4.4 shows the magnet mass used versus the achieved peak torque for the different rotor topologies.

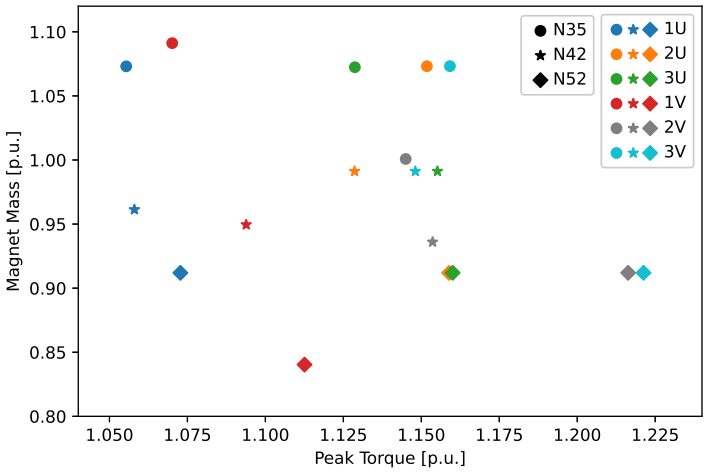

Figure 4.4: Magnet mass versus peak torque for asymmetric machines.

It is interesting to study the performance in reference to the magnet mass. In Figure 4.5 the torque in Figure 4.2 is scaled with the mass of the magnets in the respective machines compared to the symmetric 2V N42 reference machine.

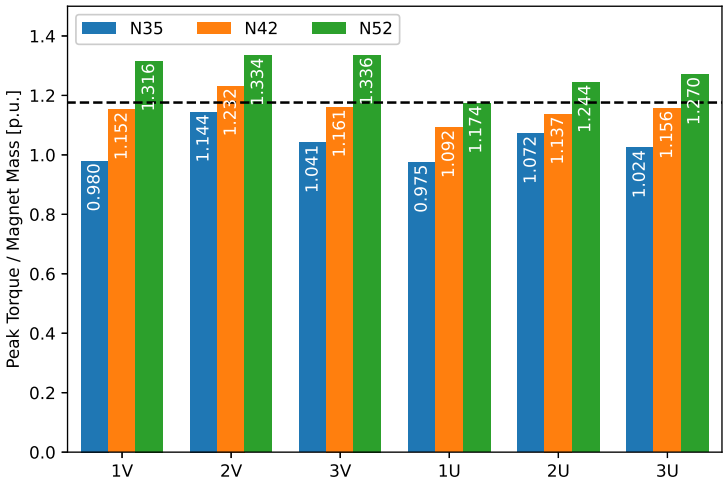

Figure 4.5: Peak torque over magnet mass for the asymmetric machines compared with the symmetric 2V N42 machines shown with the black dashed line.

The N52 machines are now superior since the higher grade magnets produced a lot of torque from the beginning and they all have a low magnet mass since they were allowed a lower maximum volume compared to the lower grade magnets. Most interestingly is that the asymmetric 2V N42 machine outperforms the symmetric 2V N42 machine with 4.8 %. This shows that it is possible to increase the peak torque of a machine while without increasing the magnet mass by introducing asymmetries in the rotor. Hence it should therefore also be possible to reduce the magnet mass and remain the same peak torque and therefore reduce cost and the environmental

impact from REEs. The power scaled with magnet mass is shown in Figure 4.6.

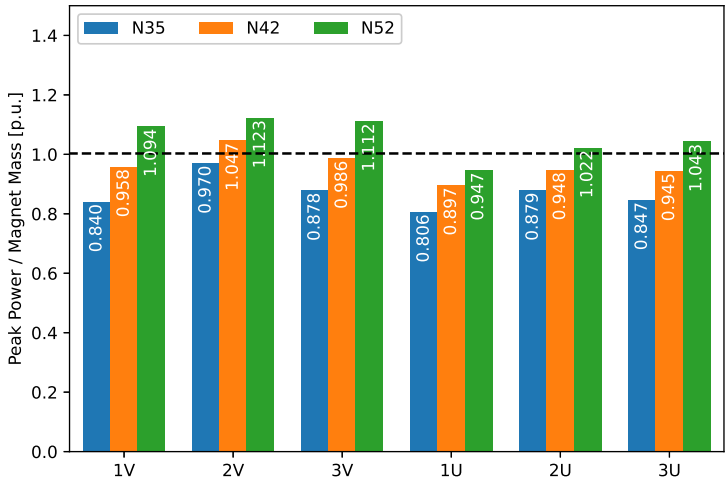

Figure 4.6: Peak power over magnet mass for the asymmetric machines compared with the symmetric 2V N42 machines shown with the black dashed line.

The asymmetric once again the beats the symmetric in power to magnet mass ratio showing promise for the asymmetric machines. To better compare the different magnet grades the power and torque is scaled with the remanence of the magnets to get a comparable magnetic moment. This is also the factor between the allowed magnet volumes of each topology. In Figure 4.7 the peak torque over magnetic moment is shown.

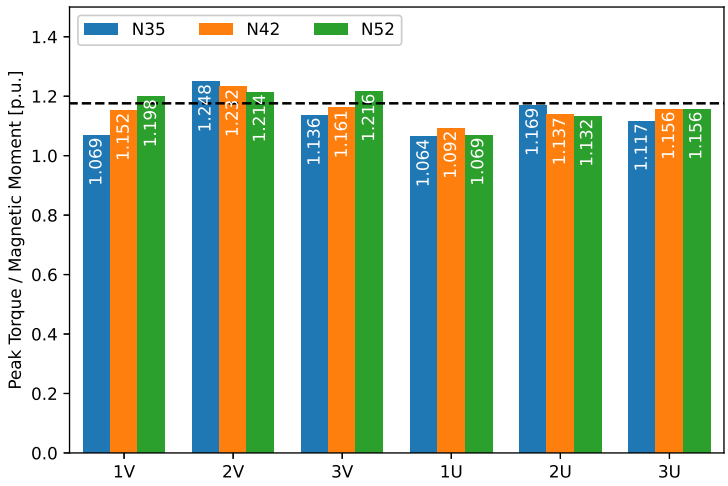

Figure 4.7: Peak torque over magnet mass scaled with the remanence for the asymmetric machines compared with the symmetric 2V N42 machines shown with the black dashed line.

All three asymmetric 2V machines has a higher peak torque over magnetic moment than the reference symmetric 2V N42 machine indicating an advantage with an asymmetric rotor topology. Interesting is that the results are inconsistent of which magnet grade that is the best for the different topologies. In Figure 4.8 the power scaled with magnetic moment for each machine is shown.

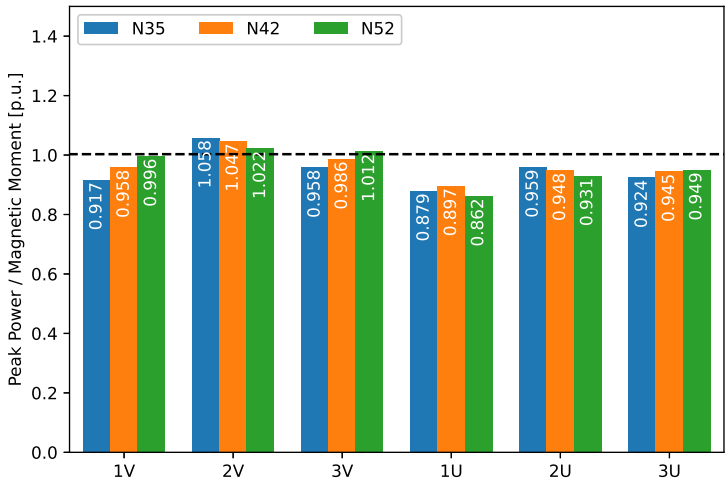

Figure 4.8: Peak power over magnet mass scaled with the remanence for the asymmetric machines compared with the symmetric 2V N42 machines shown with the black dashed line.

4.1.3 Efficiency and Power Factor

The efficiency and power factor map for the asymmetric 2V N42 machine can be seen in Figure 4.9a and 4.9b

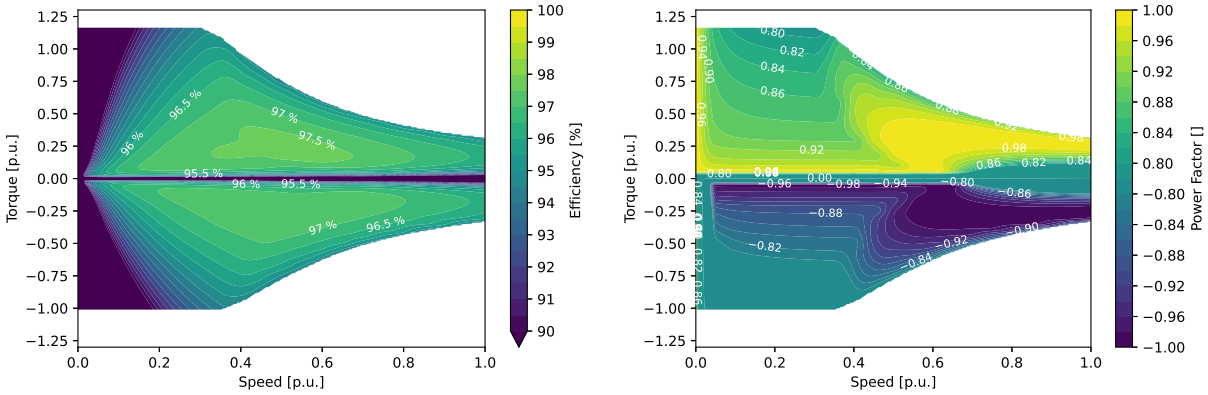

(a) Efficiency.

(b) Power factor.

Figure 4.9: Efficiency and power factor for asymmetric 2V N42 machine at 600 V DC-link voltage.

Compared to the symmetric 2V N42 machine in Figure 4.10a and 4.10b the asymmetric machine has a much bigger 97.5 % efficiency region compared the the symmetric

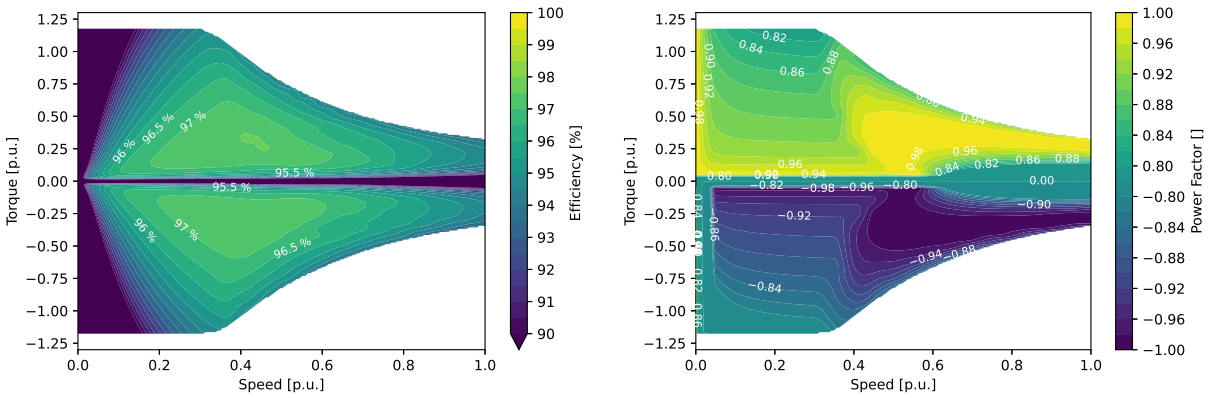

(a) Efficiency.

(b) Power factor.

Figure 4.10: Efficiency and power factor for symmetric 2V N42 machine at 600 V DC-link voltage.

To more easily compare the power factor for the symmetric and the asymmetric machine the differnce is shown in Figure 4.11.

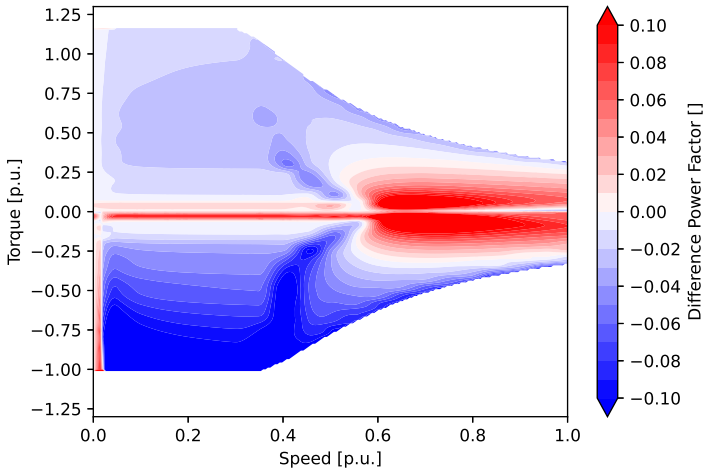

Figure 4.11: Difference in power factor between symmetric and asymmetric 2V N42 machines. The absolute values of the power factor is being compared and a positive value, red, indicates that the asymmetric machine has a higher absolute value and thereby better power factor than the symmetric and vice versa for negative, blue, values.

The asymmetric machine has considerable worse power factor than the symmetric, especially in generator mode which will reduce the over all drivetrain efficiency since it impacts the inverter efficiency negatively. The power factor in generator mode is considerably worse for all the asymmetric machine which can be seen in the efficiency and power factor maps in Appendix B. The worse power factor in generator mode is an effect of the asymmetry that shifts the reluctance and magnet torque peaks being more separated in load angle in generator mode. The asymmetric machines gets less torque per current in generator mode and for the same reason is the torque in generator mode lower than in motor mode as seen in Figure 4.14. Interestingly, the asymmetric machine is has a better power factor than the symmetric during high speed and heavy field weakening in both motor and generator mode. The iron losses for both machines can be seen in Figure 4.12a and 4.12b.

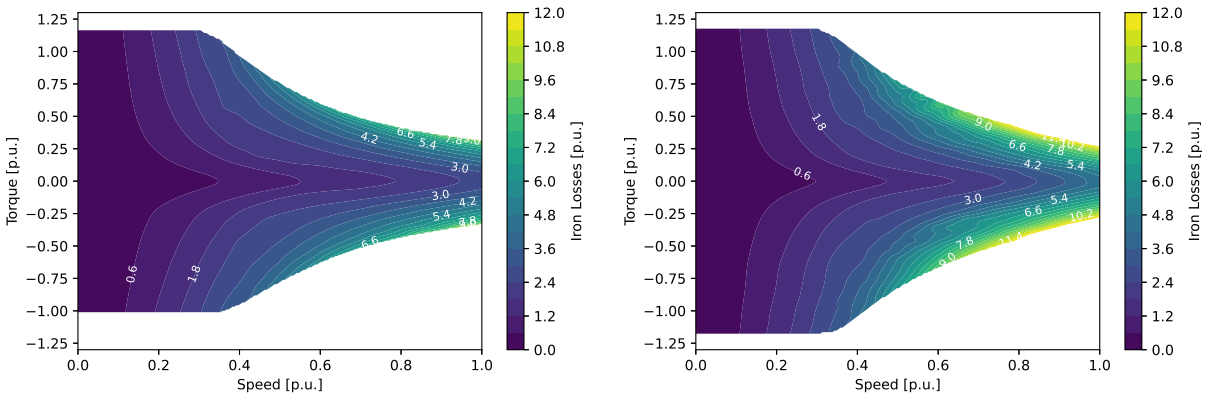

(a) Asymmetric 2V N42 machine.

(b) Symmetric 2V N42 machine.

Figure 4.12: Comparison of iron losses in asymmetric and symmetric 2V N42 machine.

The symmetric machine has considerably higher iron losses at high speed than the asymmetric one which may be a cause for the worse power factor. In Figure 4.13a and 4.13b the load angle for the respective machines is shown.

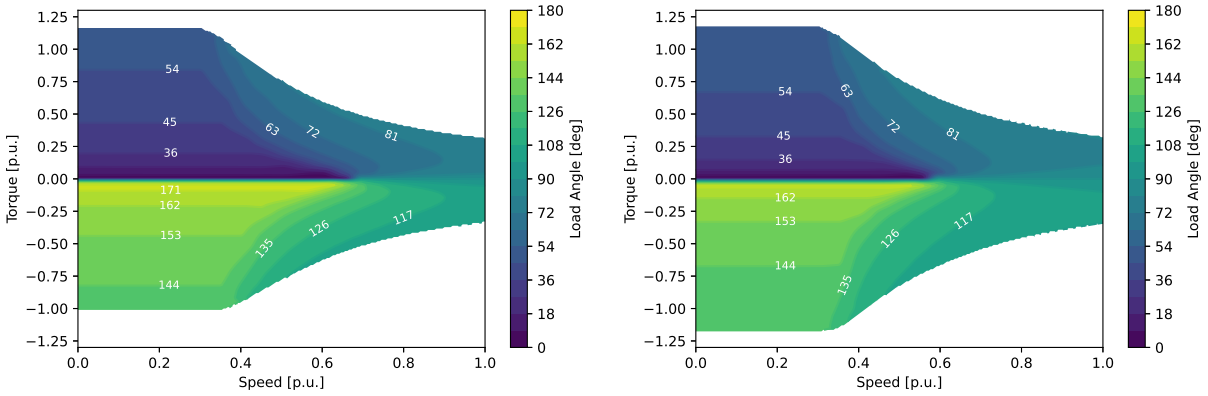

(a) Asymmetric 2V N42 machine.

(b) Symmetric 2V N42 machine.

Figure 4.13: Comparison of load angle in asymmetric and symmetric 2V N42 machine.

Here it can be seen that the asymmetric machine requires a smaller load angle at high speed which also could be a cause for the better power factor.

4.1.4 Motor Versus Generator Torque

The asymmetries in the rotor results in a lower torque in generator mode compared to motor mode. The ratio between the two can be seen in Figure 4.14.

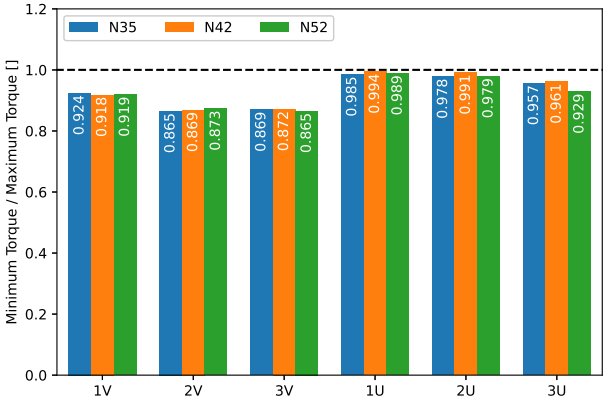

Figure 4.14: Ratio between maximum torque in motor and generator mode for the asymmetric machines compared with the symmetric 2V N42 machines shown with the black dashed line.

The factor between generator and motor torque can be seen as a figure of how asymmetric machine is. The symmetric 2V N42 has a ratio of one, that is, it can generate the same torque in either direction due to being symmetric. All the asymmetric machines on the other hand has a lower generator torque. It can be seen that the V-machines has a lower generator to motor torque ratio and are therefore more asymmetric showing that a V rotor topology benefits more from a asymmetric magnet placement in this size of machine. The ratio between generator and motor power can be seen in Figure 4.15.

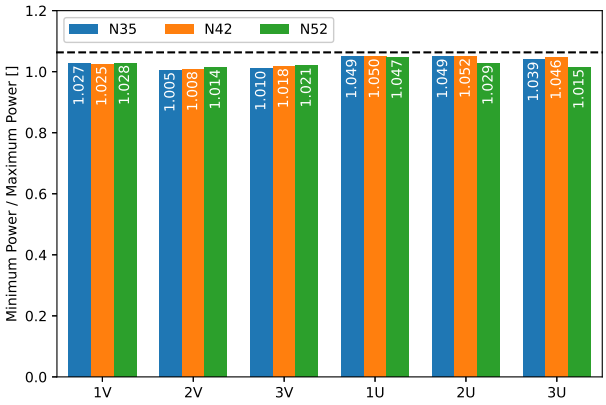

Figure 4.15: Ratio between maximum power in motor and generator mode for the asymmetric machines compared with the symmetric 2V N42 machines shown with the black dashed line.

The same story can be seen for the power but the effect is smaller due to the back-EMF also getting smaller, which allows for a higher knee point speed in generator mode. The ratio of the asymmetric machines is always lower than the ratio of the symmetric, however, they are all above one which may seem counter intuitive. The reason for them above one is that the plotted power is the mechanical power of the machine, so, the difference comes from the direction of the losses in the machine.

4.1.5 Reluctance Versus Magnet Torque

The torque components for a current angle swept from 0° to 180° is shown for the 3V N52 machine in Figure 4.16. The same thing can be seen for all the machines in Appendix C.

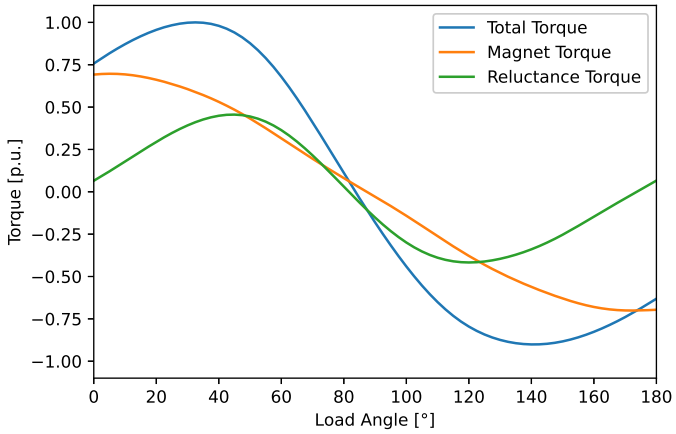

Figure 4.16: Reluctance and magnet torque components for the asymmetric 3V N52 machine.

The purpose of introducing asymmetry in the rotor is to bring the peak of the reluctance and magnet torque close and therefore have a higher peak of the total torque without necessarily increasing either of the components. With the peaks closer the torque also drops off faster with an increased load angle since the slope gets steeper. This may also explain why in Figure 4.13a and 4.13b the load angle needs to be increased less in the asymmetric machine during field weakening since the same happens with the voltage from the respective flux components. The peak of the respective torques for all machines can be seen in Figure 4.17.

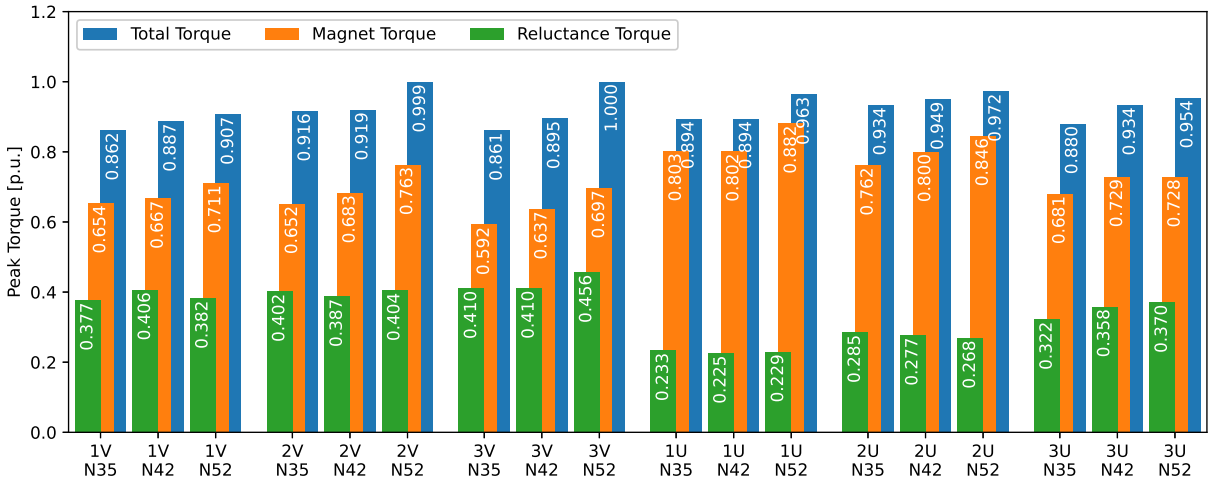

Figure 4.17: Comparison of the peak magnet, reluctance and total torque for all rotor topologies and magnet grades.

The U-machines gets considerably less reluctance torque than their respective V-shaped counter parts most likely due to the longer path of the q-axis flux in a U-shaped rotor. There is a trend for both V- and U-shaped rotors that more layers give more reluctance torque and higher magnet grades also gives more reluctance. The more layers blocks the d-axis flux more which results to more saliency, which in turn gives more reluctance torque. Higher magnet grade might for the same reason seem counter intuitive that it results in a higher reluctance torque since higher magnet grade allows for smaller magnets and thereby less blocking of the d-axis flux. However, it also results in wider flux paths in the q-axis since the magnets can be thinner which decreases the q-axis reluctance and thereby increases saliency and the reluctance torque.

There is a correlation between the magnet torque in Figure 4.17 and the asymmetry ratio in Figure 4.14. More reluctance torque correlates with more asymmetry. The V-shaped machines become more asymmetric from the optimisation due there is more performance to be found for the V compared to the U. One reason could be that there is more benefit with an asymmetric rotor topology for a machine that utilises more reluctance torque and since the U-shaped rotors don't have that much reluctance torque. The benefit from having the reluctance and magnet torque peaks closer in load angle is smaller than for the v-shaped rotors.

4.2 Efficiency and Low Cost Concept

The following section presents and analyses the results of the second part of the study where the focus of the optimisation shifted to reducing the cost and increasing the efficiency for the best topologies from the first part. The selected topology and magnet grade combinations to proceed with is 2V N35, 2V N42, 2V N52, 3V N35, 3V N42, 3V N52 and 2U N35.

4.2.1 Efficiency and Power Factor

The efficiency maps for the cost and efficiency optimised machines are as excepted very similar to their respective performance optimised machines. The efficiency and power factor map for the 2V N52 machine can be seen in Figure 4.18a and 4.18b.

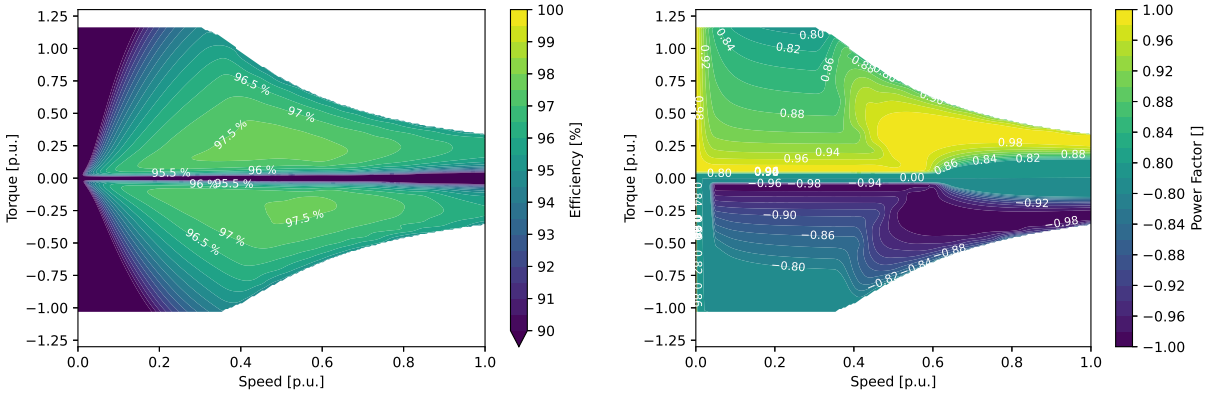

(a) Efficiency.

(b) Power factor.

Figure 4.18: Efficiency and power factor for asymmetric 2V N52 machine at 600 V DC-link voltage.

Since the 2V N52 just managed to surpass the power target for the cost and efficiency optimisation in the performance optimisation, the result of the cost and efficiency optimisation will be similar to the performance optimisation. The efficiency maps for all the efficiency optimised machines, except 2V N35 since it did not reach the performance targets, can be seen in Appendix D. The performance optimised machine is compared to the cost and efficiency optimised machine in Figure 4.19a and 4.19b.

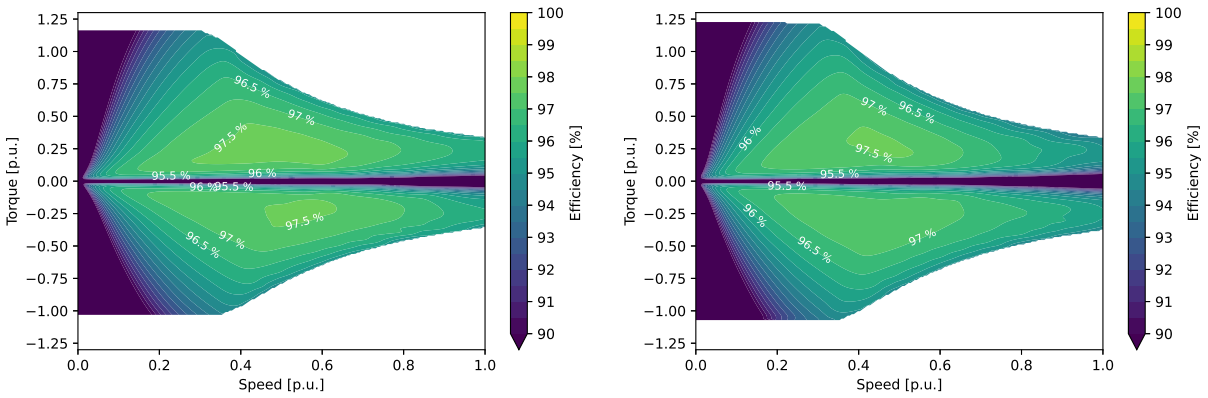

(a) Cost and efficiency optimised.

(b) Peak performance optimised.

Figure 4.19: Comparison of efficiency map between an asymmetric 2V N52 machine optimised for peak performance and an asymmetric 2V N52 machine optimised for low cost and efficiency at 600 V DC-link voltage.

The cost and efficiency optimised 2V N52 machine clearly has a higher efficiency in large parts of the operating range. The biggest gain is seen with higher speeds which indicates that optimising the rotor for efficiency has greatly reduced the iron losses. There is not any visible difference at low speed, but the efficiency is probably marginally worse since the peak torque is reduced and therefore there will be more copper losses to achieve the same torque.

The peak torque for the cost and efficiency optimised machines can be seen in Figure 4.20a and the peak power in Figure 4.20b.

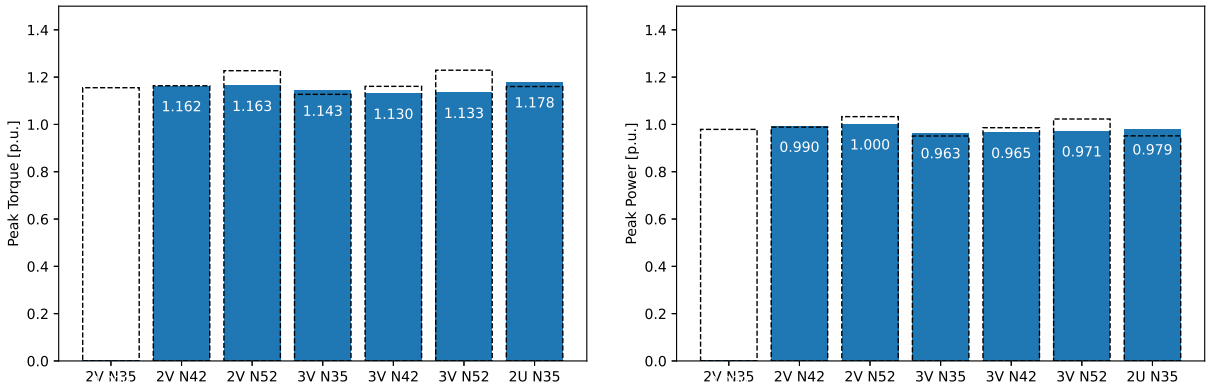

(a) Peak torque.

(b) Peak power.

Figure 4.20: Peak torque and power for the efficiency and low cost optimised machines compared to their respective peak performance counter parts shown with the dashed bars.

Many of the machines have a much higher peak torque than the optimisation target of 1 pu because they are all limited by the power they can produce and they need the extra torque to be able to produce the power target with the given space constrain. The dashed bars represent the results from the performance optimisation to show how the different targets has affected the optimisation. 2V N42 have kept similar peak torque and power and 3V N35 and 2U N35 have increased both to be able to comply with the constrain of the optimisation. Note that it is only 2V N52 that actually has enough torque and power to meet the constrains from the optimisation. However, since the optimisation was run with a simplified model and the results presented here are run with the post-process model described in section 3.1. The simpler model

may have underestimated the voltage or overestimated the torque at the peak operating point and therefore overestimated the power and therefore allowing solutions that do not meet the requirements after the post-processed model. This is however not a problem and is accounted for, since some margin is included in the torque and power targets.

The used magnet mass of the cost and efficiency optimised machines can be seen in Figure 4.21.

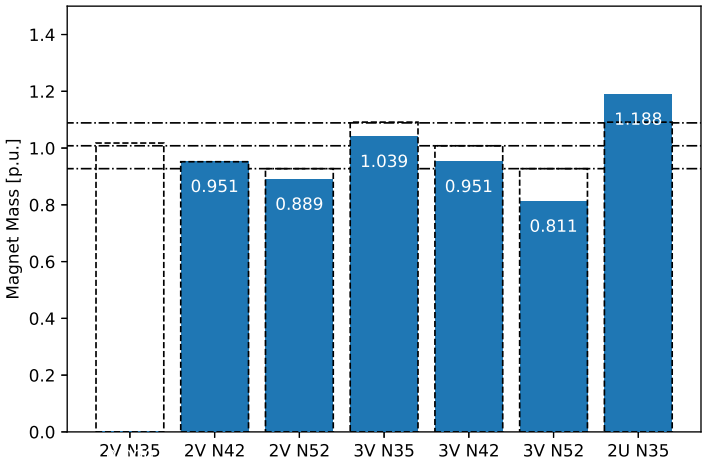

Figure 4.21: Magnet mass for the efficiency and low cost optimised machines compared to their respective peak performance counter parts shown with the dashed bars. The three allowed magnet masses for the respective magnet grades during the performance optimisations is shown with the dash-dotted lines. A lower magnet grade allowed for a higher magnet mass. 1 pu is the magnet mass of the original reference machine.

2V N52, 3V N35 and 3V N52 have managed to lower the magnet mass and 3V N35 machines did so while increasing both the power and torque. 2U N35 had to increase the magnet mass considerably to achivie marginal gains in torque and power and is now over the limit set during the performance optimisation. It again shows that the U rotor topologies are ill-suited for this size of machine with this slot, pole combination.

4.2.2 WLTP Efficiency and Cost

The efficiency map for the 3V N35 machine with a WLTP drive cycle overlaid is shown in Figure 4.22.

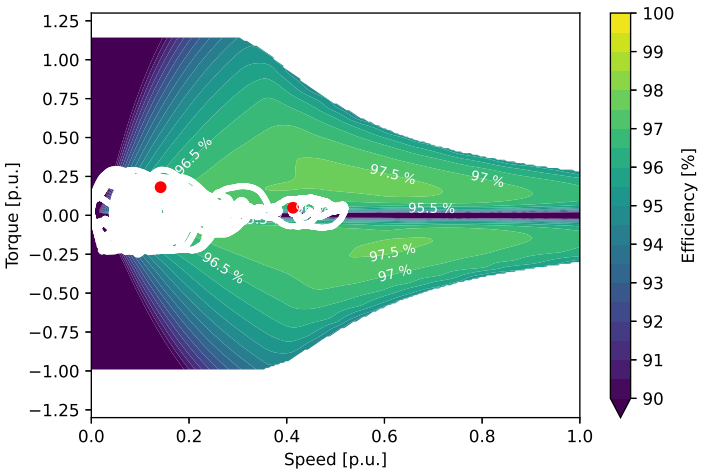

Figure 4.22: 3V N35 efficiency map with WLTP drive cycle overlaid in white as well as OP1 and OP2 highlighted in red.

WLTP does not utilise the full performance of this machine and is never in the highest efficiency region. All the machines and the performance targets for the optimisations are very over dimensioned for the WLTP cycle and a much better efficiency could be achieved with a design optimised for WLTP. The total WLTP efficiency calculated according to 3.3.3 is shown in Figure 4.23.

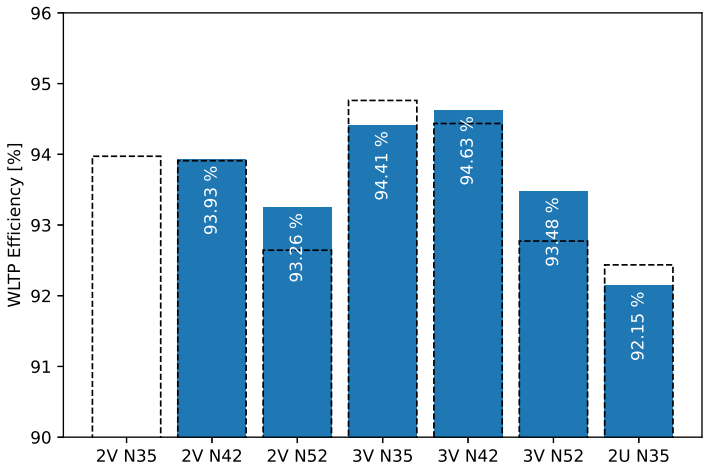

Figure 4.23: WLTP efficiency for the efficiency and low cost optimised machines compared to their respective peak performance counter parts shown with the dashed bars.

2V N52, 3V N42 and 3V N52 are the only machines that have a higher efficient compared to their performance optimised counter parts. They are also the only machines that could lower the power when optimising for cost and efficiency. The others had to sacrifice the efficiency for the cost that had a higher weight during the optimisation. The losses for OP1 and OP2 are shown in Figure 4.24.

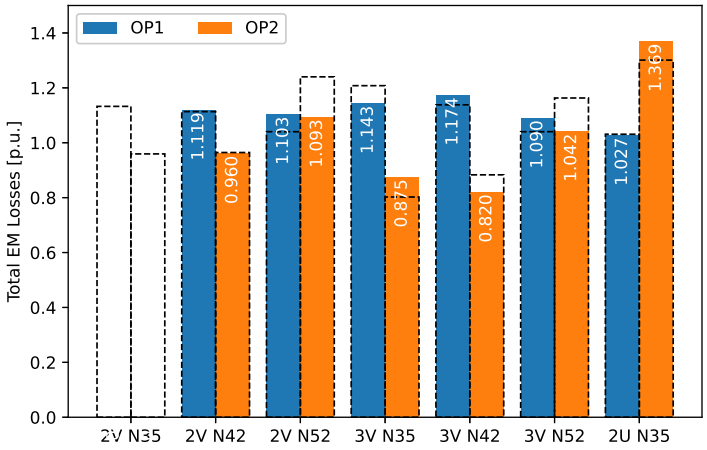

Figure 4.24: OP1 and OP2 losses for the efficiency and low cost optimised machines compared to their respective peak performance counter parts shown with the dashed bars.

The machines that had to increase the power all saw an increase in OP2 losses which impacts the WLTP efficiency negatively since the WLTP efficiency seems to be very dependant on the OP2 losses, more so than the OP1 losses. Shown by 2V N52 being able to sacrifice some OP1 efficiency, which is a side effect of the lower peak torque and thereby needing more current for OP1, for OP2 efficiency and in total gaining WLTP efficiency. The higher magnet grades also get penalised slightly by using MTPA compared to Maximum Torque per Loss (MTPL) since MTPA only minimises the current, therefore ignoring the iron losses. Seen by Figure 4.24 higher magnet grade results in higher losses in OP2 which mostly consists of iron losses and therefore would the higher grade magnets premiere more from running a MTPL control scheme. However, the difference is marginal and the study will proceed with MTPA.

The material cost for the machines is shown in Figure 4.25.

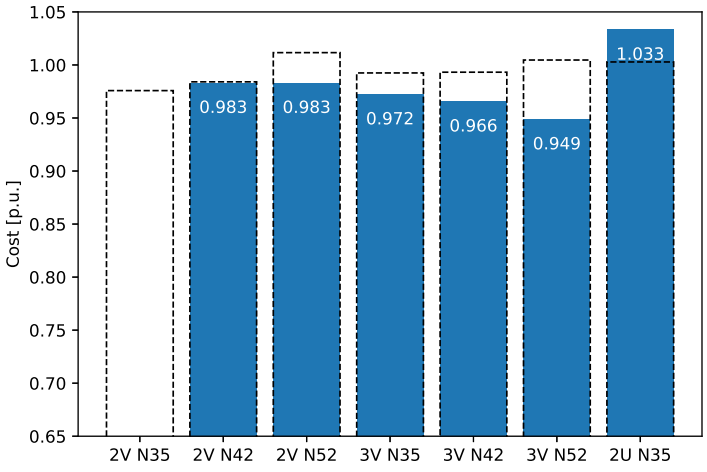

Figure 4.25: Material cost for the efficiency and low cost optimised machines compared to their respective peak performance counter parts shown with the dashed bars. 1 pu is the cost of the original reference machine.

The cost optimisation has succeeded in greatly reducing the cost of most machines except the 2V N42 that remains the same as before and the 2U N35 that has increased considerably in cost. The increase in cost for 2U N35 is most probably due to the extra magnets needed to reach the

desired power seen in Figure 4.21. The 3V N42 is the second cheapest machine and the most efficient making it interesting for future studies. The cost presented only includes material cost calculated from the mass of each element and does not consider the extra cost from having more magnet sizes and the extra work of assembly. Therefore, the 2V N42 could also be of interest since one less magnet layer reduces complexity of the assembly and requires fewer different sizes of magnets. There may also be more space for introducing flux blocking holes and in the rotor to further optimise the rotor and reduce the rotor iron cost. The cost divided into the different parts can be seen in Figure 4.26.

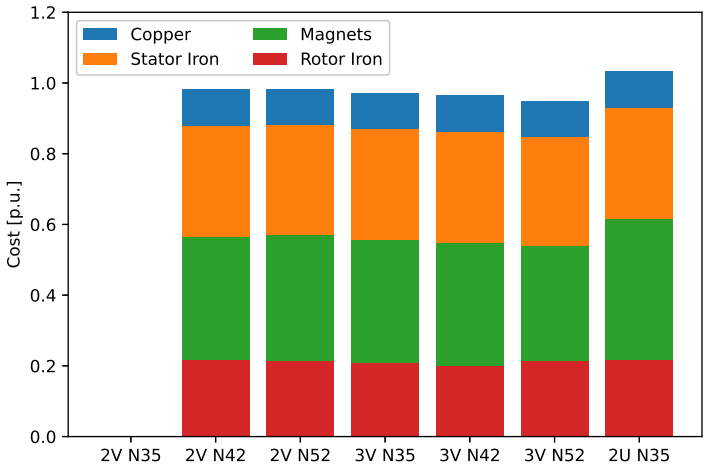

Figure 4.26: Material cost divided into copper, magnets, stator and rotor iron for the efficiency and low cost optimised machines. 1 pu is the cost of the original reference machine.

The magnet cost makes up for roughly a third of the total material cost of the machine and significant cost savings can be made from reducing the magnet mass.

4.2.3 Change of Gear Ratio for Better Efficiency

The gear ratio was fixed for the optimisations since the intention was to keep gear box unchanged but if the gear ratio is reduced it could result in higher drive cycle efficiency since all the machines achieves more torque than the target torque. The new WLTP efficiency for the cost and efficiency with a gear different gear box ratio is shown in Figure 4.27.

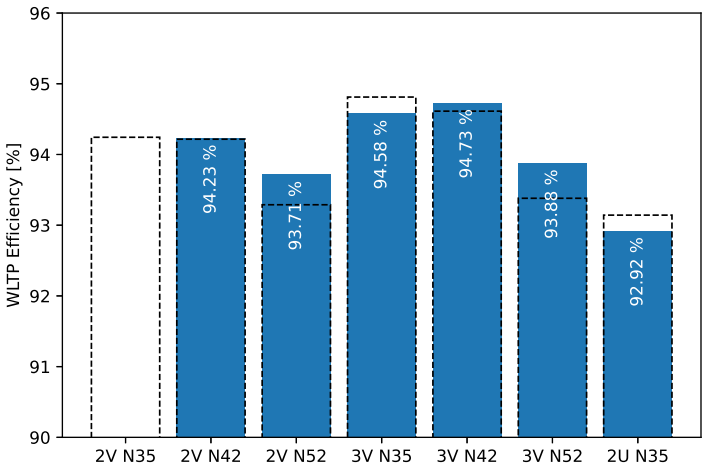

Figure 4.27: WLTP efficiency for the efficiency and low cost optimised machines with 1.143 times lower gear ratio compared to their respective peak performance counter parts shown with the dashed bars.

The efficiency has gone up across the board by reducing the gear ratio. The ratio is lowered by 1.143 times so that the peak torque of the 3V N35 machine now meets the torque target of 1 pu. This reduces the iron losses by reducing the speed of the machine but increases the copper losses since more machine torque is required to get the same torque on the wheels. Just from this quick analysis it can be seen that it could be beneficial to lower the gear ratio with these machines torque and power targets. A lower gear ratio most often also results in a lower cost and higher efficiency which would further improve the overall drive train efficiency. However, it would require more investigation to exactly determine the gains and since the scope of this study doesn't involve a change in gear box, it will not be investigated further.

4.2.4 Shortened Machine for Lower Cost

Instead of changing the gear ratio for marginally better drive cycle efficiency the active length of the machine can be shortened since the peak torque is over dimensioned. For each of the shown machines the active length is scaled so that the peak torque is 1 pu, that is the target for the optimisation. The power will still remain the same as the machines active length is shortened. The OP1 and OP2 losses and the cost of the shortened machines are shown in Figure 4.28a and 4.28b respectively.

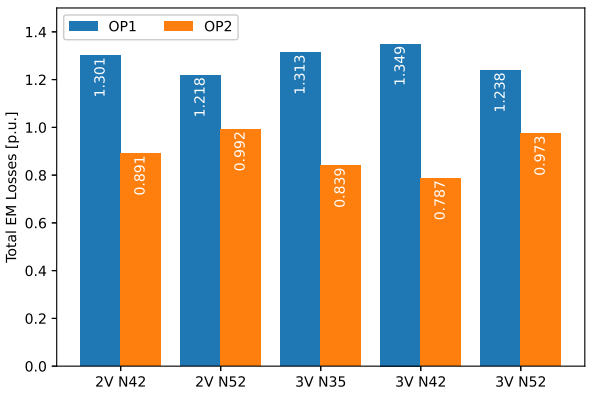

(a) OP1 and OP2 losses.

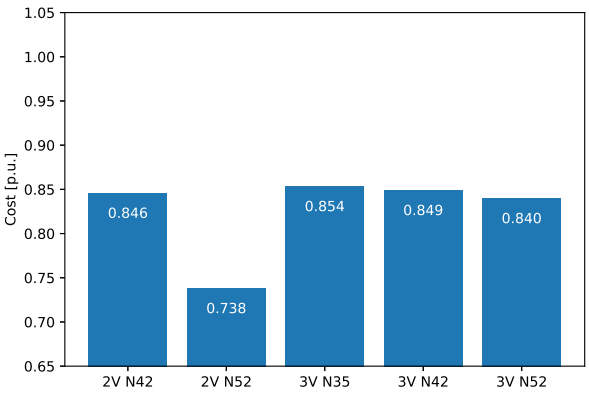

(b) Cost. 1 pu of cost is the cost of the original reference machine.

Figure 4.28: Losses and cost for shortened variants of the best efficiency and low cost optimised machines.

All machines have seen a major increase in the OP1 losses while the OP2 losses have degreased all the while the cost is considerably lower than any of the other efficiency and low cost optimised machines. The shorter machines sees a major savings potential since much less material is used with a minor decrease in the WLTP efficiency. However, the increased OP1 losses are the result of more current being needed for getting the same OP1 torque and since the inverter losses aren't accounted for in the figure and the WLTP efficiency is the efficiency of only the electric machine. Since the optimisation accounted for the inverter losses in the objective functions the optimisation results are not wrong, this just shows that a much lower cost can be achieved if the weights between efficiency and cost favoured cost more.

4.3 Control and MTPA

Shifting of the magnets poses the question of how the d-axis is defined and how it affects the current control of the inverter. The circumferential shift of the peak permanent magnet flux in reference to the reluctance flux will change due to the asymmetric magnet layout. The angle shift is so big so that it can not be neglected, but the effect will not matter in practice since it will be accounted for when calculating the MTPA angle. It does not matter what the MTPA angle is in reference to, as long as it is known and the resolver, or what ever position sensor is used, can be calibrated for it. However, the traditional torque equation for an IPM in (2.25) can not be used since the permanent magnet flux linkage no longer only is in the d-axis direction. Instead (2.22) in section 2 can be used to calculate the torque and the flux maps of the machine can be utilised instead of inductance.

The flux map over the i_d and i_q will also no longer a mirror for positive and negative q-currents, that is motor mode and generator mode, so the MTPA line no longer is a mirror for motor mode for generator mode. The MTPA lines for the low cost and efficiency optimised 3V N35 machine can be seen in Figure 4.29.

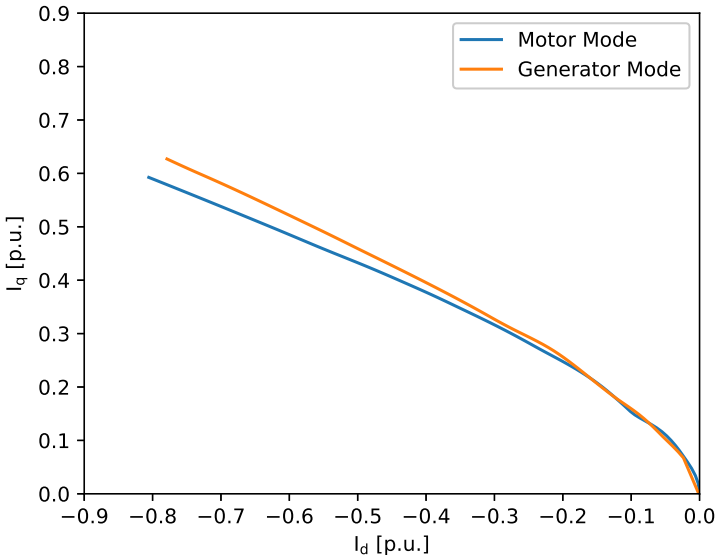

Figure 4.29: MTPA for low cost and efficiency optimised 3V N35 machine in motor and generator mode. The generator mode the q-current is flipped around the d-axis so that the values are positive instead of negative. This to enable an easier comparison between motor and generator mode.

The asymmetry results in that a smaller load angle delivers more torque per ampere in generator mode compared to motor mode due to the lower contribution from the reluctance torque. Note that the d-axis direction in this plot is defined as the middle of the simulated pole and that may no longer be in-line with the magnetic flux, but as stated earlier, it doesn't matter when flux mapping is used. Where to define the d-axis direction can as usual be found by either simulating or measuring the back-EMF at no-load and then it is known that the flux linkage is 90° behind and the link between simulation and motor control in reality can be made that way.

4.4 Demagnetisation Investigation

The following section presents and analyses the results from the brief study done on the risk of demagnetisation during normal operation and ASC.

4.4.1 Normal Operation

The maximum magnetic field strength in the six magnets in the fourth skew layer in the low cost and efficiency optimised 3V N35 machine is shown in Figure 4.30a, 4.30b, 4.30c, 4.30d, 4.30e and 4.30f. The magnetic field strength in the magnets in all six skew layers can be seen in Appendix E.

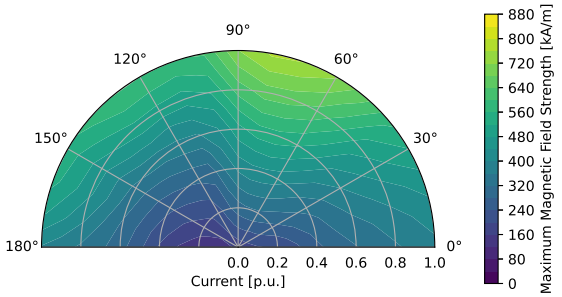

(a) Outer layer, upper magnet.

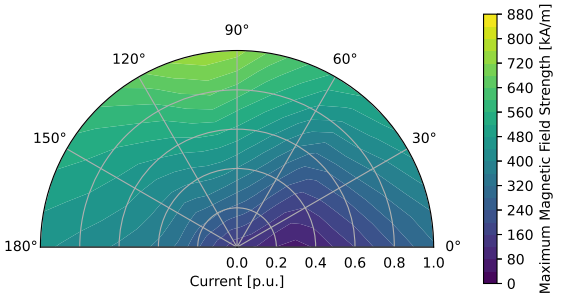

(b) Outer layer, lower magnet.

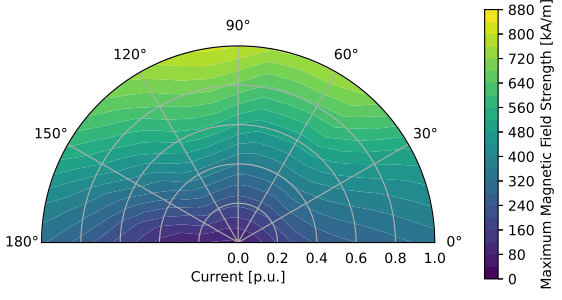

(c) Middle layer, upper magnet.

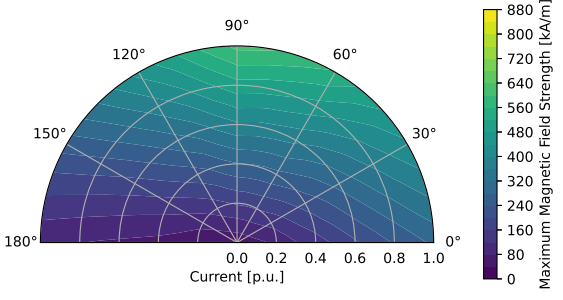

(d) Middle layer, lower magnet.

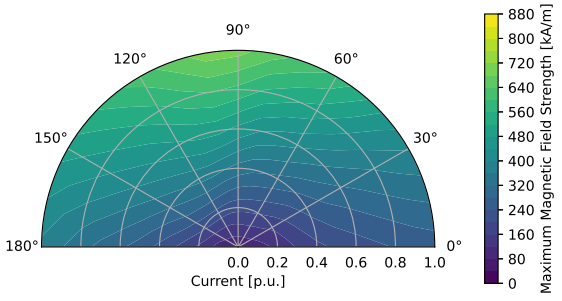

(e) Inner layer, upper magnet.

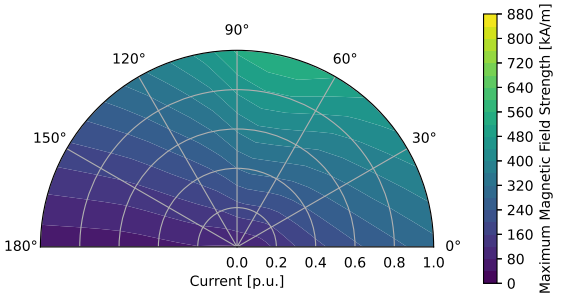

(f) Inner layer, lower magnet.

Figure 4.30: Maximum magnetic field strength in all magnets in fourth skew layer in low cost and efficiency optimised 3V N35 machine for all current amplitudes and angles.

The two outer and the upper middle magnet sees the highest magnetic field strength during normal operation. Both outer layer magnets experience similar but mirrored reverse magnetic field strength with the lower magnet being worse during generator mode and the upper magnet during motor mode. The rotation direction is anti-clockwise to the upper magnets are leading. All magnets have relatively low levels and there is no risk of demagnetisation during normal operation with the current magnets.

4.4.2 ASC

The magnets can be permanently demagnetised during ASC if the magnetic field strength is higher than the coercivity of the magnet. The maximum magnetic field strength of each magnet in the 3V N35 machine during eight periods of ASC operating at the negative knee point is shown in Figure 4.31a, 4.31b, 4.31c, 4.31d, 4.31e and 4.31f. The negative knee point is chosen due it being the worst case for this machine out of the studied operating points.

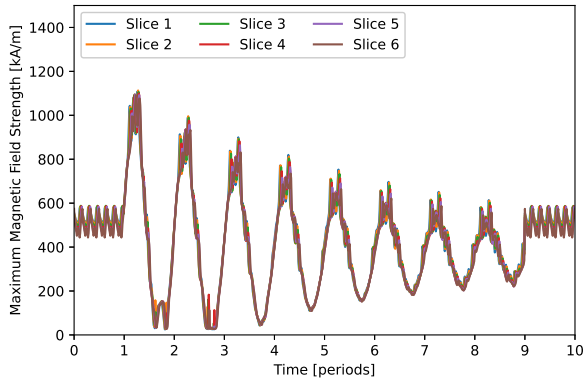

(a) Outer layer, upper magnet.

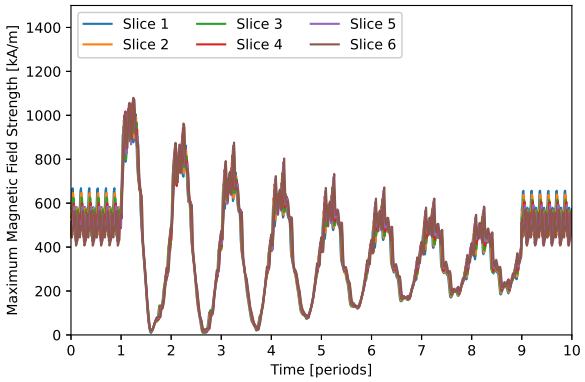

(b) Outer layer, lower magnet.

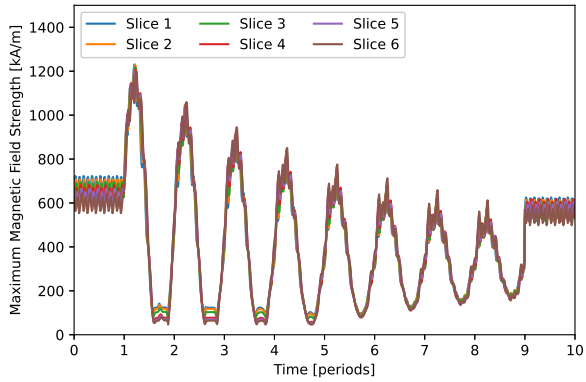

(c) Middle layer, upper magnet.

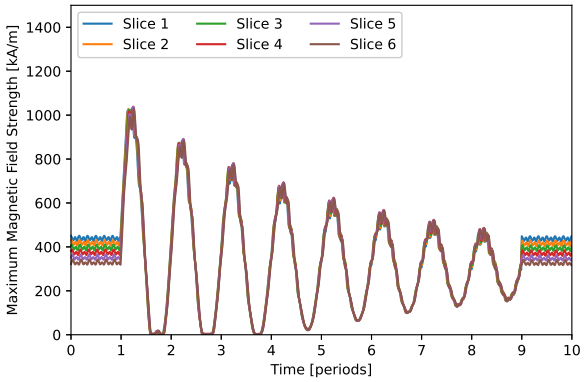

(d) Middle layer, lower magnet.

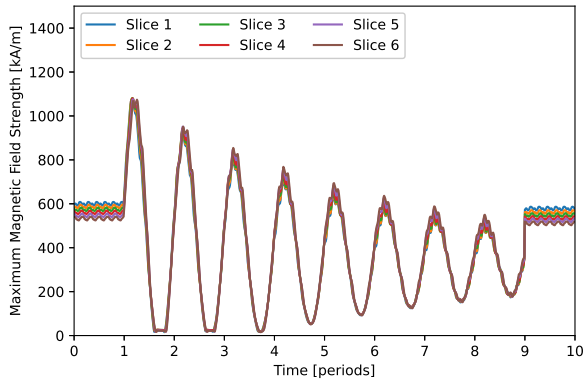

(e) Inner layer, upper magnet.

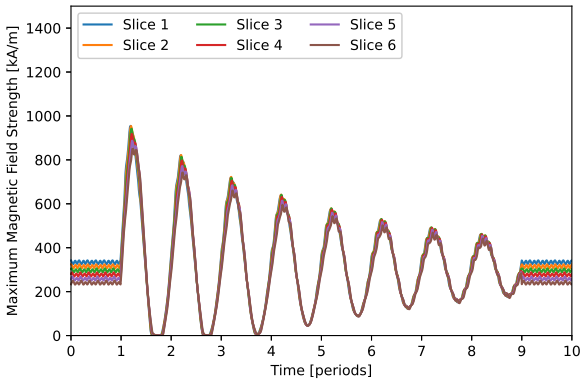

(f) Inner layer, lower magnet.

Figure 4.31: Maximum magnetic field strength in the six magnets for all six skew slices before, during and after ASC of 3V N35 machine at the negative knee point operation.

The maximum magnetic field strength surpasses the coercivity of the magnets at the maximum temperature of the used magnets in all of the upper magnets and is very close in the lower magnets. There will be some harm and demagnetisation due to the ASC. The extent of the harm can be seen in Figure 4.32a and 4.32b.

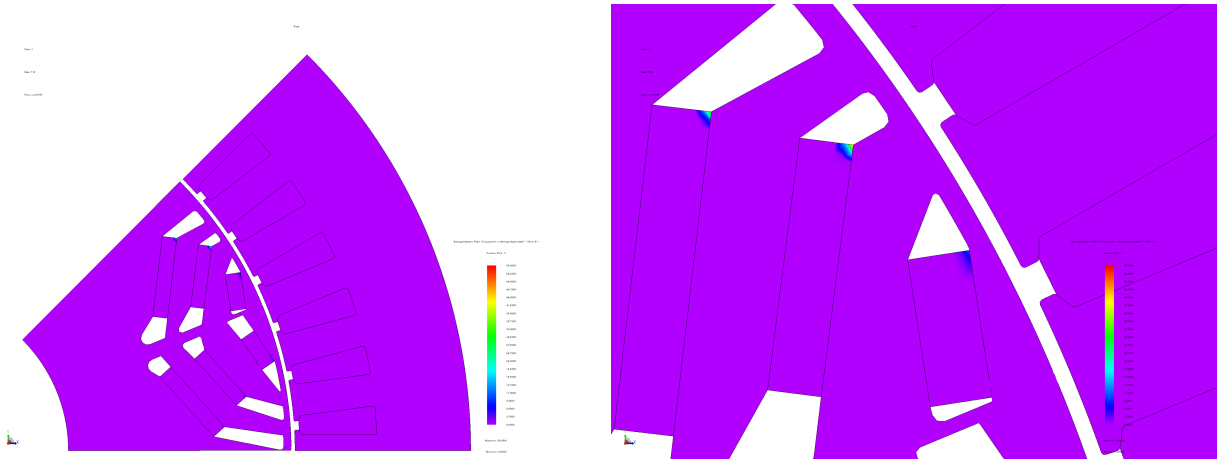

(a) The whole machine.

(b) Zoomed in on the upper magnets showing the demagnetised region.

Figure 4.32: Demagnetisation ratio contour plot of 3V N35 machine after eight periods of ASC at the negative knee point operation.

There are some demagnetisation on the edge of the magnets but the area is relatively small and the demagnetisation ratio is also very low with the highest level of 30 % in the corner of the upper magnet in the middle layer. To see if the demagnetisation has harmed the performance of the machine a period of normal operation is simulated and is shown and the torque is shown in Figure 4.33.

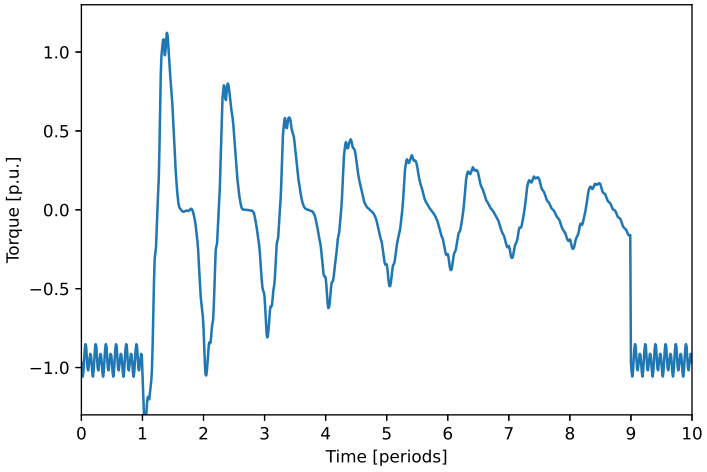

Figure 4.33: Torque before, during and after ASC of 3V N35 machine at the negative knee point operation.

The torque before and after ASC is unchanged and the marginal demagnetisation does not have a meaningful impact on the machines performance. The current during ASC is shown in Figure 4.34.

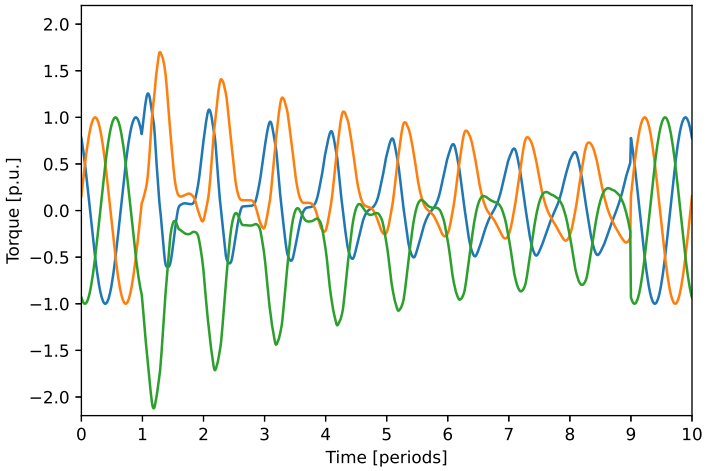

Figure 4.34: Current before, during and after ASC of 3V N35 machine at the negative knee point operation.

The current is much greater during worst case ASC than the maximum current during normal operation and could harm the machine with excessive temperature of the windings, but since the thermals of the machines is not part of this study. The effects of the ASC current will not be investigated.

Chapter 5

Conclusions

From the study it can be concluded that asymmetric machines can achieve more torque per magnet mass than a comparable symmetric machine in motor mode, but less torque in generator mode. The lower torque in generator mode is an effect of the worse alignment of the reluctance and magnet torque which also results in a considerable worse power factor for the asymmetric machine. This is not a big problem since the required torque in generator mode is much smaller than the motor mode torque for automotive applications and when only considering the losses of the electric machine the WLTC efficiency is not notably affected. However, it will lower the inverter efficiency and with a worse power factor so it should be investigated further with the full drivetrains efficiency in mind.

More layers does in general give more torque with some diminishing returns between two and three layers and a higher magnet grade results in a higher torque as well. The magnet torque sees a reduction with more layers but the increased reluctance makes up for it. The reluctance torque increases both with the number of layers and with higher magnet grade since the higher magnet grade has thinner magnets and therefore blocks less of the q-axis flux. The V-machines have a higher reluctance torque than the U and therefore become more asymmetric from the optimisation. Since there is more benefit for bringing the reluctance and magnet torque closer together when the there is more reluctance torque.

The short demagnetisation study during normal operation and ASC showed that there is no apparent risks of demagnetisation in the designed machine. However, it is only one example and it can not say if asymmetric machines in general are better or worse when it comes to demagnetisation.

From the study it is found that there can be benefits with having an asymmetric rotor for IPMs in an automotive and there has not been any findings against the suitability for the application. It will however have to be studied further in terms of how it affects aspects that has not been covered by this study.

Bibliography

[1] B. Raghuraman, S. Nategh, N. Sidiropoulos, L. Petersson, and A. Boglietti, "Sustainability aspects of electrical machines for e-mobility applications part i: A design with reduced rare-earth elements," in *IECON 2021 – 47th Annual Conference of the IEEE Industrial Electronics Society*, 2021, pp. 1–6. DOI: 10.1109/IECON48115.2021.9589246.

[2] A. Shukla and S. Basak, "Driving cycle-based design and optimization of reduced rare-earth interior permanent magnet synchronous motor for electric vehicle," in *2023 IEEE 2nd Industrial Electronics Society Annual On-Line Conference (ONCON)*, 2023, pp. 1–6. DOI: 10.1109/ONCON60463.2023.10430557.

[3] G. Dajaku, H. Zhou, X. Dajaku, and D. Gerling, "Novel rotor design with reduced rare-earth material for pm machines," in *2019 IEEE International Electric Machines & Drives Conference (IEMDC)*, 2019, pp. 1–7. DOI: 10.1109/IEMDC.2019.8785202.

[4] I. Santantonio, S. Nategh, A. Carlsson, G. Franceschini, P. Farah, and D. Zefack, "High-frequency rotor excitation system part i: Modeling method and optimization," in *2023 AEIT International Conference on Electrical and Electronic Technologies for Automotive (AEIT AUTOMOTIVE)*, 2023, pp. 1–6. DOI: 10.23919/AEITAUTOMOTIVE58986.2023.10217231.

[5] C. Zeng, Y. Chen, K. Liu, *et al.*, "Torque optimization of a dual three-phase permanent magnet synchronous machine with asymmetric rotor core for electric vehicles," in *2023 26th International Conference on Electrical Machines and Systems (ICEMS)*, 2023, pp. 2612–2617. DOI: 10.1109/ICEMS59686.2023.10344549.

[6] Y. Ji, Y. Li, and Q. Lu, "Investigation of a novel hybrid less-rare-earth consequent-pole interior permanent magnet machine with asymmetric rotor," in *2023 26th International Conference on Electrical Machines and Systems (ICEMS)*, 2023, pp. 5354–5359. DOI: 10.1109/ICEMS59686.2023.10344715.

[7] M. Suphama, P. Seangwong, N. Fernando, J. Jongudomkarn, A. Siritaratiwat, and P. Khunkitti, "A novel asymmetric hybrid-layer del-shaped rotor interior permanent magnet motor for electric vehicles," *IEEE Access*, vol. 12, pp. 2793–2802, 2024. DOI: 10.1109/ACCESS.2023.3347777.

[8] C. Diao, W. Zhao, Y. Liu, and X. Wang, "Permanent magnet assisted synchronous reluctance motor with asymmetric rotor for high torque performance," *CES Transactions on Electrical Machines and Systems*, vol. 7, no. 2, pp. 179–186, 2023. DOI: 10.30941/CESTEMS.2023.00016.

[9] Y. Xiao, Z.-Q. Zhu, J.-T. Chen, D. Wu, and L.-M. Gong, "A novel asymmetric rotor interior pm machine with hybrid-layer pms," in *2020 IEEE Energy Conversion Congress and Exposition (ECCE)*, 2020, pp. 4029–4035. DOI: 10.1109/ECCE44975.2020.9236015.

[10] Z.-Q. Zhu and Y. Xiao, "Novel magnetic-field-shifting techniques in asymmetric rotor pole interior pm machines with enhanced torque density,"
IEEE Transactions on Magnetics, vol. 58, no. 2, pp. 1–10, 2022.
DOI: 10.1109/TMAG.2021.3076418.

[11] C. C. Pavel, C. Thiel, S. Degreif, *et al.*, "Role of substitution in mitigating the supply pressure of rare earths in electric road transport applications,"
Sustainable Materials and Technologies, vol. 12, pp. 62–72, 2017, ISSN: 2214-9937.
DOI: https://doi.org/10.1016/j.susmat.2017.01.003. [Online]. Available:
https://www.sciencedirect.com/science/article/pii/S2214993716300641.

[12] V. Balaram, "Rare earth elements: A review of applications, occurrence, exploration, analysis, recycling, and environmental impact,"
Geoscience Frontiers, vol. 10, no. 4, pp. 1285–1303, 2019, ISSN: 1674-9871.
DOI: https://doi.org/10.1016/j.gsf.2018.12.005. [Online]. Available:
https://www.sciencedirect.com/science/article/pii/S1674987119300258.

[13] P. Zapp, A. Schreiber, J. Marx, and W. Kuckshinrichs, "Environmental impacts of rare earth production," *MRS Bulletin*, vol. 47, Mar. 2022.
DOI: 10.1557/s43577-022-00286-6.

[14] D. K. Cheng, *Field and Wave Electromagnetics*.
Harlow, United Kingdom: Pearson Education Limited, 2014, vol. 2.

[15] J. Pyrhönen, T. Jokinen, and V. Hrabovcová, *Design of Rotating Electrical Machines*.
Chichester, United Kingdom: John Wiley & Sons, Ltd, 2008, vol. 1.

[16] Hitachi Metals America, LTD., *Hitachi magnet handbook*, Magnetic Materials Division.

[17] C. J. O'Rourke, M. M. Qasim, M. R. Overlin, and J. L. Kirtley, "A geometric interpretation of reference frames and transformations: Dq0, clarke, and park,"
IEEE Transactions on Energy Conversion, vol. 34, no. 4, pp. 2070–2083, 2019.
DOI: 10.1109/TEC.2019.2941175.

[18] J. Loumi, *Transient phenomena in electrical machines*,
Lecture notes for a course in electrical machines, Chalmers University of Technology, 1998.

[19] A. Krings and J. Soulard,
"Overview and comparison of iron loss models for electrical machines,"
in *Proceedings of the 2010 International Conference on Electrical Machines (ICEM)*,
KTH Royal Institute of Technology, 2010.

[20] J. S. ARORA, *Introduction to Optimum Design*.
Oxford, United Kingdom: Academic Press, 2012, vol. 3.

[21] *Uniform provisions concerning the approval of light duty passenger and commercial vehicles with regards to criteria emissions, emissions of carbon dioxide and fuel consumption and/or the measurement of electric energy consumption and electric range (WLTP)*, United Nations Economic Commission for Europe, UN Regulation No. 154, Geneva, Switzerland, Feb. 2021.

[22] JSOL Corporation, *Jmag version 24.0, user's manual, parameter explanation*,
JMAG Business Company, Tokyo, Japan, 2024.

Appendix A

Peak Performance: Max Line

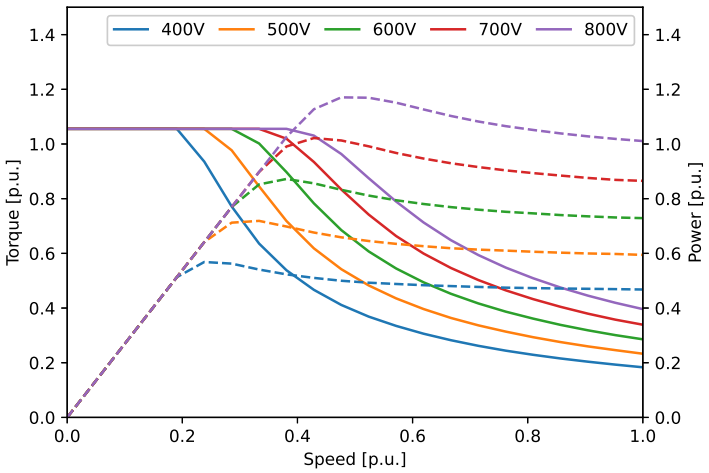

Figure A.1: Asymmetric 1U N35 machine torque and power max lines at different DC-link voltages.

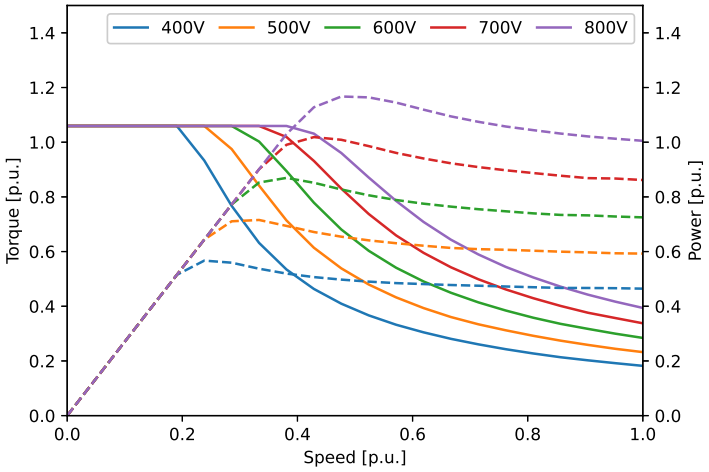

Figure A.2: Asymmetric 1U N42 machine torque and power max lines at different DC-link voltages.

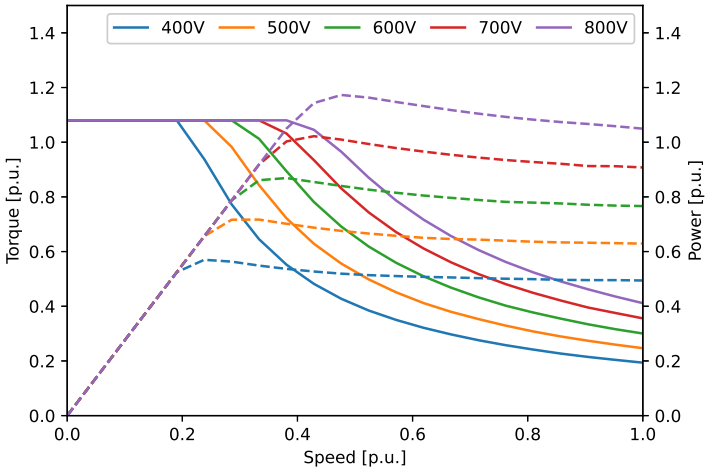

Figure A.3: Asymmetric 1U N52 machine torque and power max lines at different DC-link voltages.

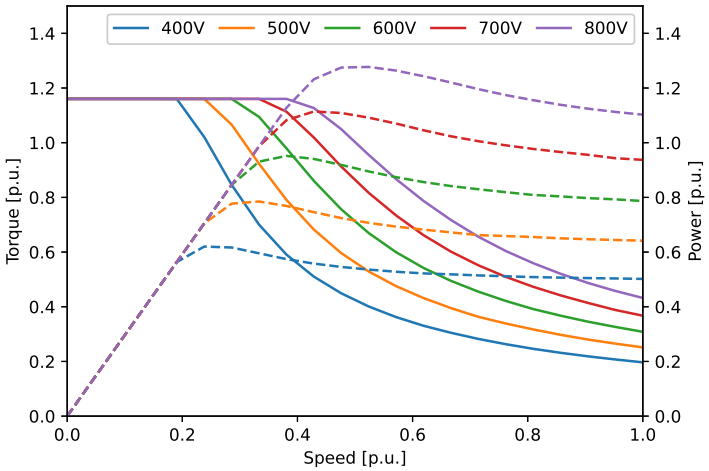

Figure A.4: Asymmetric 2U N35 machine torque and power max lines at different DC-link voltages.

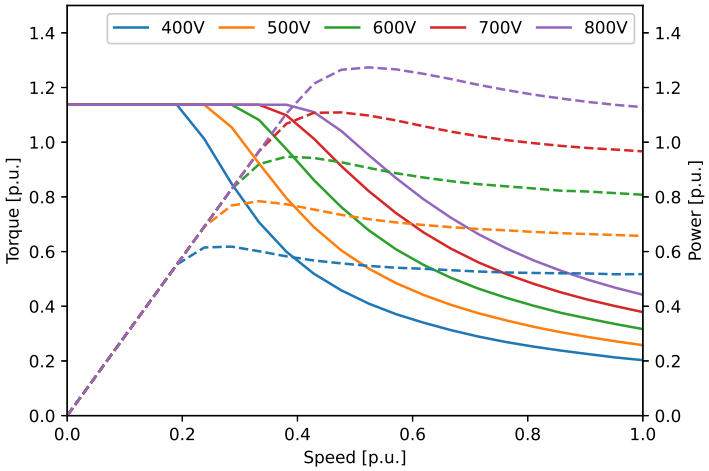

Figure A.5: Asymmetric 2U N42 machine torque and power max lines at different DC-link voltages.

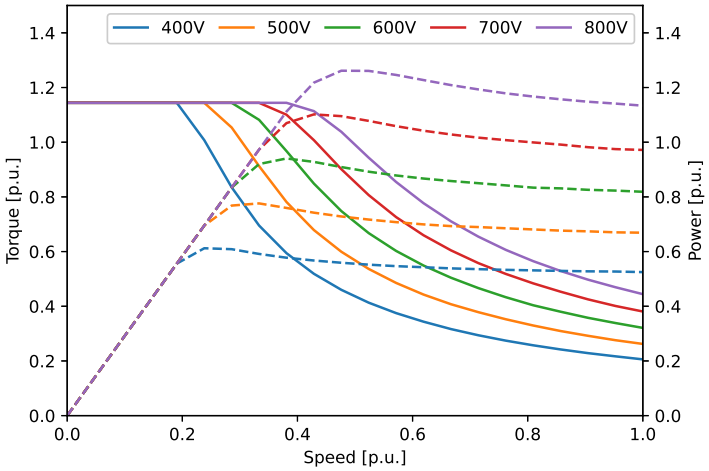

Figure A.6: Asymmetric 2U N52 machine torque and power max lines at different DC-link voltages.

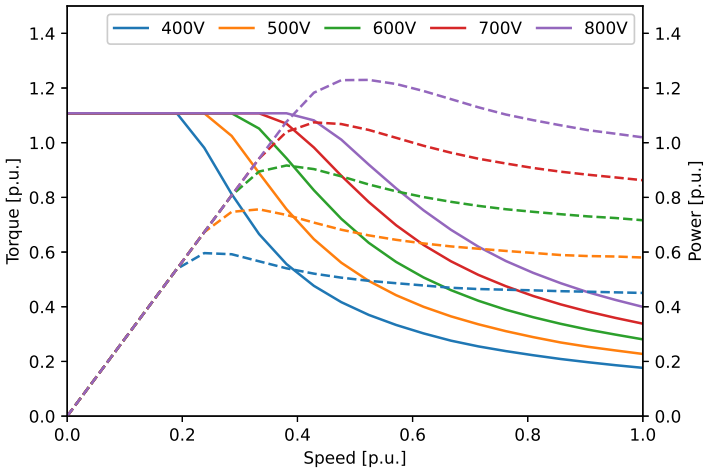

Figure A.7: Asymmetric 3U N35 machine torque and power max lines at different DC-link voltages.

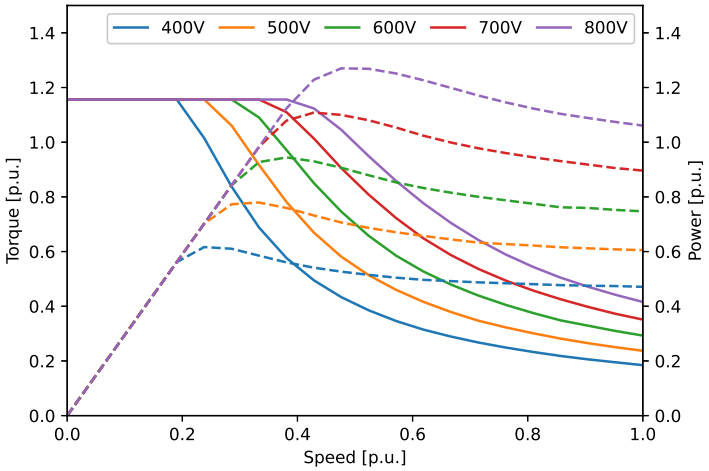

Figure A.8: Asymmetric 3U N42 machine torque and power max lines at different DC-link voltages.

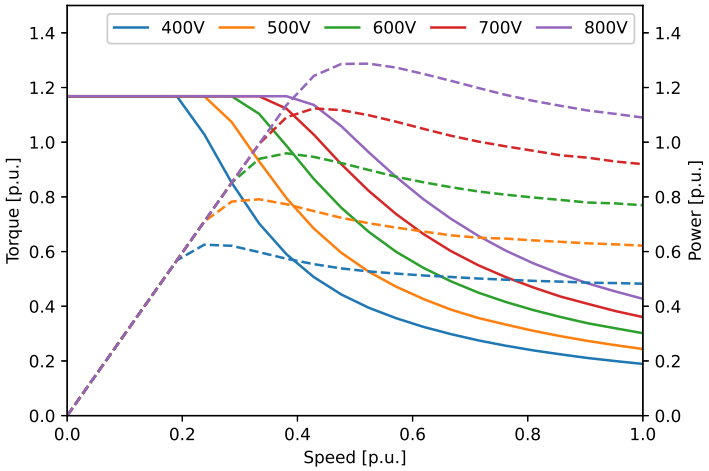

Figure A.9: Asymmetric 3U N52 machine torque and power max lines at different DC-link voltages.

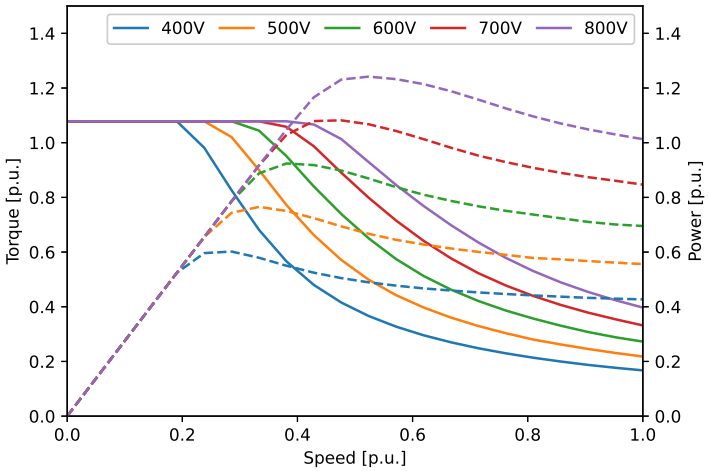

Figure A.10: Asymmetric 1V N35 machine torque and power max lines at different DC-link voltages.

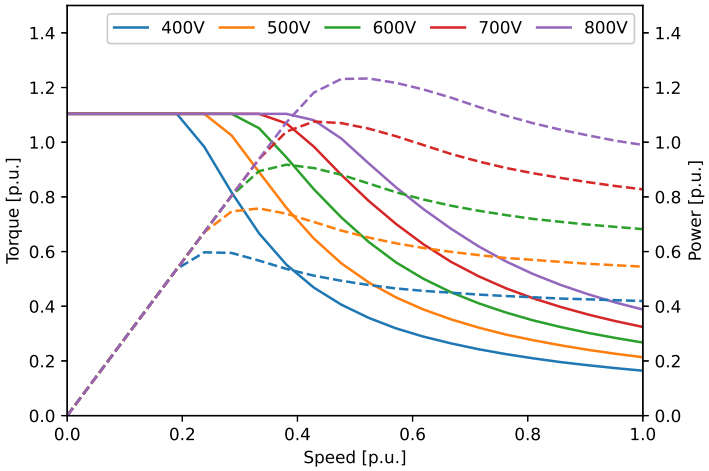

Figure A.11: Asymmetric 1V N42 machine torque and power max lines at different DC-link voltages.

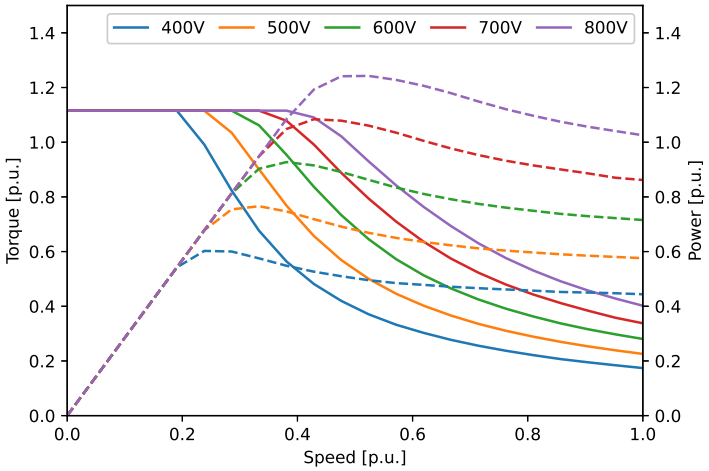

Figure A.12: Asymmetric 1V N52 machine torque and power max lines at different DC-link voltages.

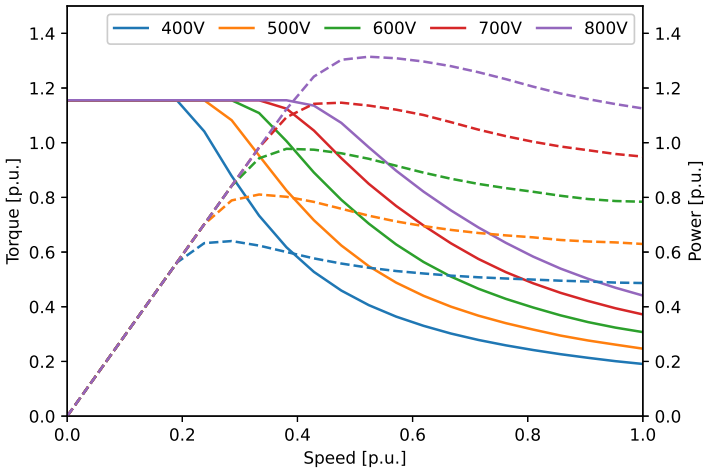

Figure A.13: Asymmetric 2V N35 machine torque and power max lines at different DC-link voltages.

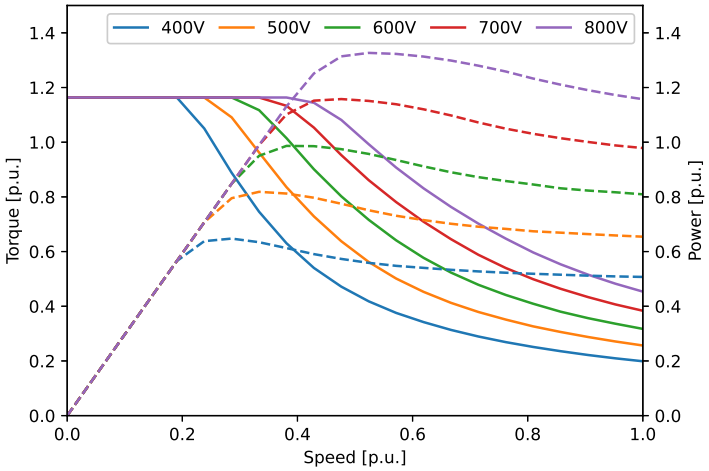

Figure A.14: Asymmetric 2V N42 machine torque and power max lines at different DC-link voltages.

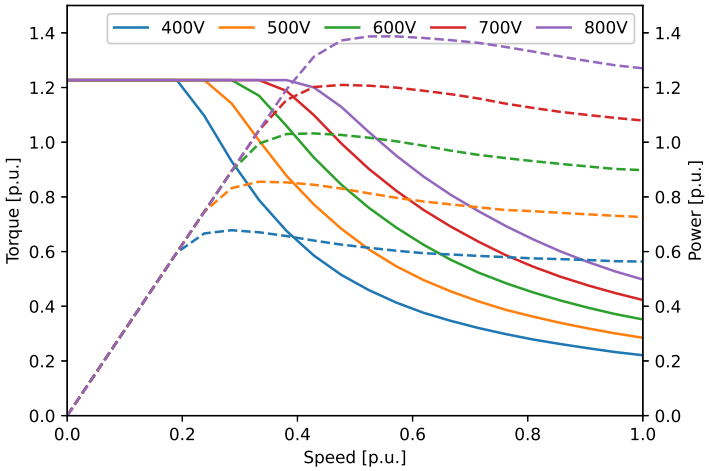

Figure A.15: Asymmetric 2V N52 machine torque and power max lines at different DC-link voltages.

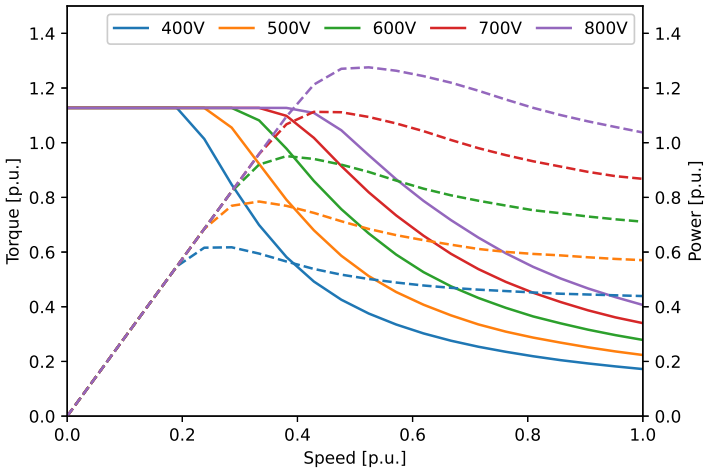

Figure A.16: Asymmetric 3V N35 machine torque and power max lines at different DC-link voltages.

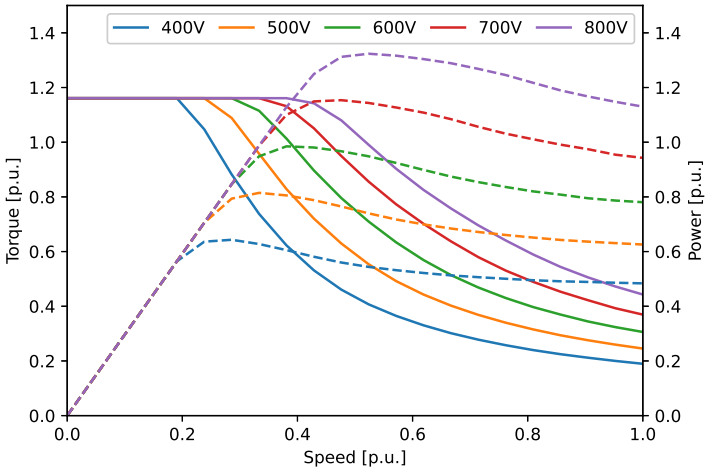

Figure A.17: Asymmetric 3V N42 machine torque and power max lines at different DC-link voltages.

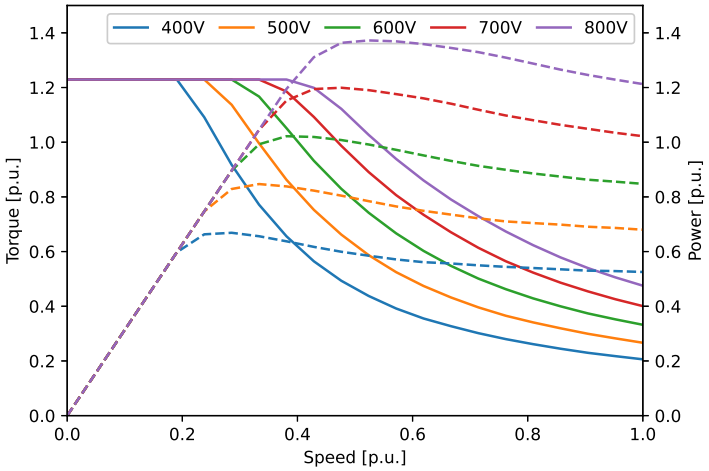

Figure A.18: Asymmetric 3V N52 machine torque and power max lines at different DC-link voltages.

Appendix B

Peak Performance: Efficiency and Power Factor

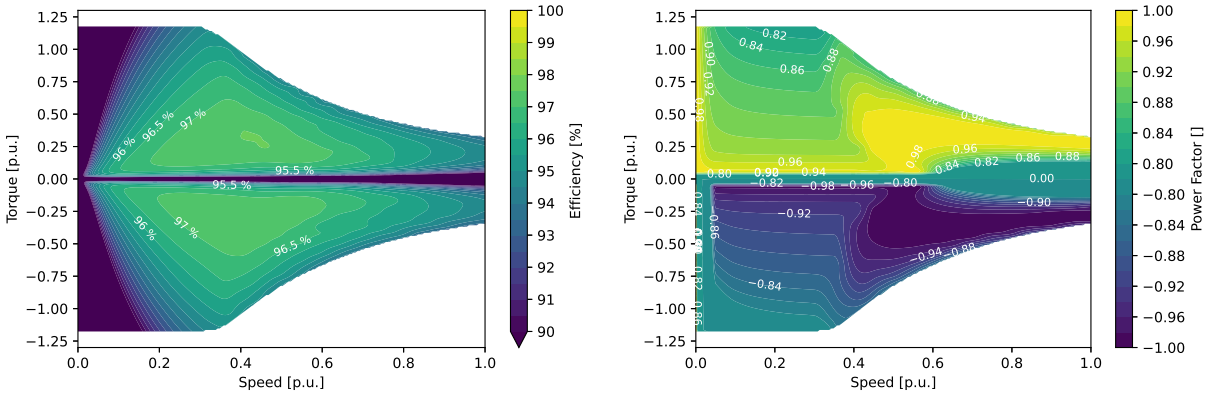

(a) Efficiency. (b) Power factor.

Figure B.1: Efficiency and power factor for symmetric 2V N42 machine at 600 V DC-link voltage.

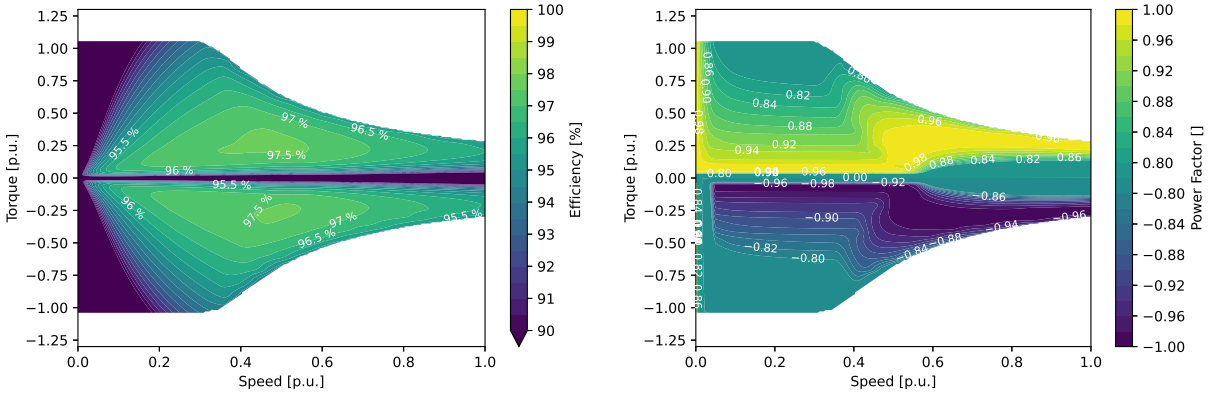

(a) Efficiency. (b) Power factor.

Figure B.2: Efficiency and power factor for asymmetric 1U N35 machine at 600 V DC-link voltage.

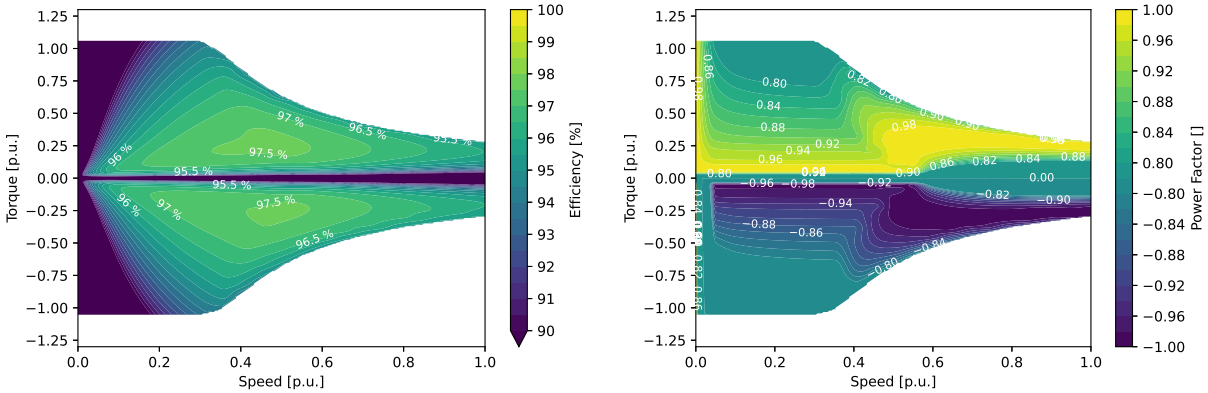

(a) Efficiency. (b) Power factor.

Figure B.3: Efficiency and power factor for asymmetric 1U N42 machine at 600 V DC-link voltage.

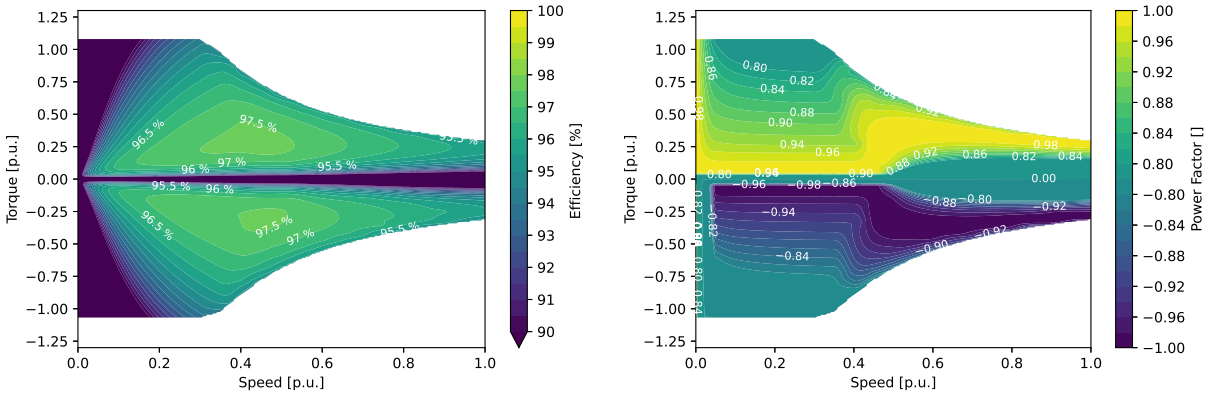

(a) Efficiency. (b) Power factor.

Figure B.4: Efficiency and power factor for asymmetric 1U N52 machine at 600 V DC-link voltage.

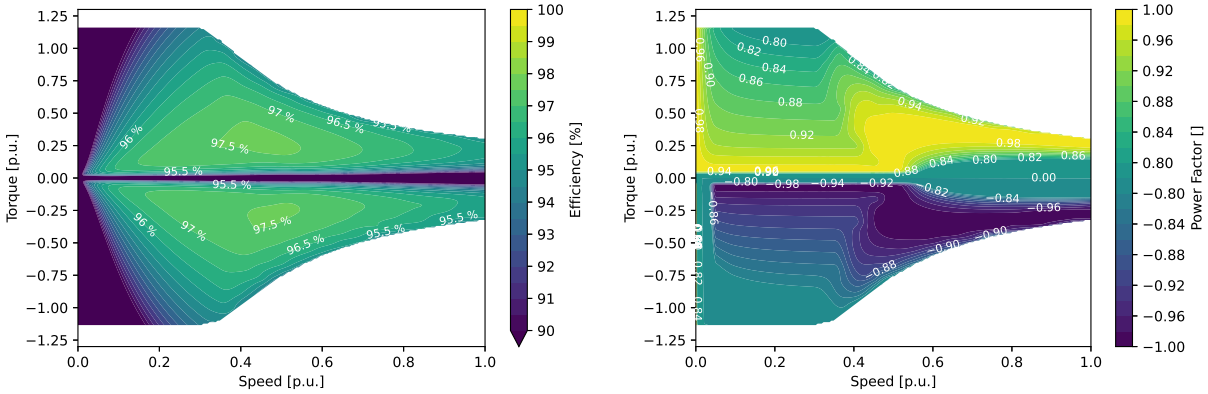

(a) Efficiency. (b) Power factor.

Figure B.5: Efficiency and power factor for asymmetric 2U N35 machine at 600 V DC-link voltage.

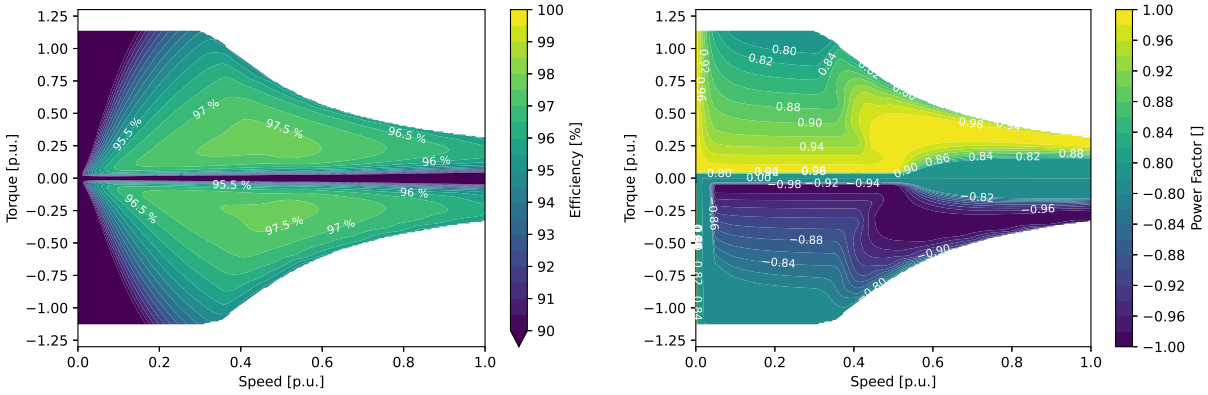

(a) Efficiency. (b) Power factor.

Figure B.6: Efficiency and power factor for asymmetric 2U N42 machine at 600 V DC-link voltage.

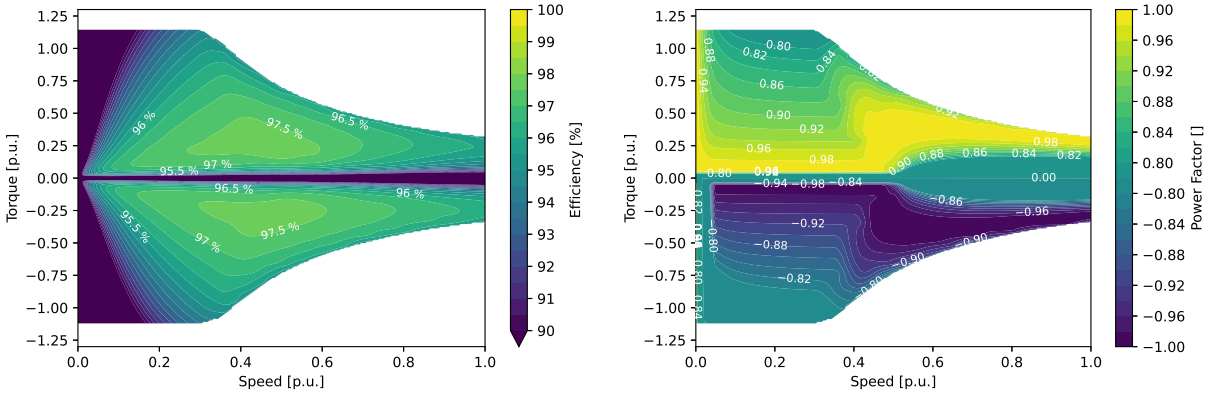

(a) Efficiency. (b) Power factor.

Figure B.7: Efficiency and power factor for asymmetric 2U N52 machine at 600 V DC-link voltage.

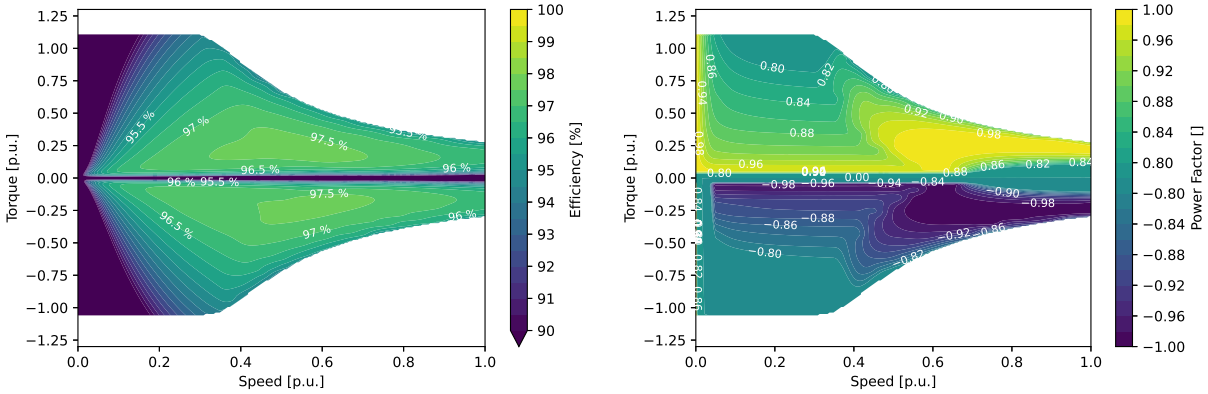

(a) Efficiency. (b) Power factor.

Figure B.8: Efficiency and power factor for asymmetric 3U N35 machine at 600 V DC-link voltage.

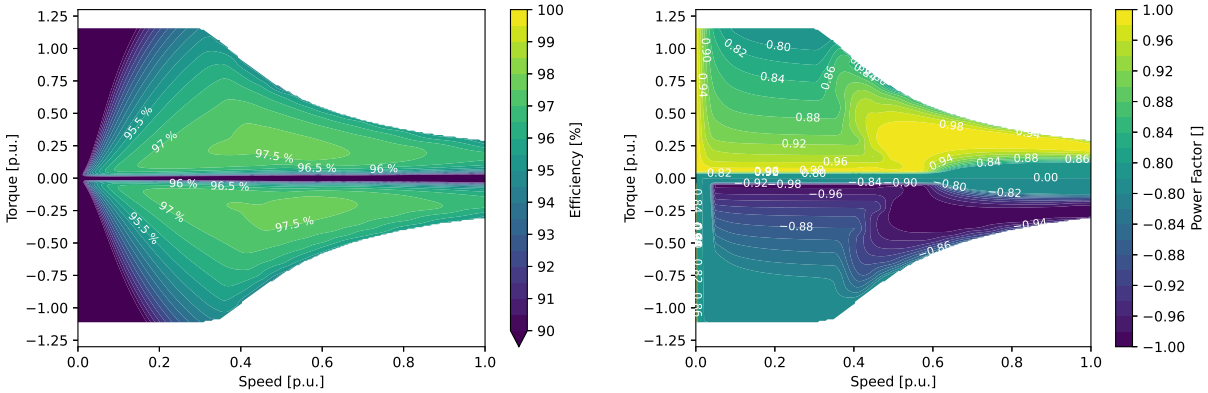

(a) Efficiency. (b) Power factor.

Figure B.9: Efficiency and power factor for asymmetric 3U N42 machine at 600 V DC-link voltage.

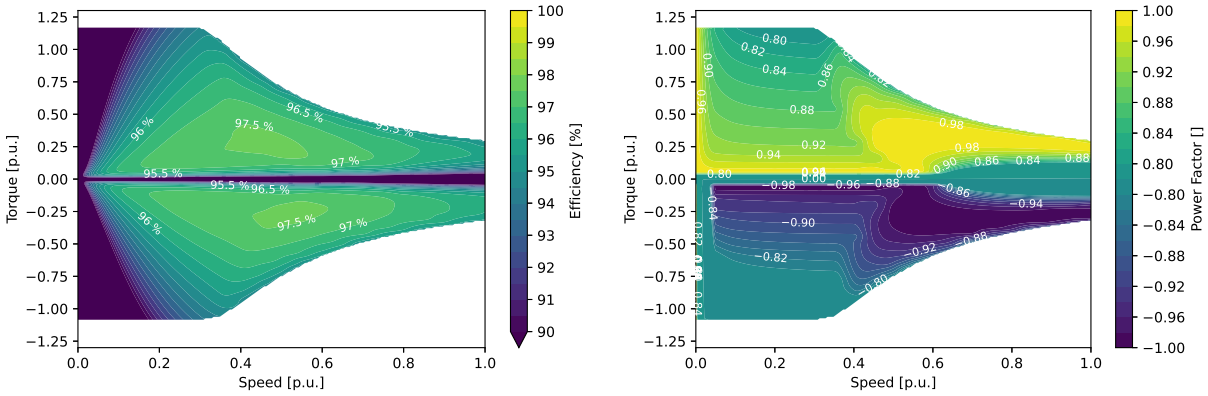

(a) Efficiency. (b) Power factor.

Figure B.10: Efficiency and power factor for asymmetric 3U N52 machine at 600 V DC-link voltage.

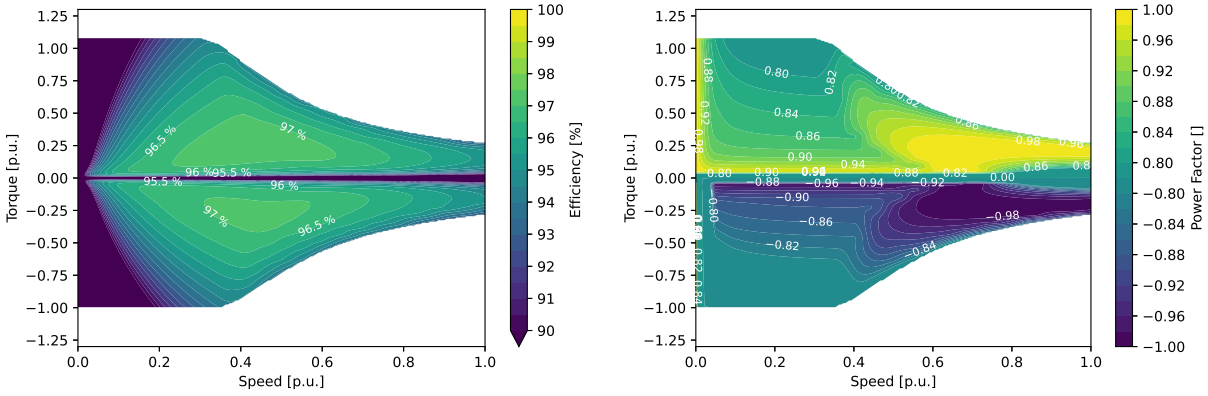

(a) Efficiency. (b) Power factor.

Figure B.11: Efficiency and power factor for asymmetric 1V N35 machine at 600 V DC-link voltage.

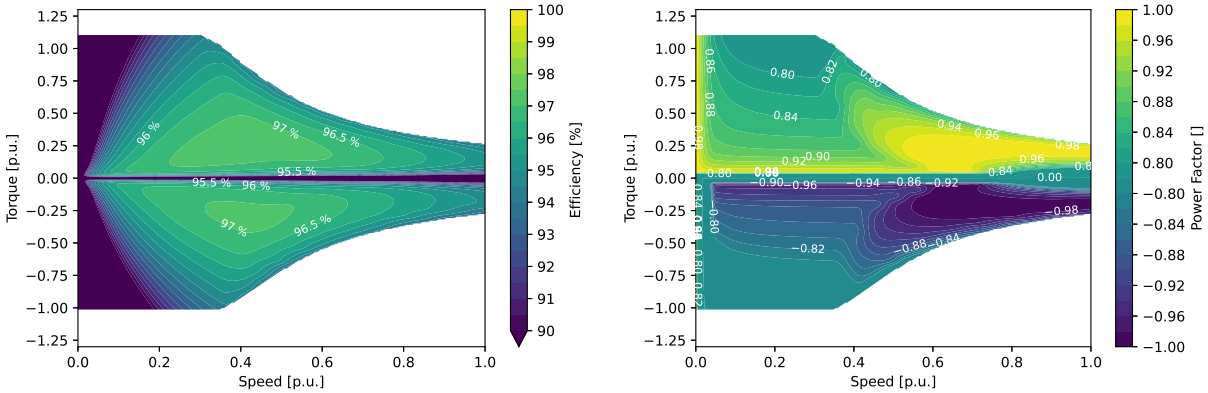

(a) Efficiency. (b) Power factor.

Figure B.12: Efficiency and power factor for asymmetric 1V N42 machine at 600 V DC-link voltage.

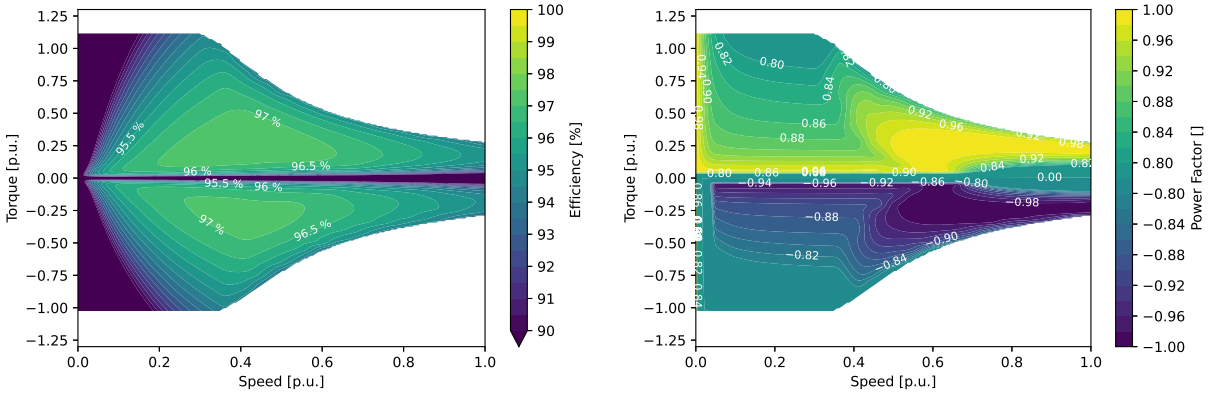

(a) Efficiency. (b) Power factor.

Figure B.13: Efficiency and power factor for asymmetric 1V N52 machine at 600 V DC-link voltage.

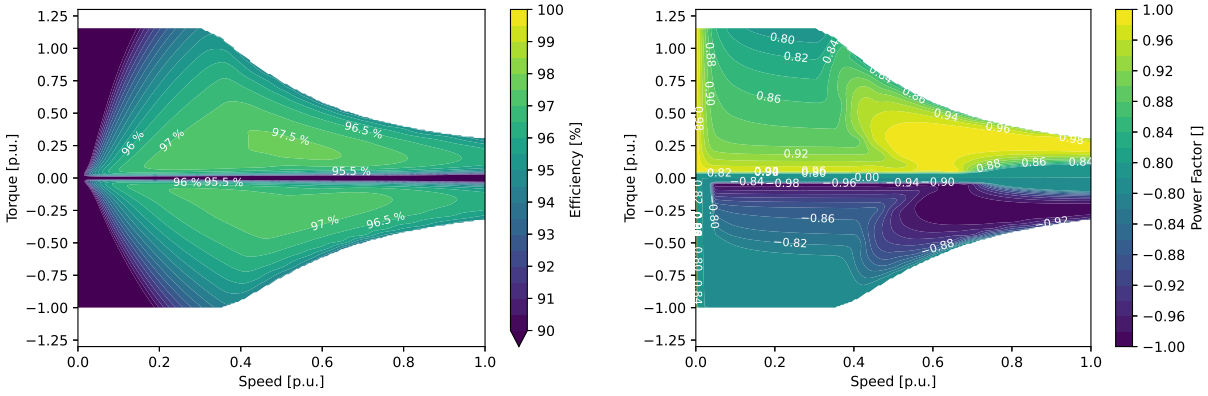

(a) Efficiency. (b) Power factor.

Figure B.14: Efficiency and power factor for asymmetric 2V N35 machine at 600 V DC-link voltage.

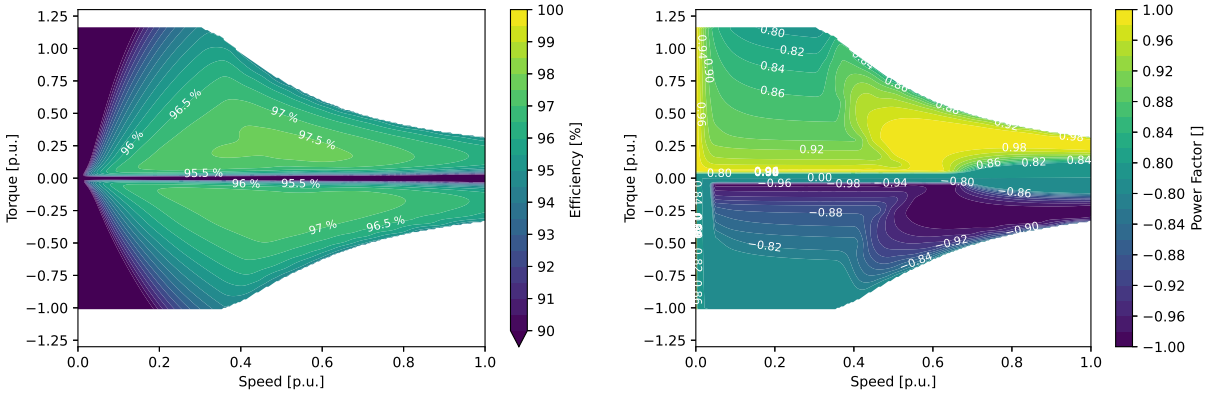

(a) Efficiency. (b) Power factor.

Figure B.15: Efficiency and power factor for asymmetric 2V N42 machine at 600 V DC-link voltage.

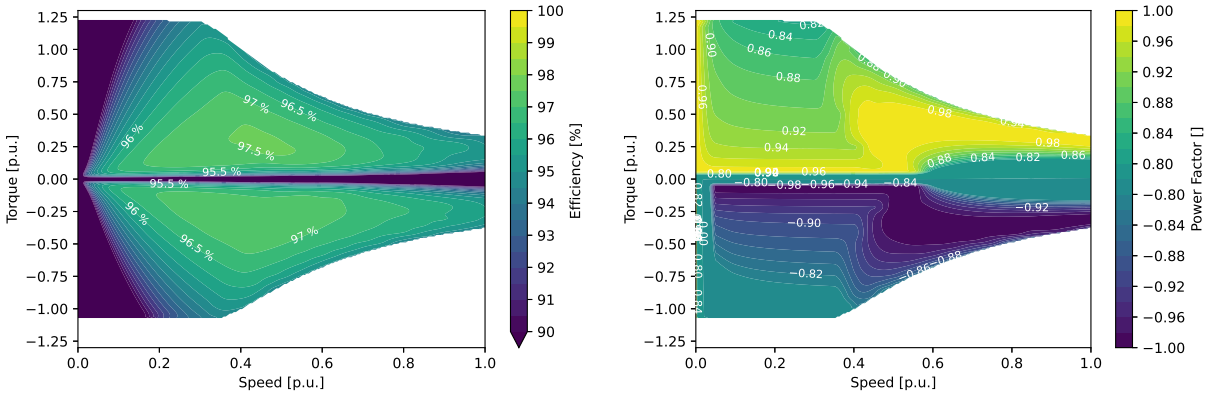

(a) Efficiency. (b) Power factor.

Figure B.16: Efficiency and power factor for asymmetric 2V N52 machine at 600 V DC-link voltage.

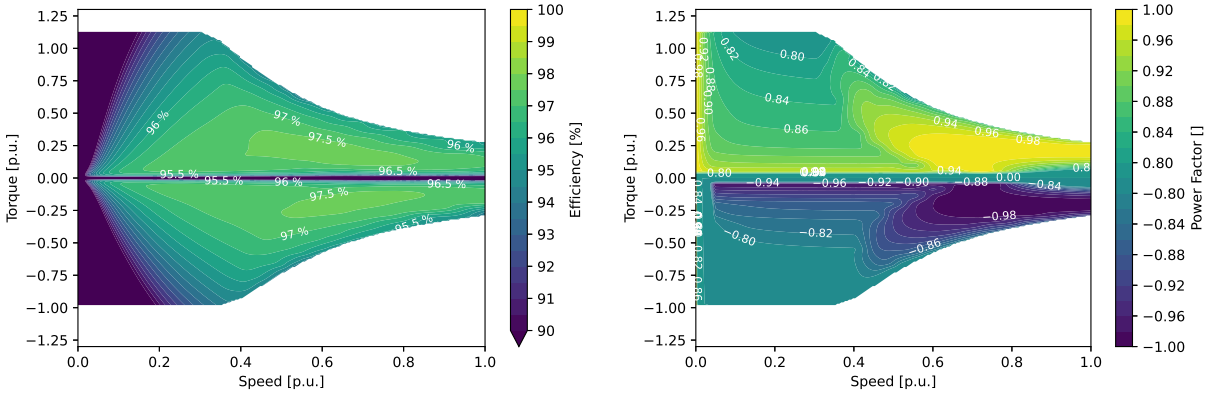

(a) Efficiency. (b) Power factor.

Figure B.17: Efficiency and power factor for asymmetric 3V N35 machine at 600 V DC-link voltage.

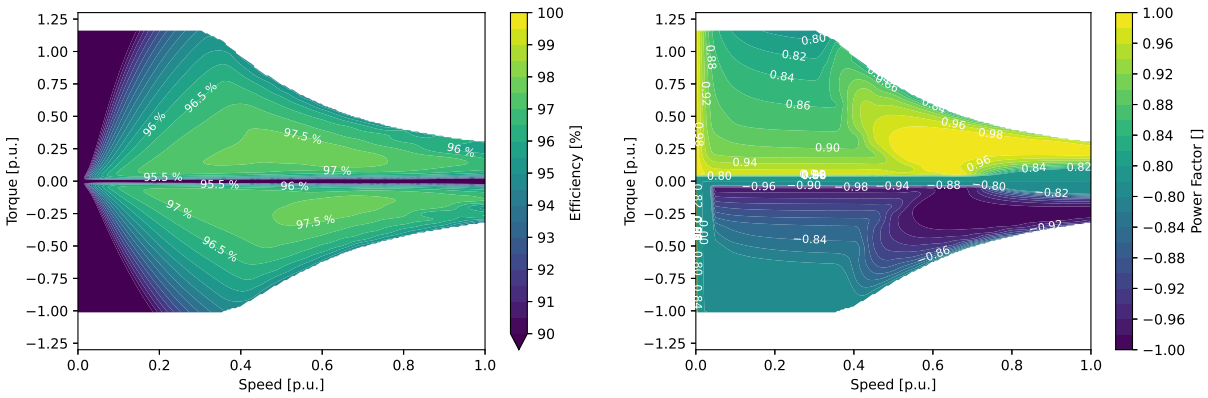

(a) Efficiency. (b) Power factor.

Figure B.18: Efficiency and power factor for asymmetric 3V N42 machine at 600 V DC-link voltage.

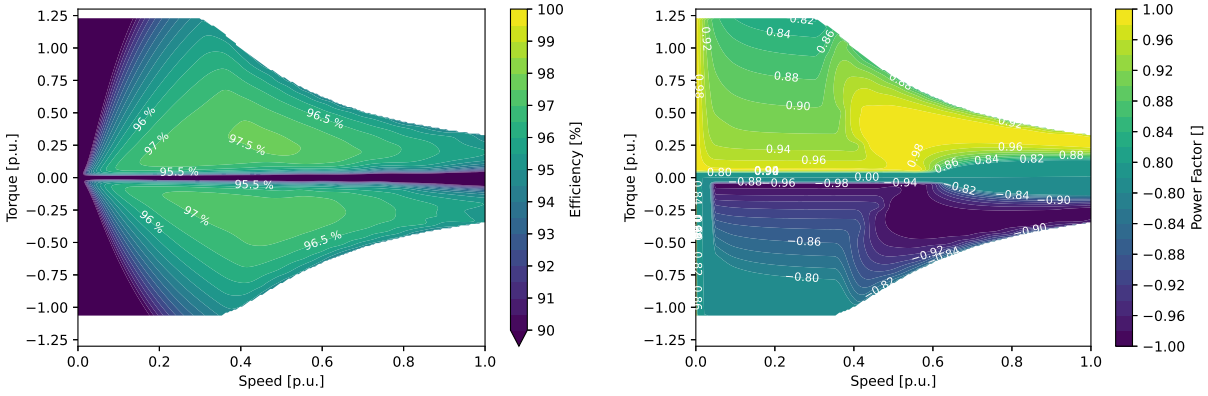

(a) Efficiency. (b) Power factor.

Figure B.19: Efficiency and power factor for asymmetric 3V N52 machine at 600 V DC-link voltage.

Appendix C

Peak Performance: Reluctance Versus Magnet Torque

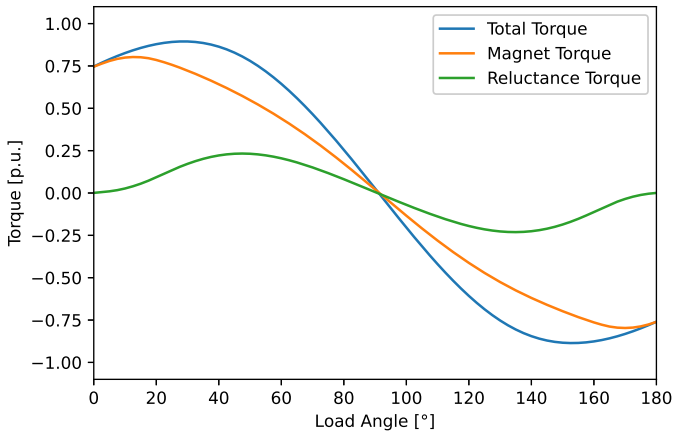

Figure C.1: Reluctance and magnet torque components for the asymmetric 1U N35 machine.

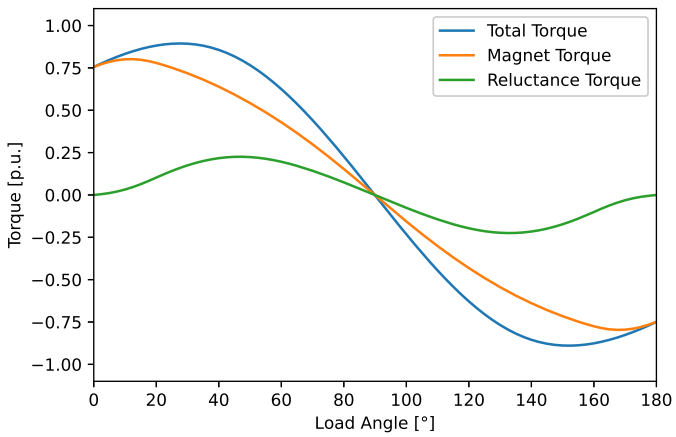

Figure C.2: Reluctance and magnet torque components for the asymmetric 1U N42 machine.

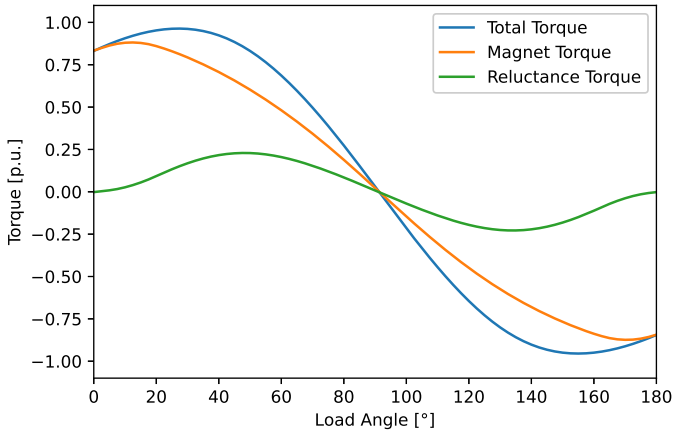

Figure C.3: Reluctance and magnet torque components for the asymmetric 1U N52 machine.

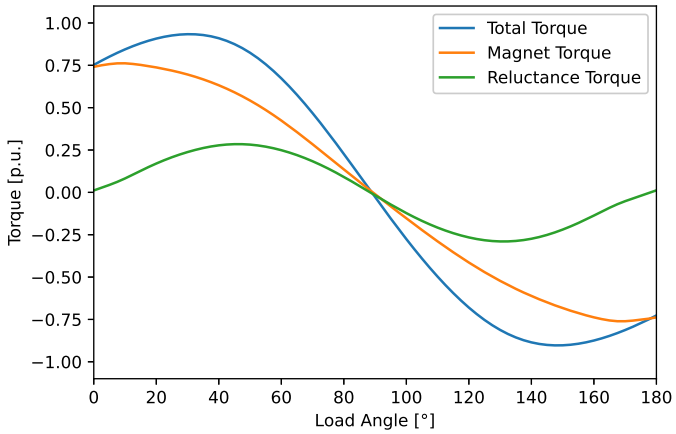

Figure C.4: Reluctance and magnet torque components for the asymmetric 2U N35 machine.

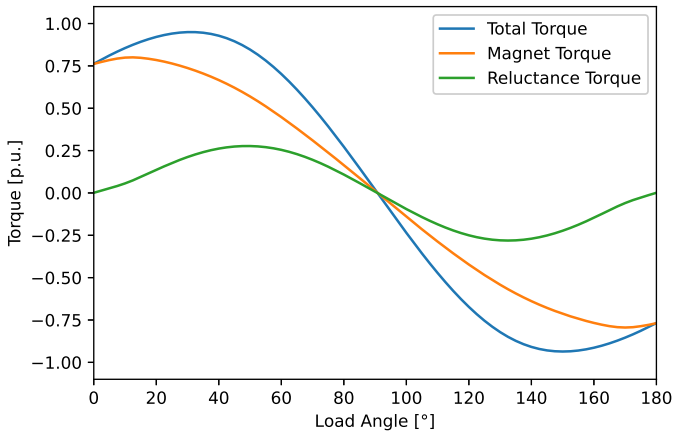

Figure C.5: Reluctance and magnet torque components for the asymmetric 2U N42 machine.

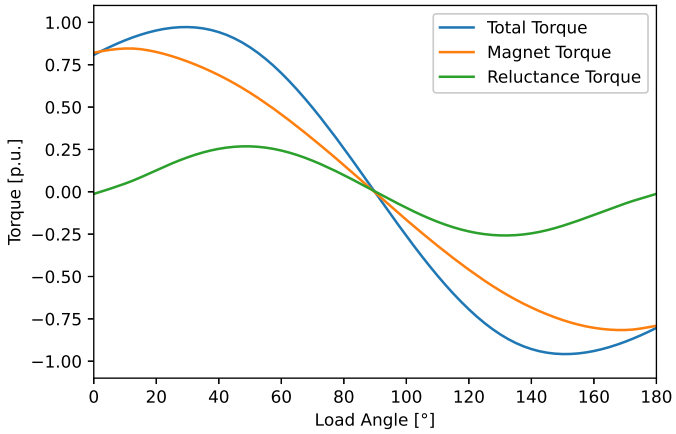

Figure C.6: Reluctance and magnet torque components for the asymmetric 2U N52 machine.

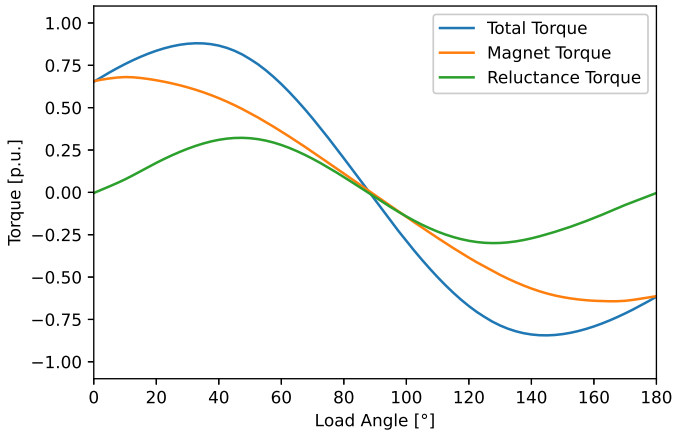

Figure C.7: Reluctance and magnet torque components for the asymmetric 3U N35 machine.

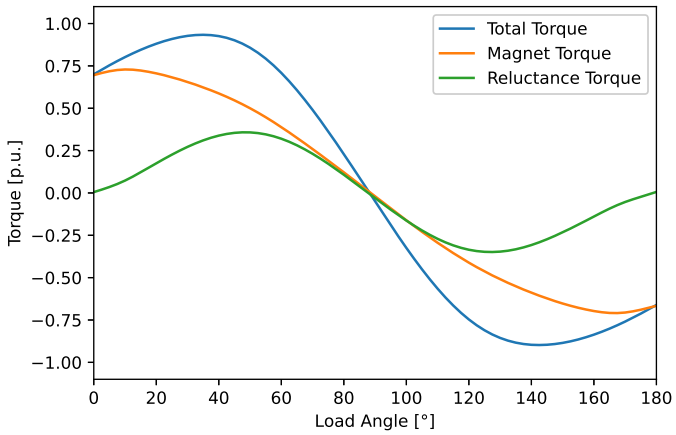

Figure C.8: Reluctance and magnet torque components for the asymmetric 3U N42 machine.

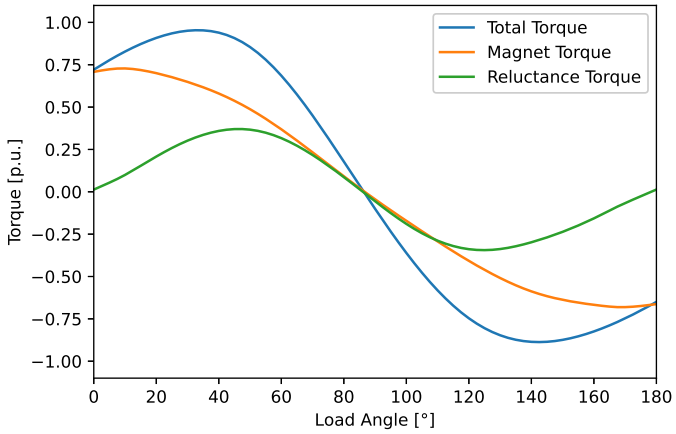

Figure C.9: Reluctance and magnet torque components for the asymmetric 3U N52 machine.

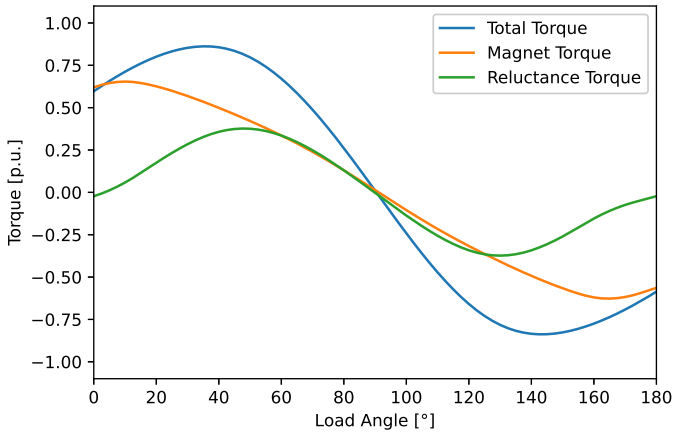

Figure C.10: Reluctance and magnet torque components for the asymmetric 1V N35 machine.

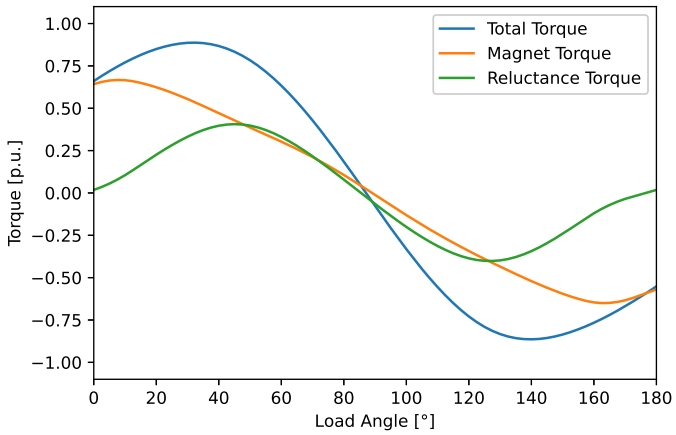

Figure C.11: Reluctance and magnet torque components for the asymmetric 1V N42 machine.

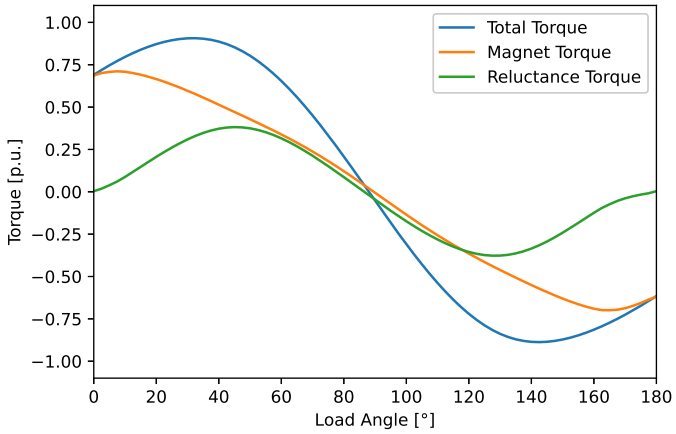

Figure C.12: Reluctance and magnet torque components for the asymmetric 1V N52 machine.

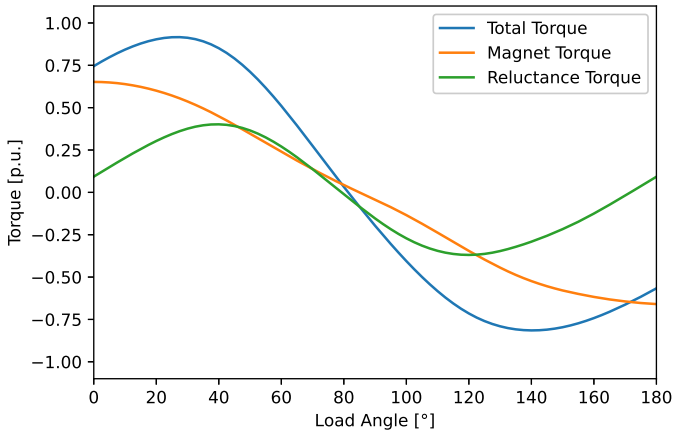

Figure C.13: Reluctance and magnet torque components for the asymmetric 2V N35 machine.

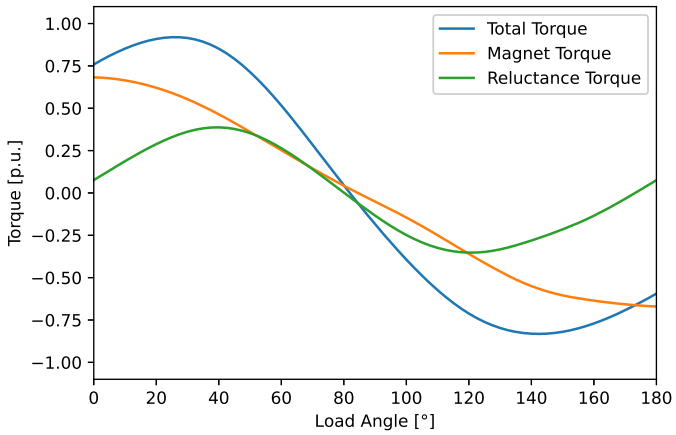

Figure C.14: Reluctance and magnet torque components for the asymmetric 2V N42 machine.

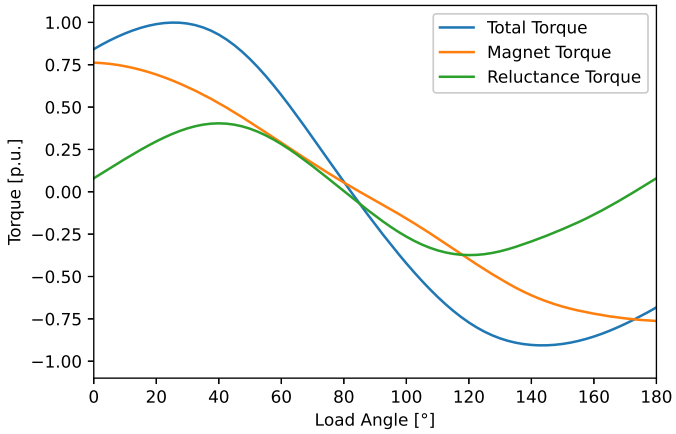

Figure C.15: Reluctance and magnet torque components for the asymmetric 2V N52 machine.

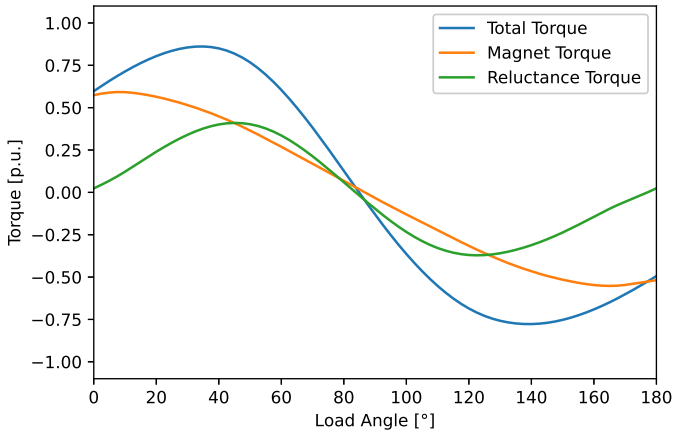

Figure C.16: Reluctance and magnet torque components for the asymmetric 3V N35 machine.

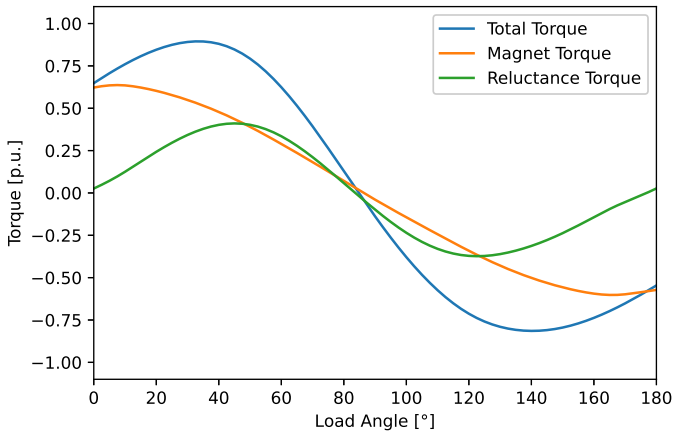

Figure C.17: Reluctance and magnet torque components for the asymmetric 3V N42 machine.

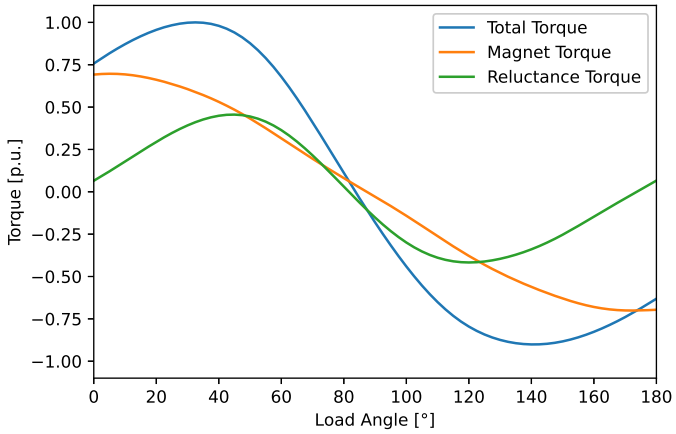

Figure C.18: Reluctance and magnet torque components for the asymmetric 3V N52 machine.

Appendix D

Efficiency and Cost: Efficiency and Power Factor

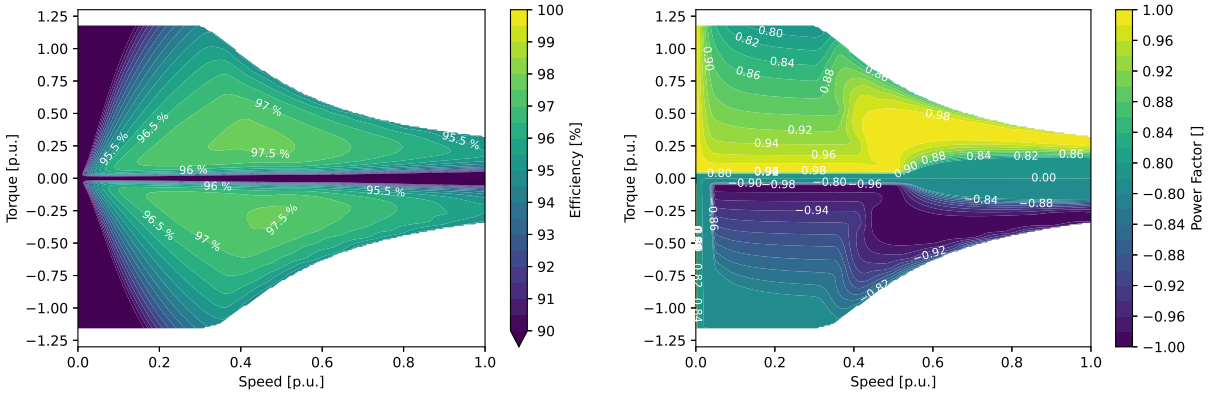

(a) Efficiency. (b) Power factor.

Figure D.1: Efficiency and power factor for asymmetric 2U N35 machine at 600 V DC-link voltage.

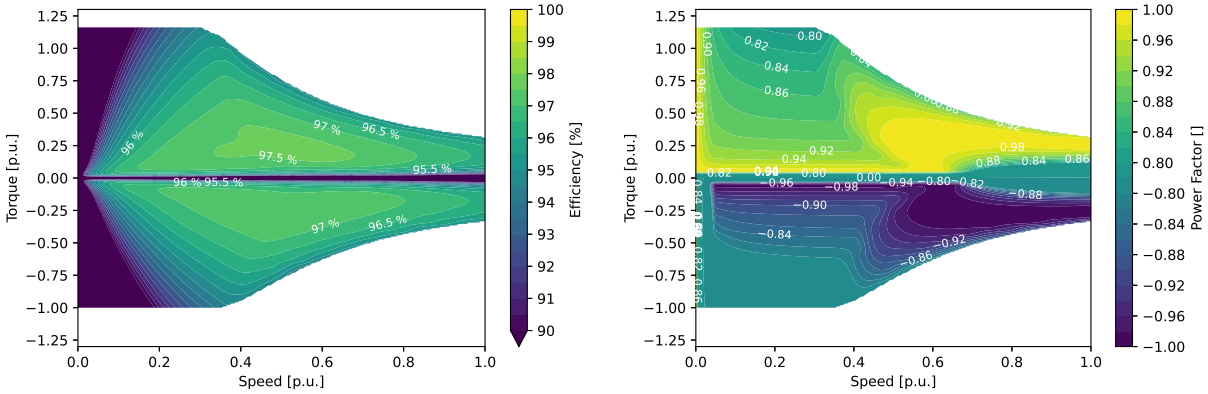

(a) Efficiency. (b) Power factor.

Figure D.2: Efficiency and power factor for asymmetric 2V N42 machine at 600 V DC-link voltage.

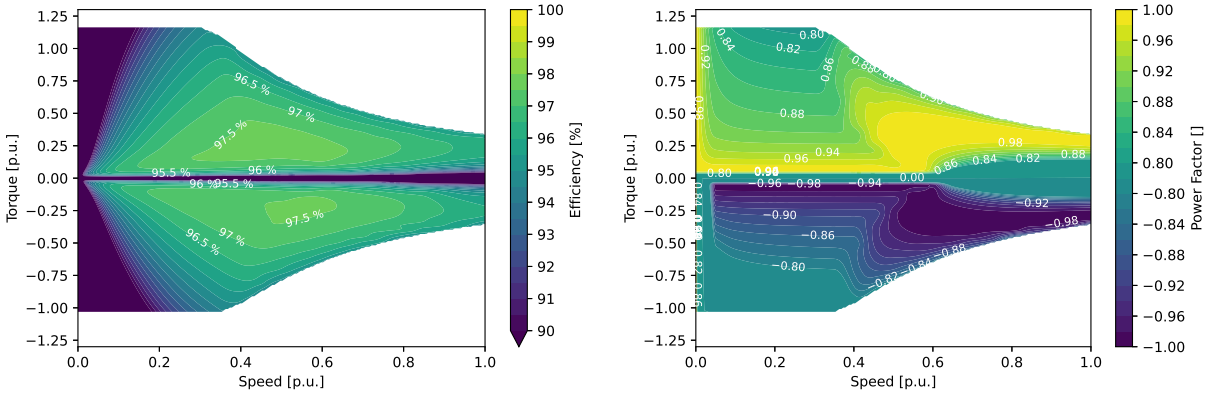

(a) Efficiency. (b) Power factor.

Figure D.3: Efficiency and power factor for asymmetric 2V N52 machine at 600 V DC-link voltage.

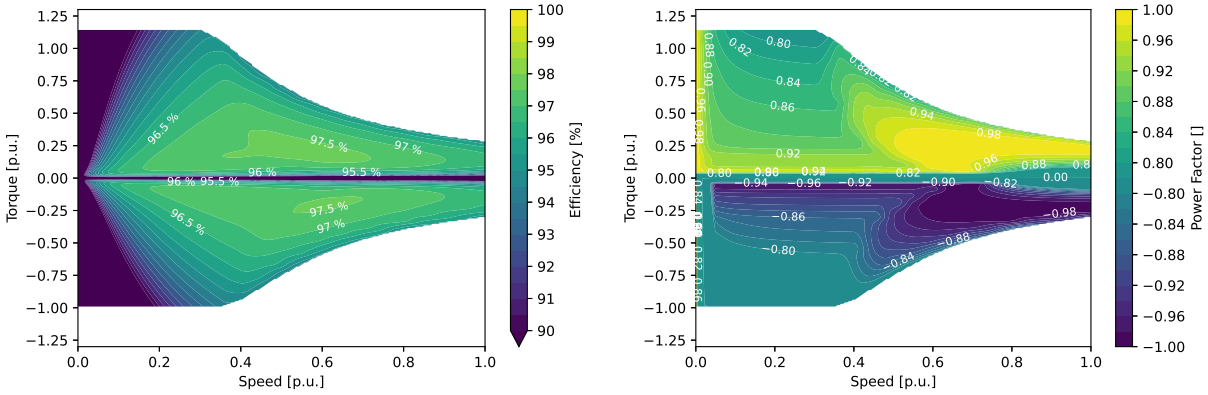

(a) Efficiency. (b) Power factor.

Figure D.4: Efficiency and power factor for asymmetric 3V N35 machine at 600 V DC-link voltage.

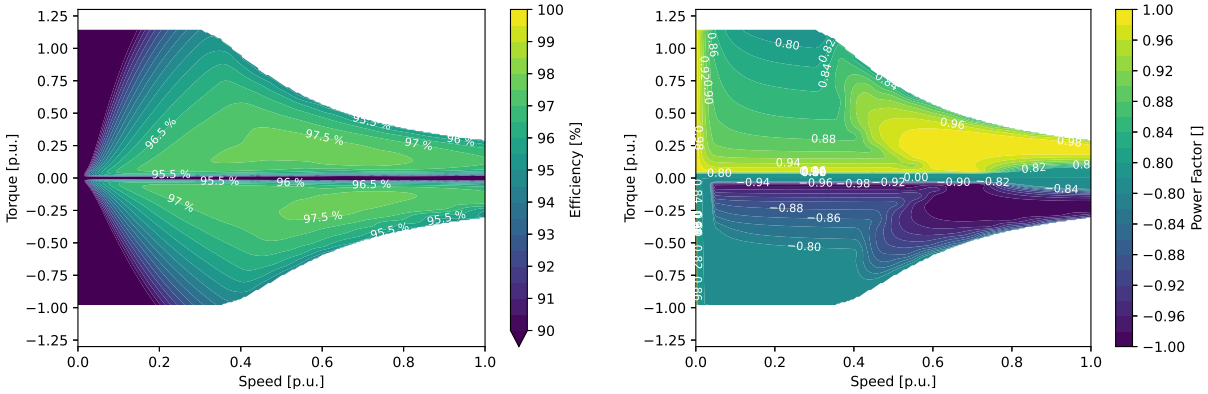

(a) Efficiency. (b) Power factor.

Figure D.5: Efficiency and power factor for asymmetric 3V N42 machine at 600 V DC-link voltage.

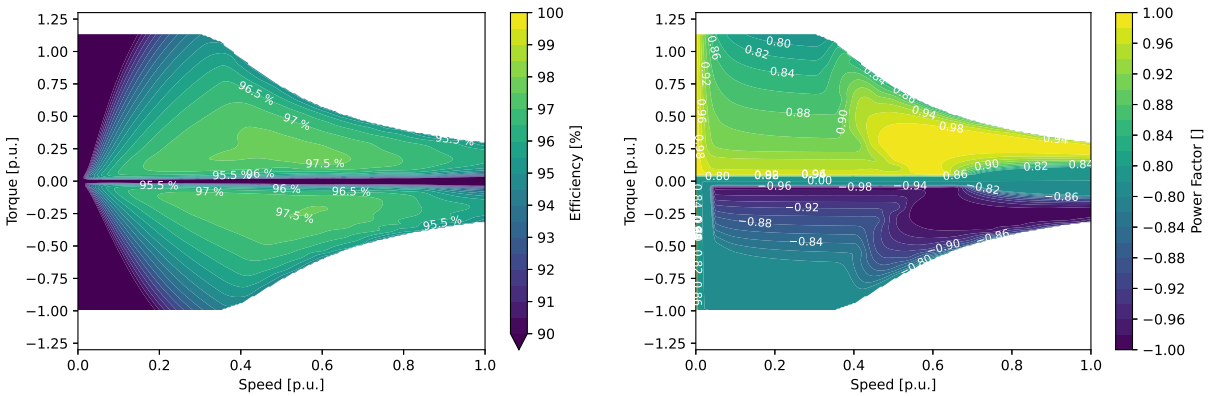

(a) Efficiency.

(b) Power factor.

Figure D.6: Efficiency and power factor for asymmetric 3V N52 machine at 600 V DC-link voltage.

Appendix E

Demagnetisation Current Sweep

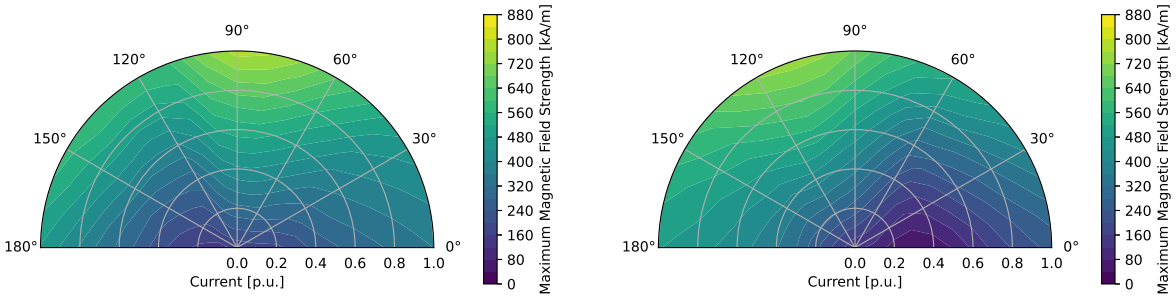

(a) Outer layer, upper magnet.

(b) Outer layer, lower magnet.

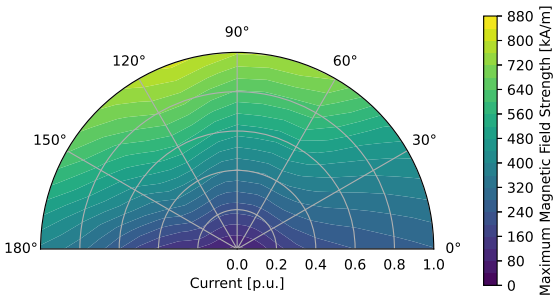

(c) Middle layer, upper magnet.

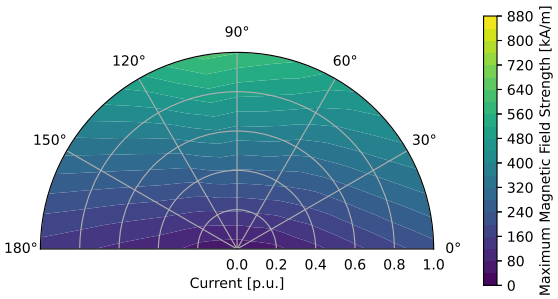

(d) Middle layer, lower magnet.

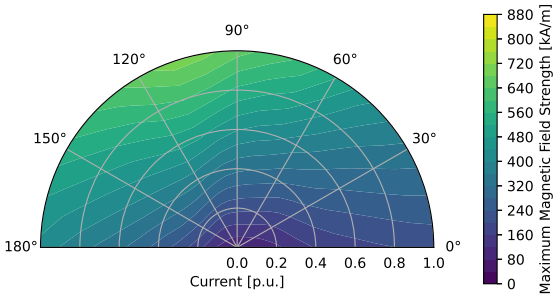

(e) Inner layer, upper magnet.

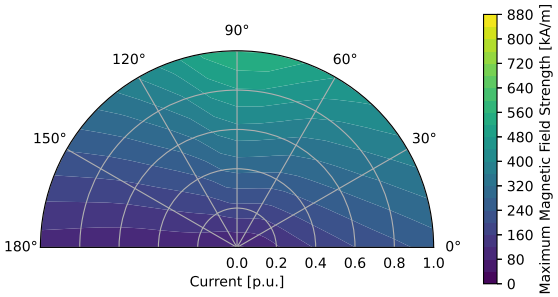

(f) Inner layer, lower magnet.

Figure E.1: Maximum magnetic field strength in all magnets in first skew layer in 3V N35 low cost and efficiency optimised machine for all current amplitudes and angles.

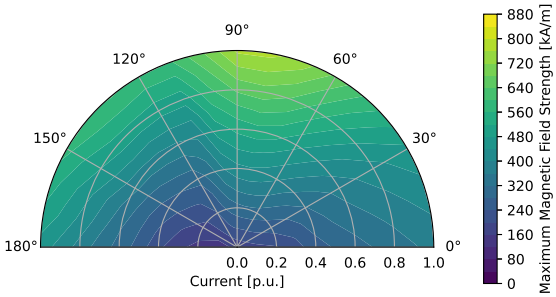

(a) Outer layer, upper magnet.

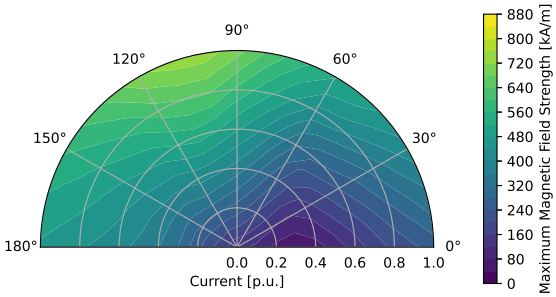

(b) Outer layer, lower magnet.

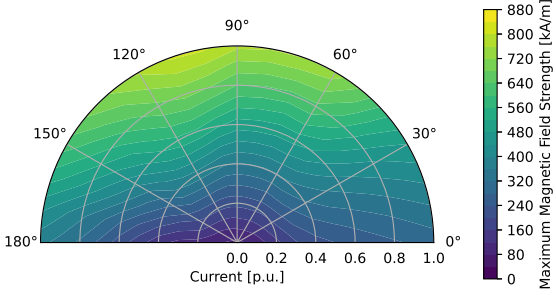

(c) Middle layer, upper magnet.

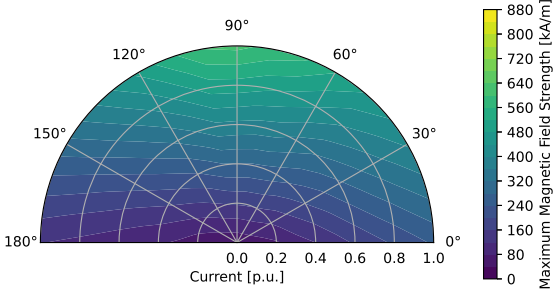

(d) Middle layer, lower magnet.

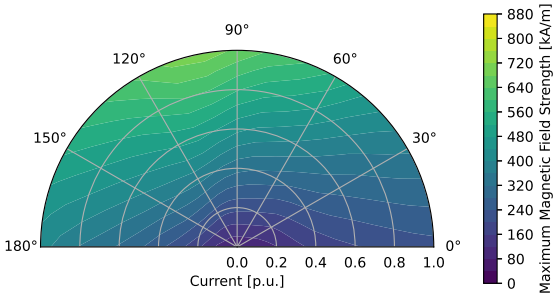

(e) Inner layer, upper magnet.

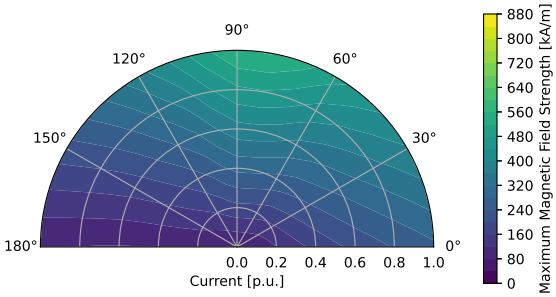

(f) Inner layer, lower magnet.

Figure E.2: Maximum magnetic field strength in all magnets in second skew layer in 3V N35 low cost and efficiency optimised machine for all current amplitudes and angles.

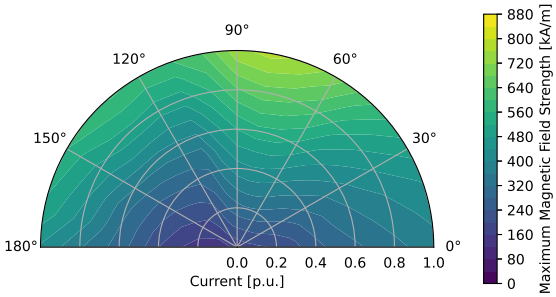

(a) Outer layer, upper magnet.

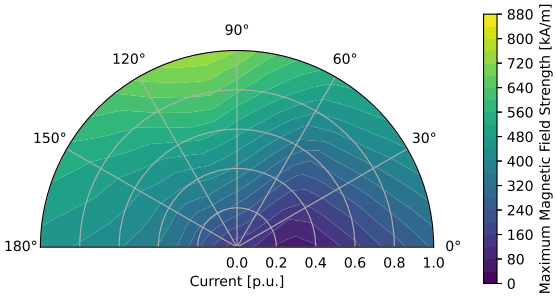

(b) Outer layer, lower magnet.

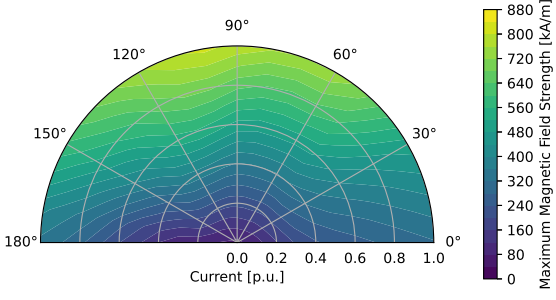

(c) Middle layer, upper magnet.

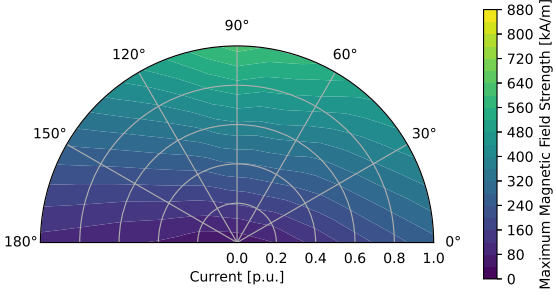

(d) Middle layer, lower magnet.

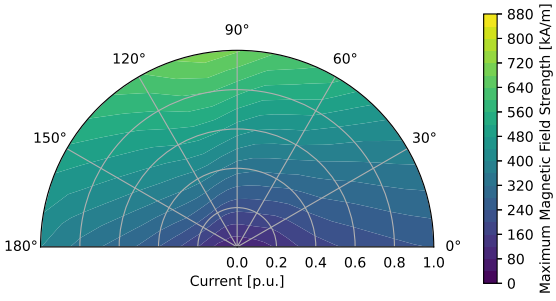

(e) Inner layer, upper magnet.

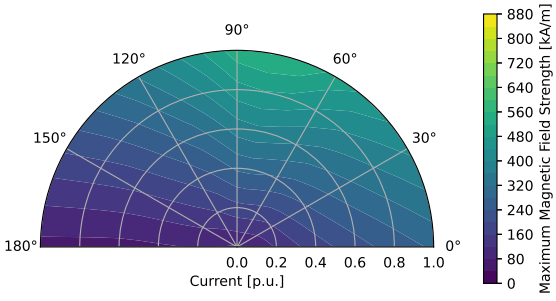

(f) Inner layer, lower magnet.

Figure E.3: Maximum magnetic field strength in all magnets in third skew layer in 3V N35 low cost and efficiency optimised machine for all current amplitudes and angles.

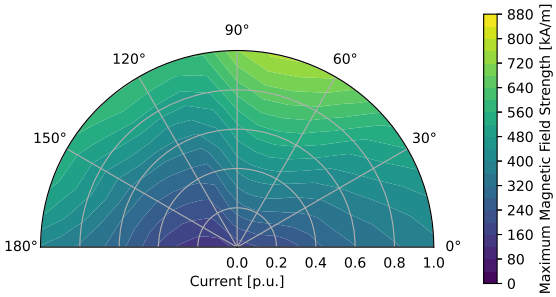

(a) Outer layer, upper magnet.

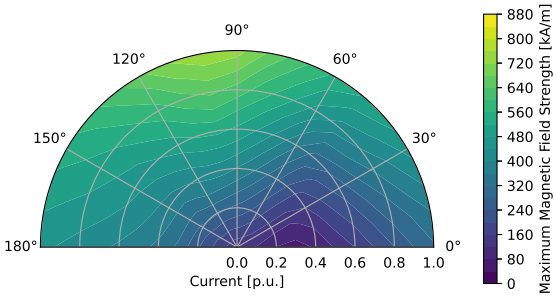

(b) Outer layer, lower magnet.

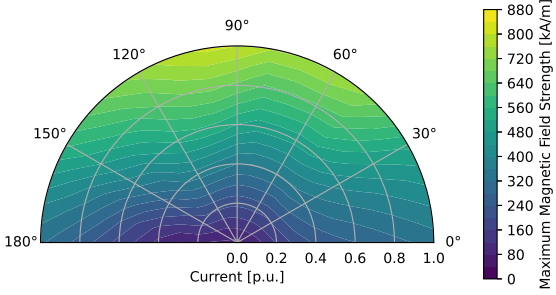

(c) Middle layer, upper magnet.

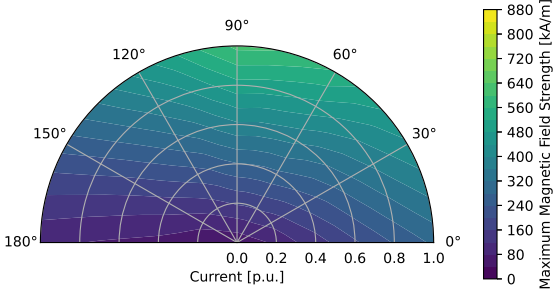

(d) Middle layer, lower magnet.

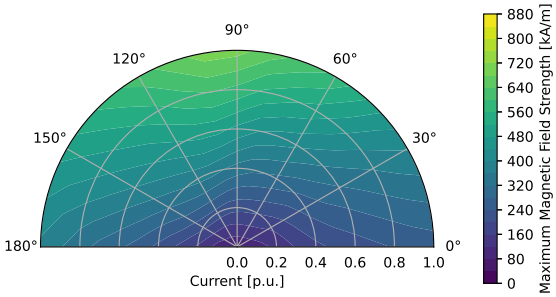

(e) Inner layer, upper magnet.

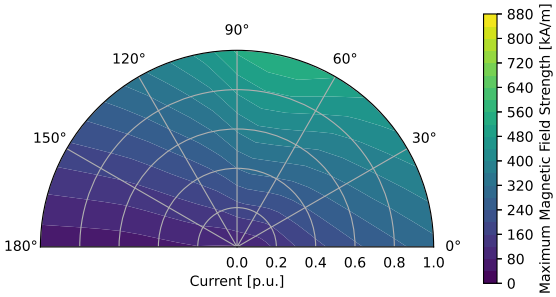

(f) Inner layer, lower magnet.

Figure E.4: Maximum magnetic field strength in all magnets in fourth skew layer in 3V N35 low cost and efficiency optimised machine for all current amplitudes and angles.

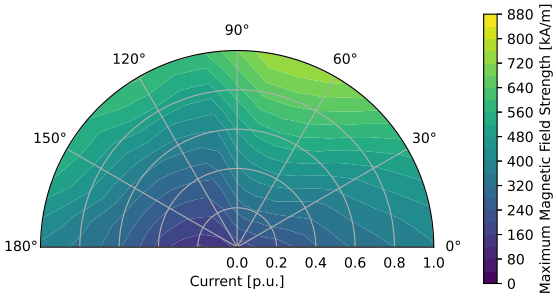

(a) Outer layer, upper magnet.

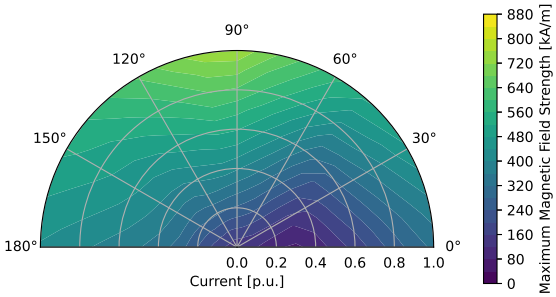

(b) Outer layer, lower magnet.

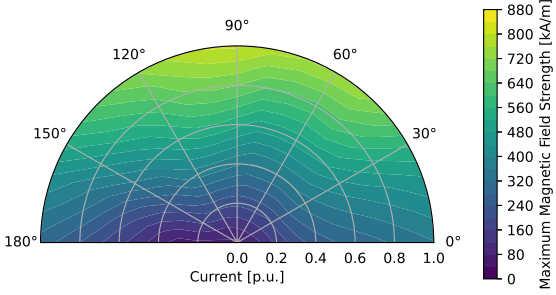

(c) Middle layer, upper magnet.

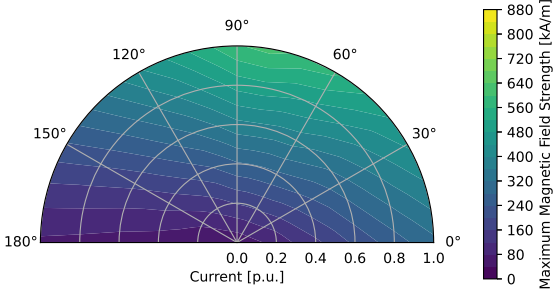

(d) Middle layer, lower magnet.

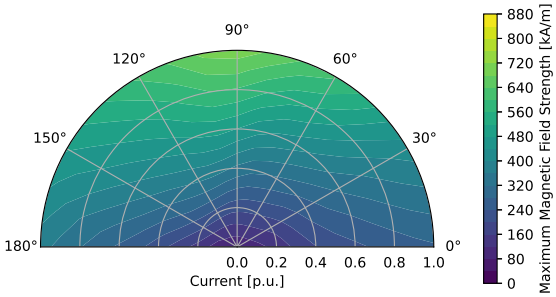

(e) Inner layer, upper magnet.

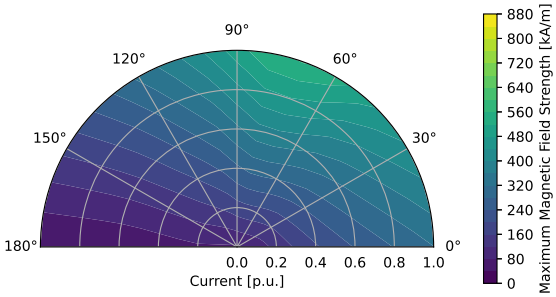

(f) Inner layer, lower magnet.

Figure E.5: Maximum magnetic field strength in all magnets in fifth skew layer in 3V N35 low cost and efficiency optimised machine for all current amplitudes and angles.

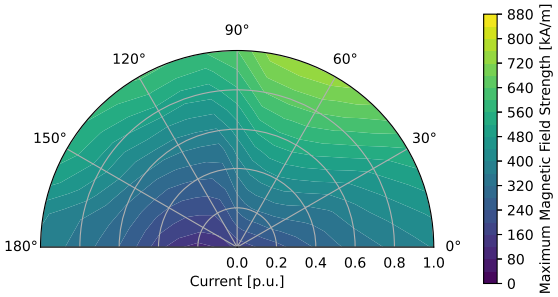

(a) Outer layer, upper magnet.

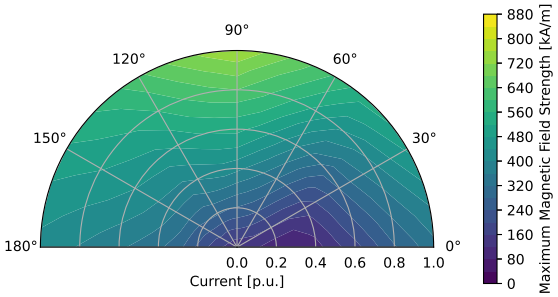

(b) Outer layer, lower magnet.

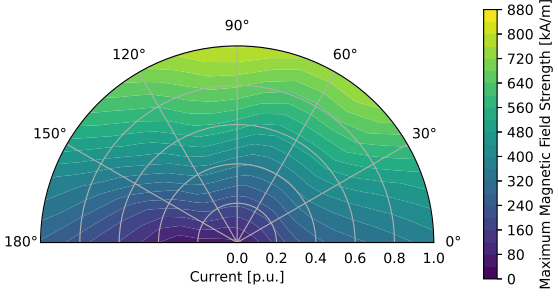

(c) Middle layer, upper magnet.

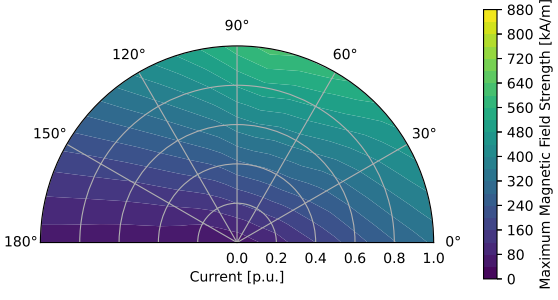

(d) Middle layer, lower magnet.

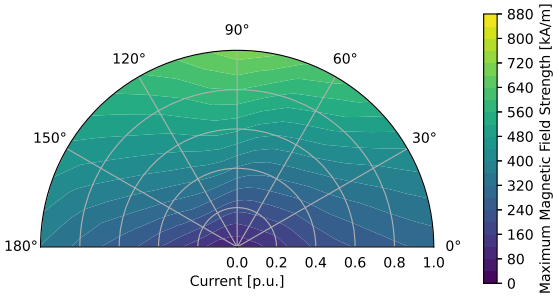

(e) Inner layer, upper magnet.

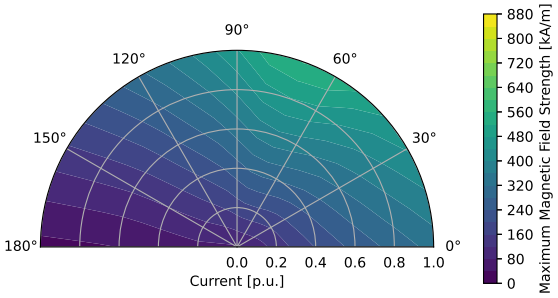

(f) Inner layer, lower magnet.

Figure E.6: Maximum magnetic field strength in all magnets in sixth skew layer in 3V N35 low cost and efficiency optimised machine for all current amplitudes and angles.

DEPARTMENT OF ELECTRICAL ENGINEERING
DIVISION OF ELECTRIC POWER ENGINEERING
CHALMERS UNIVERSITY OF TECHNOLOGY
Gothenburg, Sweden 2025
www.chalmers.se

CHALMERS
UNIVERSITY OF TECHNOLOGY